Development of Compound-Specific Hydrogen Isotope Ratio Analysis of Biomarkers and their Application as New Proxy for Reconstruction of Palaeoenvironment and Palaeoclimate

Entwicklung komponentenspezifischer Wasserstoffisotopen-Analyse von Biomarkern und deren Anwendung als neuartiger Proxy zur Rekonstruktion von Paläoumwelt und Paläoklima

Dissertation

zur Erlangung des akademischen Grades doctor rerum naturalium
(Dr. rer. nat.)

vorgelegt dem Rat der Chemisch-Geowissenschaftlichen Fakultät der
Friedrich-Schiller-Universität Jena
von Diplom Geologe Jens Radke
geboren am 20.2.1967 in Bremerhaven

Gutachter:

1. Prof.Dr.R.Gaupp

2. PD.Dr.G.Gleixner

Tag der öffentlichen Verteidigung: 18.1.2006

Printed on 100% recycled paper (after ISO9706, 133 CIE, DIN 6738 LDK 24-85)

Content

ABSTRACT

The hydrogen isotope ratio (δD) of continental water is defined by the general depletion of Deuterium in precipitation during condensation and its passage over continental areas. The primary producers in aquatic marine or lacustrine environments and land plants produce a δD of synthesized organic components, which records the isotope ratios of their source water. The Deuterium enrichment of short chain *n*-alkanes in aquatic primary producers to the environmental water ($\varepsilon_{alkane/water}$) is astonishingly constant from –158‰ to –160‰ and from –122‰ to –128‰ in long chain *n*-alkanes from the epicuticular leaf surface of higher plants. The δD values of *n*-alkanes from the aquatic and terrestrial palaeoenvironment has been used in this study to reconstruct the δD of water (δD_c) in the hydrological cycle of sediments from the Mesozoic to the Palaeozoic.

Methodological investigation of extraction and chromatographic separation methods gave an excellent stability and reproducibility for δD values of organic standards (weighed mean σ_1= ±5.2‰, n=234 triplicates) and three independent Posidonienschiefer (PS) extracts as an example of natural sediments (weighed mean of all *n*-alkanes = 6.8‰). In addition, the H_3^+-factor of 7.75 indicates a high stability of the analytical system.

Maturation processes significantly change the Deuterium content in the primary hydrogen bounding of *n*-alkanes and acyclic isoprenoids during burial. The PS of the Northern German Massif with its organic matter maturation influenced by a mafic intrusion and the Kupferschiefer (KS) of the Northern Polish Zechstein Basin (NPB) with a maturation gradient to burial depth were used for the first time to develop a maturity correction on the δD values of lipids in sediments.

The δD values of the extracted alkanes positively correlate with thermal maturity in the KS (y = 56‰ × MPI1(x)-160‰ [VSMOW]) and in the PS (y = 104‰ × MPI1(x)-200‰ [VSMOW]). Isotopic ratios of isoprenoids were more affected in the PS (y = 300‰ × MPI1(x)-415‰ [VSMOW]) than in the KS (y = 179‰ × MPI1(x)-341‰ [VSMOW]). Thermal methanogenesis, thermodynamic equilibration, and hydrogen exchange with sediment water could be rejected as a source for this Deuterium enrichment. Time-related increased Deuterium transfer to C-C bounds due to differences in activation energy is seen as one main factor for Deuterium enrichment. Additionally, chemical reactions of *n*-alkanes during maturation incorporating Deuterium depleted molecules would enrich remaining *n*-alkanes.

The maturity correlation of *n*-alkanes facilitates the reconstruction of the δD of water (δD_c) in Palaeozoic equatorial intermontane climate conditions of the Westphalian-Stephanian Saar-Nahe

Basin (SNB). The increase of the initial δD_c value of +15.6‰ of palaeolakewater in the intermontane Basin to +27.8‰ explains the transition to dryer conditions during the Permo-Carboniferous glaciation. The increase of δD_c values of –32.9‰ to –17.7‰ in meteoric waters from the Westphalian D to the Stephanian A indicates changes in airmass directions of the monsoon system during the Westphalian-Stephanian. Accordingly, the appearance of first dry resistant tree ferns and gymnosperms is recorded in the same type of sediments.

In contrast to sediments from the Saar-Nahe Basin, the Early Permian Lodève Basin (LB) sediments were deposited under semi-arid climate conditions show tightly connected δD_c values of aquatic and meteoric water of +11.1‰ and -0.4‰. This fits into a reconstructed riverbank depositional area with coupled source water connections between higher plants and primary producers.

At the base of the Early Zechstein, δD_c values of the KS Basin surface water have a W-E difference of –79‰ from the lagoon of the Lower Rhine subbasin (LRB) to the North East Polish KS Basin (NPB). The absolute δD_c value of surface water is -3.5‰ in the North East Polish Basin. Conclusively, the influence of arid hinterland in the western KS is recorded in the δD values with +20‰ in the LRB and of –20‰ to –40‰ in the freshwater of the eastern Pangean coast in the source area of the KS in Poland. The lagoonal deposition supports the very high Deuterium enrichment in the surface water of the lagoonal LRB.

During the Lower Toarcian in the Epeiric Sea of the Middle European PS large anoxic oceanic events enhanced organic matter deposition correspondent to the carbon isotope depletion in organic matter (OM) and ^{13}C enrichment in carbonates. Enhanced nutrient supply from freshwater of continental areas into the Posidonienschiefer Basin is reflected in the gradient of δD values from –8.2‰ in northern surface waters to +3.3‰ in the south.

In conclusion, the relationship of δD values of biomarkers to maturity allows the correction of the maturity influence and therefore the reconstruction of the evolution of primary biosynthesis. The comparison of the reconstructed δD value of water with similar recent environment shows that the reconstructions of changes in atmospheric circulation, properties of ocean currents and nutrient supply will help to understand and quantify the palaeoenvironmental and palaeoclimatic changes during earth history.

KURZFASSUNG

Das Wasserstoffisotopenverhältnis (δD) von kontinentalem Wasser wird durch die Abreicherung von Deuterium im Niederschlag während der Kondensation von Wasser und beim Durchzug über kontinentale Gebiete bestimmt. Die Primärproduzenten in aquatischen Systemen sowie Landpflanzen produzieren ein δD in synthetisierten organischen Komponenten, welches das primäre Isotopenverhältnis der Ursprungswässer widerspiegelt. Die Anreicherung des Deuteriums in kurzkettigen *n*-Alkanen aquatischer Primärproduzenten im Vergleich zum Wasser der sie umgebenden Umwelt ($\varepsilon_{alkane/water}$) mit –158‰ bis –160‰ ist erstaunlich konstant. In langkettigen *n*-Alkanen aus der Epikutikula von Blättern höherer Pflanzen ist dieser Abstand mit -122‰ bis -128‰ ebenfalls konstant. Die δD-Werte von *n*-Alkanen aus aquatischen und terrigenen Paläoumwelten wurden in der vorliegenden Arbeit verwendet, um das δD von Wasser (δD_c) im hydrologischen Kreislauf in Sedimenten bis in das Paläozoikum hinein zu rekonstruieren.

Methodische Untersuchungen von Extraktionsverfahren und chromatographischer Trennung von Substanzen ergaben eine exzellente Stabilität und Reproduzierbarkeit von δD-Werten organischer Standards (Mittelwert = ±5,2‰, n = 234 Dreifach-Messungen) und dreier unabhängig extrahierter Posidonienschiefer Proben (PS) als ein Beispiel für natürliche Proben (gewichtete mittlere Standardabweichung σ_1 für *n*-Alkane = 6.8‰). Zusätzlich hat das analytische Messsystem mit einem H_3^+-Faktor von 7,75 eine hohe Stabilität.

Durch Reifeprozesse in Sedimenten wird der Deuteriumgehalt in primär gebundenem Wasserstoff von *n*-Alkanen und azyklischen Alkanen (*i*-Alkane) signifikant verändert. Der durch eine magmatische Intrusion bzw. unterschiedliche Subsidenzraten gereifte PS des Norddeutschen Massivs und der mit einem graduellen Reifegradienten in der Ablagerungstiefe gereifte Kupferschiefer (KS) des nördlichen polnischen Zechstein Beckens (NPB) wurden verwendet, um erstmalig eine Korrektur zu entwickeln, die den Einfluss von thermischer Reife auf die δD-Werte von Lipiden in Sedimenten ermöglicht.

Die δD-Werte der extrahierten *n*-Alkane korrelieren positiv mit der thermischen Reife im KS (y = 56‰ × MPI1(x) – 160‰ [VSMOW]) und mit (y = 104‰ × MPI1(x) – 200‰ [VSMOW]) im PS. Isotopenverhältnisse von Isoprenoiden waren mehr beeinflusst mit (y = 179‰ × MPI1(x) – 341‰ [VSMOW]) im KS und (y = 300‰ × MPI1(x) – 415‰ [VSMOW]) im PS. Thermische Methanogenese, thermodynamische Gleichgewichtsreaktion und der Wasserstoffaustausch mit dem Sediment konnten als Ursache für diese Deuteriumanreicherung ausgeschlossen werden. Als ein Hauptfaktor für die

Deuteriumanreicherung in Kohlenwasserstoffen werden die Unterschiede in der Aktivierungsenergie gesehen, die zeitlich beeinflusst einen erhöhten Deuteriumübergang zu C-C-Bindungen vorantreiben. Zusätzlich wird dieser Prozess durch chemische Reaktionen gefördert, die während des Reifeprozesses an Deuterium abgereicherte Moleküle produzieren und somit die verbleibenden *n*-Alkane anreichern.

Die Korrelation von *n*-Alkanen zur Reife ermöglicht exemplarisch die Rekonstruktion des δD-Wertes von Wasser (δD_c) in Sedimenten des Saar-Nahe Beckens (SNB). Zur Zeit des Westphal / Stephans herrschten hier äquatoriale Klimabedingungen vor. Der Anstieg des δD_c-Wertes von +15,6‰ im Paläoseewasser des intermontanen Beckens auf +27,8‰ erklärt den Übergang zu trockenerem Klima während der permo-karbonischen Vereisung. Der Anstieg der δD_c-Werte von –32,9‰ auf –17,7‰ im meteorischen Wasser vom Westphal zum Stephan zeigt Veränderungen von atmosphärischen Strömungsrichtungen im Monsun-System während des Westphal-Stephans an. Gleichzeitig mit der Ablagerung der untersuchten Sedimente erschienen erstmals Gymnospermen in der Erdgeschichte.

Im Gegensatz zu den äquatorialen Bedingungen des SNB wurden die kontinentalen Beckensedimente im Lodève während des frühen Perms unter semi-ariden Klimabedingungen abgelagert. Die δD_c-Werte des OW mit +11,1‰ und des Wassers aus dem Stoffwechsel der höheren Pflanzen mit +0,4‰ liegen nah beeinander. Dies spiegelt die Situation in Flusstälern wider, in denen das Wasser der höheren Pflanzen und der aquatischen Primärproduzenten gleiche isotopische Signaturen zeigen.

Die KS Beckensedimente an der Basis des frühen Zechsteins weisen einen W-E-Unterschied der δD_c-Werte im marinen Oberflächenwasser auf, von +75‰ im Lagunenbereich des Niederrheinischen Kupferschiefer Beckens (LRB) bis zu –3,5‰ im nord-östlichen polnischen Kupferschiefer Becken. Der Einfluss des ariden Hinterlandes wird im westlichen LRB mit δD_c-Werten von +20‰ in kontinentalen Wässern widergespiegelt und mit –40‰ im Süßwasser an der Küste des zentralen, östlichen Pangea im Gebiet des NPB. Die hoch angereicherten Deuteriumgehalte im Wasser der Lagune bestätigen den starken ariden Einfluss des Hinterlandes gegenüber dem Oberflächenwasser im Westen des mitteleuropäischen KS Beckens.

Im Unteren Toarc akkumulierte viel organisches Material während weitreichender anoxischer Ereignisse im Meer des Posidonienschiefer-Beckens, einhergehend mit einer Abreicherung des schweren natürlichen Kohlenstoffisotopes (^{13}C) im organischen Material (OM) und einer ^{13}C Anreicherung in Karbonaten. Erhöhte Nährstoffzufuhr durch Süßwasser aus nahen kontinentalen

Gebieten zeigt sich im Unterschied der δD_c-Werte des marinen Oberflächenwassers von –8,2‰ im nördlichen Posidonienschiefer Becken bis zu +3,3‰ im Süden.

Die Korrelation der δD-Werte von Biomarkern mit der Reife ermöglicht die Korrektur des Reifeeinflusses und daher die Rekonstruktion der Evolution der Biosynthese von Substanzen und der δD_c-Werte von Wässern. Der Vergleich der δD_c-Werte von Paläowässern mit denen von rezenten Wässern hilft, die atmosphärische und ozeanische Zirkulation sowie die Nährstoffkreisläufe geologischer Zeitalter zu verstehen und damit Paläoumwelt und Paläoklima zu quantifizieren.

ABBREVIATIONS

The following list summarizes the abbreviations of terms and definitions mentioned in the text

ASE	**A**ccelerated **S**olvent **E**xtractor
BSTFA	**B**i**s**-**t**rime**t**hylsilyl-**t**ri**f**luor**a**mide ($C_8H_{18}F_3NOSi_2$)
C_{org}	**O**rganic **C**arbon
$\delta^{13}C$	Carbon isotope ratio
$\delta^{13}C_{org}$	Carbon isotope ratio of bulk organic matter
δD	Hydrogen isotope ratio
$\delta^{15}N$	Nitrogen isotope ratio
$\delta^{18}O$	Oxygen isotope ratio
D	**D**euterium
DB	**D**öhlen **B**asin
EA	**E**lemental **A**nalyzer
EA-IRMS	**E**lemental **A**nalyzer **I**sotope **r**atio **m**ass **s**pectrometry
GC	**G**as**c**hromatograph
GC/MS-IRMS	Individual Organic compounds separated by **g**as **c**hromatography and simultaneously measured for organic **m**ass **s**pectrometry and **i**sotope **r**atio **m**ass **s**pectrometry
GC-AED	**G**as**c**hromatograph coupled to an **A**tomic **E**mission **D**etector
IRMS	**I**sotope **R**atio **M**ass **S**pectrometry
KS	**K**upfer**s**chiefer
LB	**L**odève **B**asin
LRB	**L**ower **R**hine Kupferschiefer **B**asin
MS	**M**ass **S**pectrometer
$NADPH+H^+$	Hydrated **N**icotinacid-amide-**a**denin-**d**inucleotid-**p**hosphate
NGB	**N**orthern **G**erman Posidonienschiefer **B**asin
NPB	**N**orth East **P**olish Kupferschiefer **B**asin
OM	**O**rganic **M**atter
PS	**P**osidonien**s**chiefer
SGB	**S**outhern **G**erman Posidonienschiefer **B**asin
SNB	**S**aar-**N**ahe **B**asin
SPE	**S**olid **P**hase **E**xtraction
C_{tot}	**T**otal inorganic and organic **C**arbon
TOC	**T**otal **O**rganic **C**arbon

TN	**T**otal inorganic and organic **N**itrogen
TG	**T**hermo **G**ravimetric Analyzer
TGA	**T**hermo **G**ravimetric **A**nalysis
TC	**T**hermo **C**onversion
TC-IRMS	**T**hermal **C**onversion **i**sotope **r**atio mass **s**pectrometry
MEP	1-Deoxy-D-xylulose-5-phosphate/2 *C*-**M**ethyl**e**rythritol **p**athway)
Units	
1 bar	0.1 Mega Pascal
0 °C	273.15 K

1 Introduction

To reconstruct the palaeotemperature of the atmosphere and the trajectories of atmospheric circulation the hydrogen and oxygen isotope ratio of water in ice from glaciers and ice sheets are generally used. In marine sediments the information comes from the oxygen isotope ratio of carbonaceous shells, additionally serving the palaeotemperature of water (EREZ and LUZ, 1983; MCCREA, 1950; SPERO et al., 1997). However, in non-carbonaceous sediments at former geological timescales with no preservation of the primary source water the hydrogen isotope ratio of organic matter or clay minerals can serve as a quantitative proxy for palaeoclimate reconstruction (YEH, 1980). Recent results indicate that the hydrogen isotope ratio of the water used during biosynthesis is directly preserved in the compound specific hydrogen isotope ratio of biomarkers in sediments (HUANG et al., 2004; SACHSE et al., 2004b).

To understand the fractionation steps, which are involved in the reconstruction of δD values of source water chapter 2 is exclusively reserved for the hydrogen isotope fractionation in the biosphere. The uncertainties of compound specific hydrogen isotope analysis are addressed in chapter 3 under Sediments and Methods. To be able to reconstruct the δD_c values of source water in Palaeozoic and Mesozoic sediments in chapter 5, at first the effects and possible corrections of the influence of maturation on the natural hydrogen isotope ratio of *n*-alkanes and acyclic isoprenoids have to be evaluated in chapter 4.

This offers the possibility to have one proxy for palaeoclimate reconstructions for all types of environmental samples. However, the maturation of organic matter during burial might potentially change this primary hydrogen isotope ratio and limit the use of the new proxy to earlier timescales. Therefore this work investigates whether the use of compound specific isotope ratios of biomarkers can be extended to the geological past.

2 Fractionation of water isotopes in the environment

2.1 Fractionation of water isotopes in the climate system

Evaporation of water determines the hydrogen isotope content of the vapor phase relative to the liquid source (GAT, 1996). Consequently, water in world oceans is more enriched in Deuterium and ^{18}O and remaining water vapor of clouds is depleted after rainout events.

This isotope fractionation depends on physical parameters and results into an average global relationship of the hydrogen and oxygen isotope content of precipitation (Global meteoric water line, GMWL; $\delta D = 8 \times \delta^{18}O + 10$, (CRAIG, 1961)). Mainly temperature and humidity determine the isotope fractionation (DANSGAARD, 1964; GAT and BOWSER, 1991; MAJOUBE, 1971; MERLIVAT, 1978; MERLIVAT and JOUZEL, 1979). The slope and the interception (deuterium excess) of this relation differ regionally and important information for the local meteoric situation in a specific region (Local meteoric water line) can be elaborated.

Mainly, Rayleigh fractionation increases the isotopically lighter isotope in vapor traveling over the continents and continental precipitation is depleted in Deuterium relative to coastal precipitation (*continental effect*, Figure 2.1). Other effects explain the deviation of the isotope signal of precipitation, which would be expected from the Rayleigh fractionation. A similar isotope effect is introduced by temperature related fractionation as known from global latitudinal distribution of isotopic ratios in precipitation (*latitude effect*) and in precipitation over topographical heights (GONFIANTINI et al., 2001) (*altitude effect*). In tropical areas the recycling of larger water masses enhances the enrichment of the heavier isotope in the source water due to evaporation (*amount effect*) (INGRAHAM and TAYLOR, 1986).

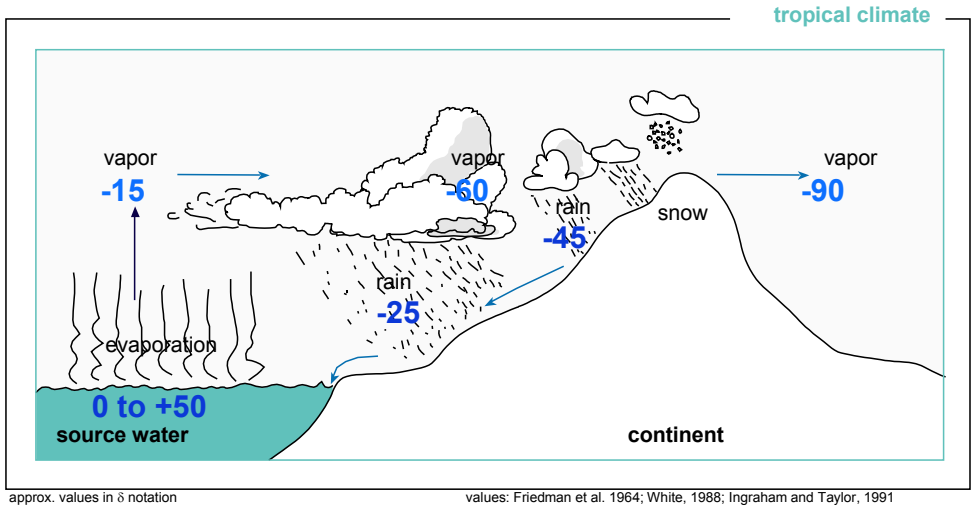

Figure 2.1. Deuterium enrichment during rainout over the continent in the tropics. (FRIEDMAN et al., 1964; INGRAHAM and TAYLOR, 1991; WHITE, 1988)

2.2 Fractionation of hydrogen in the biosynthesis of plant biomass

Physical and biosynthetic fractionations determine the δD value of biomarkers in plants. These fractionations influence the δD values of biomarkers before their preservation in sediments. Firstly, the δD value of leaf water reflects the δD value of precipitation under equilibrium conditions during transpiration. (ALLISON et al., 1985; LUO and STERNBERG, 1992; RODEN and EHLERINGER, 1999; WALKER et al., 1989). Consequently, the plant organic matter also reflects the isotopic signal of precipitation and supports Deuterium being a tracer for palaeoclimate reconstructions. However, the "peclet" effect enriches in the transpiration process the heavy water isotope in the leaf water and consequently biosynthesis of biomass starts using a heavier water pool (BARBOUR et al., 2004; RODEN et al., 2000). The different latitudinal distribution of plant associations (i.e. gymnosperms vs. angiosperms) should influence the δD value of biomarkers due to their different transpiration processes (CHIKARAISHI and NARAOKA, 2003). In Europe the plants associations change from mainly gymnosperms in the north, broad-leaved in the middle, to hard-leaved, evergreen plants in the south. The effect of the transpiration process from different plant associations on the δD value of biomarkers from higher plants is not recorded over such a latitudinal gradient (HUANG et al., 2002; SACHSE et al., 2004a). It is more reflected by a constant fractionation of the lipids to the source water, i.e precipitation, of the higher plants.

First investigations of hydrogen isotope fractionation in biomass compared to the δD value of environmental water started with the determination of δD values from bulk organic biomass (LUO and STERNBERG, 1991; NISSENBAUM, 1972; RUNDEL et al., 1979; SMITH and ZIEGLER, 1990; STERNBERG et al., 1984; ZIEGLER et al., 1976). Discriminations against Deuterium in the biomass were attributed to differences in the photosynthetic mechanism (i.e. C3, C4, CAM), environmental factors like evapotranspiration effects or simply differences in growth and age of the biomass, and synthesis of compound classes in different cellular compartments.

First differences in δD values of CAM and C_3 plant biomass were found comparing the δD values of nitrate cellulose to the Deuterium depleted lipid fraction (STERNBERG et al., 1984). In contrast to the influence of photosynthetic mechanisms in carbon isotope fractionation, the evapotranspiration was attributed as a factor for isotope enrichment in C_4 plants (LUO et al., 1991; ZIEGLER et al., 1976). Later the differences of δD values in C3, C4 and CAM plant biomass were related to the use of different cellular water pools during synthesis (SMITH and ZIEGLER, 1990; ZIEGLER, 1989) in addition to differences in intercellular biosynthesis of compounds (STERNBERG and DENIRO, 1983).

To explain the influence of Deuterium depletion in compounds versus the source water the first fractionation step seems to exist in the formation of $NADPH+H^+$ (–600‰) during

photoreduction to produce highly depleted H ions (CHIKARIAISHI et al., 2004; LUO et al., 1991; SESSIONS et al., 1999). Lipids are 120‰ more depleted in Deuterium as carbohydrates. In a simplified view, SCHMIDT (2003) add to the $NADPH+H^+$ (–250‰) the reduced form of FAD (–350‰) as possible sources for depleted deuterium addition during fatty acid synthesis. Additionally, the isotope ratios of compounds and reductants must be different in distinct compartments. It must be assumed that the H^+ source in the $NADPH+H^+$ of the pentose phosphate cycle is distinct from the H^+ source in $NADPH+H^+$ during photoreduction in the photo system of the plant cell. This explains that the isotope discriminations in compounds are dependent on the pool size, metabolic fluxes and branchings of products, and the origin of the reduction equivalents.

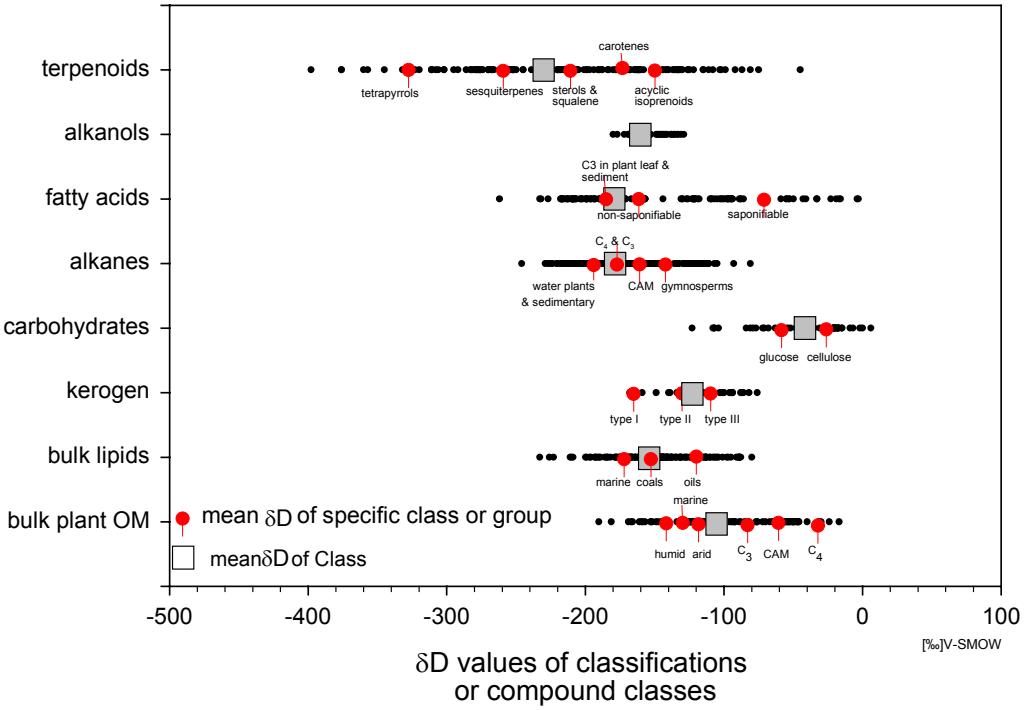

Figure 2.2. General distribution of hydrogen isotope signal of different organic matter of plants and sediments in nature. Sources: bulk plant OM: (MEDINA et al., 1991; SMITH and EPSTEIN, 1970; STERNBERG and DENIRO, 1983); (ESTEP and HOERING, 1980; RUNDEL et al., 1979; STILLER and NISSENBAUM, 1980), bulk lipids: (ESTEP, 1984; QUANDT et al., 1977; SCHIEGL and VOGEL, 1970; STERNBERG, 1988; STERNBERG et al., 1986) (RUNDEL et al., 1979; SCHIEGL, 1972), kerogen: (HASSAN and SPALDING, 2001; REDDING et al., 1980; SMITH et al., 1983), carbohydrates: (STERNBERG, 1988; ZHANG et al., 2002), *n*-alkanes: (CHIKARAISHI and NARAOKA, 2003; CHIKARIAISHI et al., 2004; DAWSON et al., 2004; ESTEP and HOERING, 1980; LI et al., 2001; SESSIONS et al., 1999; YANG and HUANG, 2003), fatty acids: (DOSSANTOS et al., 1996; ESTEP and HOERING, 1980; SESSIONS et al., 1999; SESSIONS et al., 2002), alkanols: (CHIKARIAISHI et al., 2004; ESTEP and HOERING, 1980; SESSIONS et al., 1999), Terpenoids: (CHIKARIAISHI et al., 2004; ESTEP and HOERING, 1980; LI et al., 2001; SESSIONS et al., 1999; SESSIONS et al., 2002; STERNBERG, 1988)

As two main compound classes lipid molecules are synthesized by acetogenic pathway in the cytosol and isoprenoids are produced in the cytosol via MVA pathway or in plastids via MEP pathway (LANGE and CROTEAU, 1999; LICHTENTHALER et al., 1997; SCHWENDER et al., 1996). The metabolism during biosynthesis of these compounds, the pool sizes and involved isotope discrimination of reactants seem to label the biosynthetic origin of lipids and isoprenoids (Figure 2.1) (CHIKARIAISHI and NARAOKA, 2005; CHIKARIAISHI et al., 2004; HAYES, 2001; SCHMIDT,

2003; SCHMIDT et al., 2003; SESSIONS et al., 1999; SESSIONS et al., 2002; SMITH and EPSTEIN, 1970). MVA-Isoprenoids and acetogenic lipids are more enriched in Deuterium compared to MEP-isoprenoids. Organisms exist in which only one of the pathways exists to produce isoprenoids or the metabolism of a specific isoprenoid class is genetically related to one of the pathways. Consequently, the evaluation of significant isotope fractionation or enrichment factors in recent biomass promotes the ability to reconstruct the biomass source of compounds in sediments and to step forward to elucidate the evolution of pathways in the past.

3 Sediments and Methods

3.1 Sediment samples and stratigraphic framework

The sample distribution of this study is part of the stratigraphic distribution for samples set up for the priority program SPP 1054 “Evolution des Systemes Erde während des jüngeren Paläozoikums im Spiegel der Sediment-Geochemie” of the German Science foundation. From 40 samples only 11 samples plus 8 already extracted samples from the North East Polish Kupferschiefer Basin (NPB) had a sufficient amount of compounds (>300 ng alkane / compound) for compound specific analysis. The number of samples from the Palaeozoic with high hydrocarbon contents is restricted and it is difficult to get not-weathered borehole or outcrop samples (Table 3.1). Hence, the selection of samples was focused on climate transitions in the Permo-Carboniferous icehouse and greenhouse conditions and to sedimentary sections with different sediment burial and organic matter maturation. Posidonienschiefer (PS) of the Northern German Posidonienschiefer Basin (NGB) and Kupferschiefer (KS) of the North East Polish Kupferschiefer Basin (NPB).

A warming phase (Westphalian / Stephanian) in the Permo-Carboniferous might have affected the tropical climate system. Saar-Nahe Basin (SNB) samples of the Westphalian / Stephanian transition were taken together with samples from the supposedly more humid Gzhelian / Asselian Döhlen Basin and the Gzhelian / Artinskian Lodève Basin (LB) to investigate possible effects on the equatorial eastern Euramerican climate system over a large area. NPB and NGB samples were used to be able to investigate the effect of maturation on the organic matter in sediments. Besides this main focus both sediments represent relative short time sedimentation with major climatic and carbon cycle distortions. The δD_c values of surface water mass properties were exemplarily reconstructed for the KS basin area of the Lower Rhine Kupferschiefer Basin (LRB) and the PS Basin area of the Southern German Posidonienschiefer Basin (SGB) to evaluate differences within the sub-basins of the two basins.

Samples were classified after the stratigraphic table of the German stratigraphic commission (GERMAN-STRATIGRAPHIC-COMMISSION, 2002) and applied to the IUGS stratigraphic table (IUGS, 2002) to be able to correlate with other sediments (GERMAN-STRATIGRAPHIC-COMMISSION, 2002; IUGS, 2002). Core samples from the SNB were taken from the Wemmetsweiler core with clay-rich coals and coals (R^{25}7915, H^{54}7262) from the Westphalian D (928 m to 947 m) to the lower Stephanian A (820 m to 810 m) including the Eilert and Waldwiese coal seam and assumingly the Leia VII horizon. Samples from the Stephanian A of the Bilsdorf and Hirzweiler cores are connected stratigraphically to the top of Wemmetsweiler core. All cores were correlated according to depth profiles of in all cores appearing coal seams.

Similar accumulation rates were assumed. The Bilsdorf core (R^{25}6525, H^{54}5542 1675 m to 1665 m) and the top Hirzweiler core (R^{25}7537, H^{54}7045; 925 m to 927m) shall give information about lateral facies differences and possible regional changes in the isotope ratios of sediments. They belong to the top of the Westphalian / Stephanian boundary, which is represented by the Holzer Conglomerates in the area of the Saarbrückener Hauptsattel.

Table 3.1. Investigated samples in this study. Posidonienschiefer (NGB: (LITTKE, 1993), U. Mann, pers. commun.), SGB: (RÖHL et al., 2001a); KS (OSZCZEPALSKI and RYDZEWSKI, 1987; VAUGHAN et al., 1989; WEDEPOHL, 1964), Lodève Basin und St. Afrique Basin (BROUTIN et al., 1994; COGNE et al., 1990; COGNE et al., 1993), Döhlen Basin (SCHNEIDER et al., 1999), Upper Carboniferous (STOLLHOFEN, 1999), boundary of Stephan A / Stephan B (MENNING et al., 2001), boundary Westphal / Stephanian (BURGER et al., 1997), boundary Westphalian C / Westphalian D (Seam B & claystone D).

location	*serie* / era	stage	*group* / stage	lithology	formation (name)	country	boreholes / outcrop
	global		regional				
Southern German Basin	*L. Jurassic*	L. Toarcian	Lower Toarcian	black shale	(Posidonienschiefer) (PS)	**Germany**	Dotternhausen
Northern German Basin	*L. Jurassic*	L. Toarcian	Lower Toarcian	black shale	(PS)	**Germany**	Rheinberg
Vlotho Massif	*L. Jurassic*	L. Toarcian	Lower Toarcian	black shale	(PS)	**Germany**	Wenzen / Wickensen / Dohnsen / Hadessen
Lower Rhine Basin	*U. Permian* / Guadalupian	Wuchiapingian	*Zechstein* / Thuringian	shallow marine	(Kupferschiefer) (KS)	**Germany**	Richelsdorf
NE Polish Basin	*U. Permian* / Guadalupian	Wuchiapingian	*Zechstein* / Thuringian	marine	(KS)	**Poland**	different boreholes
Lodève Basin	*L. Permian* / Cisuralian	Gzhelian to Asselian	*Rotliegend* / Autun	black shale / plant remains	Usclas St.-Privat, Tuilieres Loiras	**SE-France**	outcrop
Döhlen Basin	*L. Permian* Cisuralian	Sakmar / Asselian	*Rotliegend* / Autun	sapropelite / coal / silt to organic rich clay-like	Niederhäslich / Döhlen	**Germany**	Schweinsdorf / Freital-Zauckerrode / Gittersee / Niederpesterwitz
Saar-Nahe Basin	*U. Carboniferous*	Kasimovian	*Stephanian* / Stephan A	coal / coal bearing clay	Göttelborn-/ Dilsburg	**Germany**	Hirzweiler / Bilsdorf / Wemmetsweiler
Saar-Nahe Basin	*U. Carboniferous*	Moskovian	*Westphalian* Westphalian D	coal	Geisheck / Heiligenwald / Luisenthal	**Germany**	Hirzweiler / Bilsdorf / Wemmetsweiler

Both Kupferschiefer samples, the samples of the NPB and the LRB, were extracted samples by A. Bechtel, L. Schwark and kindly provided S. Oszczepalski for measurement. The NPB are taken from the barren zone of the KS. Geochemical information about the NPB samples is published in (BECHTEL et al., 2000a). The LRB sample is also from the barren zone and taken from the Richelsdorf coal mine. The PS samples of the Vlotho Massif were assembled at core depository at the FZ Jülich, Germany. Samples are from the Wenzen (56 m from surface), Wickensen (66 m), Dohnsen (82 m), Hadessen (75 m) cores. The PS sample from the Dotternhausen quarry is directly sampled from carbonaceous black shale located directly under the first carbonate bank (falciferum zone, see (RÖHL et al., 2001a).

3.2 Sample preparation for bulk and compound specific analysis

3.2.1 Sample preparation

37 sediments were investigated to characterize their differences in terrestrial and aquatic palaeoenvironmental and palaeoclimatic history using compound specific hydrogen isotope analysis. After homogenization by grinding under low temperature in a Retsch S 100 ball mill samples were freeze-dried and stored in glass bottles under vacuum to avoid contamination and aerobe biodegradation. All glassware for organic solvent extraction and sample storage has been acid treated and heated to 500 °C before analysis to remove contaminates.

3.2.2 Extraction method

1L bottles of research grade organic solvents (*n*-hexane, chloroform, dichlormethane, methanol) were used for extraction (VWR International GmbH, Darmstadt, Germany). The batch of contaminant-free solvents was tested continuously in the GC-AED system.

Soxhlet extraction

20 g to 30 g of samples were extracted in a 300 ml Soxhlet apparatus (VWR International GmbH, Darmstadt, Germany) with 500 ml beaker for distillation. Extraction thimbles were pre-cleaned with the same organic solvents used for extraction. The soxhlet distillation with chloroform / methanol mixture (v:v, 9:1) for 72 h yielded the extractable bituminous fraction. Added HCl activated copper removed the elementary sulfur in the sample.

Accelerated solvent extraction

PS samples from the Vlotho Massif were extracted in an accelerated solvent extractor (ASE 200, Dionex, Idstein, Germany). Additionally a homogenized PS (Dotternhausen, Germany) will serve as a new working reference sample for compound-specific hydrogen analysis. For this a fast solvent extraction is attained. The extraction method was optimized at 100 °C for 30 min. under pressurized nitrogen (3.8 MPa). 60% of a 33 ml sample vial volume were filled with sample and extracted with a ~20 ml Dichlormethanol / Methanol mixture (9:1 v / v). Added HCl activated copper removed the elementary sulfur in the sample.

Flash chromatography

After filtration the bituminous fraction of soxhlet and ASE extracts was separated in a rotary evaporator (Büchi Labortechnik AG, Flawil, Switzerland) from the organic solvent. Using flash-chromatography (borosilicate flash chromatographic column with glass frite, 40 cm long, i.d.1 cm^2; QVF Labortechnik, Ilmenau, Germany) under 0.5 bar N_2 the bituminous extract was separated into the saturated hydrocarbon fraction (45 ml hexane), aromatic hydrocarbon fraction (35 ml chloroform) and heterocomponents fraction (N, S, O components) (40 ml methanol). The

stationary phase, 16 cm^3 of silica gel (KG 60, 0.040-0.063 meshsize, VWR International GmbH, Darmstadt, Germany), was heated at 170 °C and conditioned with *n*-hexane under 0.5 bar N_2 pressure in the glass column. The bituminous extract was adsorbed on a mixture of silica gel and acid-treated, preheated sand, before filled into the 1cm hexane supernatant. Yielded fractions were again evaporated in a rotary evaporator and filled into pre-clean 5 ml glass vials capped with Teflon. Before analysis all extracts were stored in freezer at –18°C.

3.2.3 Chemical treatment to reduce sample matrix

In gas chromatography peaks unresolved baseline separation, co-elution of peaks and matrix effects often prevent proper peak analysis. Quantification and isotope ratio determination of those compounds results in wrong values and have to be omitted. However, different chemical treatment with selective chemical degradation, silver nitrate adduction, polarity separation (SPE) or size separation by molecular sieves are possible to reduce these effects (ELLIS and FINCANNON, 1998). For chemical degradation remaining isotope ratios of the compound can depend on the intra-molecular distribution of isotopes in the molecule. Isotope fractionation by polarity separation and adduction techniques may be rather low because of the complete transfer of compounds during solvent elution. Aromatic and aliphatic standards were tested for the influence of urea adduction and chemical degradation by comparing the δD values of pretreated and post-treated standards.

Silica gel chromatography-urea adduction

Saturated aliphatic compounds can be isolated from the unsaturated aliphatic fraction after solvent extraction by elution of the not separated aliphatics through a 10 ml clean glass pipette packed with glass fiber at the tip and 4 g silicate gel conditioned with 8 ml of $AgNO_3$ solution (40 g of $AgNO_3$ in 300 ml $C_2H_4O_2$, 100 ml distilled H_20). The problem of the elution with hexane is the reduction of the low chained *n*-C_{16} to *n*-C_{18} alkanes (BARRICK et al., 1980).

Chemical degradation (Rutheniumoxide oxidation)

The selective chemical degradation of alkenes is of common usage to remove interfering aromatic hydrocarbons (hopanoids, hopanes, hopenes) for 14C-AMS measurements of bulk and individual aliphatic hydrocarbons (HUANG et al., 1996; PEARSON and EGLINTON, 2000). Additionally this artificial oxidation of kerogen was chosen to obtain its individual and polymeric linked alkyl compounds (BOUCHER et al., 1991; STANDEN et al., 1991). Fresh RuO_4 solution is prepared in a separatory funnel by dissolving 10 mg of RuO_2 in·10 ml de-ionized H_2O. 6 ml of CCl_4 was added with 50 ml of $NaIO_4$ as catalyzing re-oxidant to oxidize the RuO_2 solution and shaken rigorously for 5 min. before mixing it with the hydrocarbon fraction. The mixture will be dried under N_2 stream until a bright yellowish color of the RuO_4 is persisting.

5 mg of reaction products were extracted with Hexane in a silica-packed glass column to elute the saturated hydrocarbons. The yield of the saturated hydrocarbons were filtered in 0.45 Millipore filter to remove carried ruthenium tetroxide particles. Different aromatic and aliphatic standards are used for evaluating the effect of chemical degradation of hetero components (N, S, O) bounded to and within the ring of an aromatic compound.

3.3 Elemental analysis - organic C, N, S and inorganic C

3.3.1 Elemental analysis of C, N, S

The elemental analysis of organic and inorganic C, S, N has been performed in an elemental analyzer vario EL for C, H, N, S, O and for C and N only with vario MAX CN (both Elementar Analysensysteme GmbH, 63452 Hanau, Germany).
In a tin foil an amount of 20 mg to 200 mg bulk sediment (depending on the amount of C) was combusted with O_2 and WO_3 as catalysts at 1150 °C in a vario EL elemental analyzer to CO_2, H_2O, NO_x and SO_3/SO_2. Reduction to remaining reaction gases (CO_2, H_2O, N_2, SO_2) was reached with elemental Cu at 830 °C in a reduction tube. Quantitative elemental detection with thermal conductivity was enabled by adsorption of the reaction gases. Simultaneous C/N analysis is applied with vario MAX CN. Main methodological differences exist in sample supply to the analytical system via Al_2O_3 shuttle and constant purge with O_2, which enhances the sample per time ratio and amount of sample. Additionally, after combustion with O_2 remaining gaseous carbon compounds are oxidized with CuO and Pt as catalyzing reagent at 900 °C. Reduction is applied with W at 830 °C as reductive reagent. Analysis is reduced to C and N, which are available for detection by adsorption. Each analysis is done by triplicate and inter-laboratory standardization.

3.3.2 Determination of the inorganic carbon and organic carbon

The organic carbon fraction (TOC) of the total carbon (C_{tot}) was determined by removal of the total inorganic carbon fraction (TIC). At first, the total carbon content of the sediment has to be detected. Additionally, the carbonaceous carbon dioxide was extracted with 1 M HCl solution. After complete CO_2 extraction the remaining sediment has been neutralized to pH 7 with deionized water and the TOC can be quantified via elemental analysis. The amount of TIC can be derived from the subtraction of TOC from the total amount of carbon in the sediment (differential method, Equation 3.1).

$$TIC[\%] = C_{tot}[\%] - TOC[\%] \qquad \text{Equation 3.1}$$

3.4 Elemental analysis of individual compounds (C, N, H, Si)

For elemental analysis of individual compounds (C, H, Si, N) an atomic emission detector (HP G 2350 Agilent Technologies, Palo Alto, USA) was coupled to a gas chromatograph (HP 6890, Agilent Technologies, Palo Alto, USA). To separate compounds in a gas chromatographic column. (HP1-MS, 0.32 mm i.d., 0.17 µm thickness, 25 m) the column was heated with a 15°C / min. temperature gradient to 325 °C and isothermally held for 25 min.. Prior to separation compounds were injected at a temperature of 80 °C (1 min. holding time) and transferred at a 1 / 10 to 1 / 5 split rate according to the concentration of substances. Compounds are transferred to the detector at 300 °C, by spark emission they are vaporized and excited in a microwave induced plasma to a high energy level, which is formed after ignition and ionization with the mass specific reaction gases. Element specific emission spectra are produced after the atoms are decaying back to lower energy levels. The elemental composition of the organic compound can be quantified simultaneously when the spectral atomic lines are passing through a diffraction grid into a polychromator composed of a photodiode array.
Different simultaneous element detection was applied within these combinations: C (193 nm), N (174 nm), S (101 nm); C (248 nm), Si (252 nm) and C (496 nm) and H (486 nm). In parentheses the specific emission wavelength for detection of the atoms is indicated. All detections were used for qualitative analysis. The organic C, N, S and H composition were investigated in order to confirm the elemental composition of the organic mass spectrometric chromatograms, for approximation of the amount of hydrogen in compound specific hydrogen analysis and to assure purity of organic solvents.

3.5 Isotope ratio mass spectrometry

To determine the isotopic natural abundance of lower mass elements a sector-field isotope ratio mass spectrometer (IRMS) is used (Figure 3.1). Prior to electronic impact ionization (70 eV to 110 eV) of the gaseous molecule in the ion source of the mass spectrometer, the organic or inorganic sample has to be transfered via oxidising and other physical and chemical reactions to a gas phase (BRAND, 2004). The preparation of a sample gas from a single component is possible under a continuous carrier gas flow with He, namely “continuous flow system”. After ionization the gaseous ions are then deflected by a stable magnetic field with a static permanent magnet according to their mass to charge ratio and kinetic energy (WIESER and BRAND, 2000). By either changes of the accelerating electronic potential field of the ion source or of the magnetic field strength the mass-dependent ion beam path of different ions is focused simultaneous into a multiple Faraday cup detector system. Therefore, at the same time different isotope abundances

can be read and in each collector the mass dependent ion current is converted into an analog electronic signal.

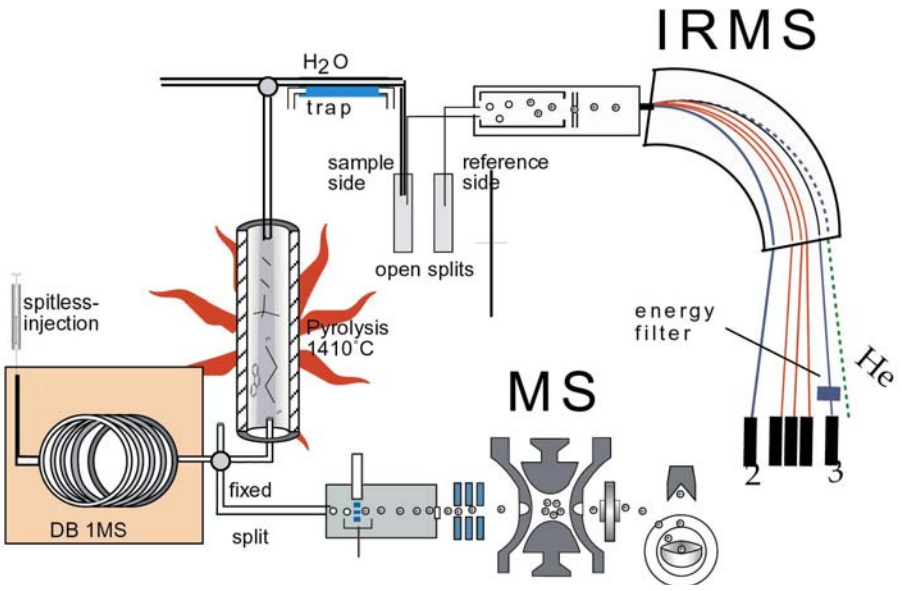

Figure 3.1. Schematics for hydrogen gas isotope ratio monitoring and simultaneous organic mass spectroscopy of organic compounds.

For sample gas transfer from organic compounds an IRMS system is used with a constant diluted He flow (i.e. Continuous Flow Mode). The sample / standard gases are separately diluted with additional Helium (1 / 10) in an open-split device. The separation in two open split systems allows the injection of a working standard gas to be able do referencing of the sample isotope ratio against the international scale.

To measure the $\delta^{13}C$ value of standards an elemental analyzer coupled to an IRMS was used (EA-IRMS). For the δD of standards a pyrolysis reactor coupled to an IRMS was used (TC-IRMS). In comparison to the compound-specific analysis the principle of conversion to sample gas is the same. For compound specific carbon isotope analysis the sample will be combusted to CO_2 by CuO and Pt, Ni as catalysts at 940 °C. Interfering N_2O has to be reduced in the sample gas flow by downstream reduction in a reduction furnace (Cu) at 640 °C. CO_2 and N_2 were generated by chromatography in an elemental analyzer (see section elemental analyzer). Organic compounds will be converted to H_2 sample gas by pyrolysis (TC= thermal conversion) in an empty Al_2O_3 ceramic tube at 1400 °C to 1450 °C in the TC-IRMS and the GC-TC-IRMS system.

3.5.1 Referencing strategy for gas isotope ratios

For isotope abundance measurements the *absolute* isotope abundance of isotopomers is mandatory but a higher precision is achieved by using the difference between to samples. This *relative* isotope abundance (δ notation, Equation 3.2) becomes important for normalization of the sample isotopic ratio and smaller errors due to its availability for comparison with international and inter- / intralaboratorial standard materials.

$$\delta\,{}^{\text{'heavy isotope'}}\text{value'in}\left[‰\right] \equiv \frac{R_{sample} - R_{standard}}{R_{standard}} \times 1000 \qquad \text{Equation 3.2}$$

where R is the elemental ratio between the heavier and the lighter isotope. Which generally means that the heavier isotope is less abundant than its lighter isotope and for ease of use, a notation of the relative isotopic abundance in permil is generally accepted.

3.5.1.1 *Hydrogen, carbon, nitrogen isotope referencing*

For isotope standardization the generally accepted isotope reference standards for hydrogen, carbon, nitrogen and oxygen isotope ratios data were used (Table 3.2) (ROSMAN and TAYLOR, 1997; WERNER and BRAND, 2001). Normalized δ values of compounds in this work are reported as VSMOW for hydrogen, VPDB for carbon and Air-N_2 for nitrogen according to the IAEA guidline using available reference materials (COPLEN, 1996).

Table 3.2. Absolute isotope abundance of international standards.

element	abundance of light reference isotope Atom [%]	stable isotope	abundance of heavy reference isotope Atom [%]	International scale (Reference material)
^{1}H	99.984426	^{2}H	0.01557	VSMOW (VSMOW)
^{12}C	98.892200	^{13}C	1.10780	VPDB (NBS 19)
^{14}N	99.633700	^{15}N	0.36630	AIR-N_2 (Air)
^{16}O	99.762800	^{18}O	0.20004	VSMOW (VSMOW)

Carbon

The $\delta^{13}C$ value of inorganic and organic solid material and gases are determined after conversion of the compounds to CO_2 gas. CO_2 constitutes different isotopes, which are detected by their molecular ion currents (44: [$^{12}CO^{16}O^{16}$], 45: [$^{13}C^{16}O_2$], [$^{12}C^{16}O^{17}O$], 46: [$^{12}C^{18}O^{16}O$] [$^{13}C^{17}O^{16}O$] [$^{12}C^{17}O^{17}O$]). In addition, the calculation of the ion current mass ratios (Equation 3.3) follows the partial pressure of the ion constituents in the gas:

$$\frac{I_{45}}{I_{44}} = \frac{c45}{c44} \times {}^{45}Rm\,, \quad \frac{I_{46}}{I_{44}} = \frac{c46}{c44} \times {}^{46}Rm \qquad \text{Equation 3.3}$$

where coefficient *c* is proportional to the partial pressure of the ion current constituents in the ion source; *Rm* is the ratio of the isotope containing CO_2 concentration. According to low ionization efficiency *c* cannot be excluded from the equation. Therefore, the sample isotope ratio has to be referred to a working standard isotope ratio to eliminate the efficiency factors. Further calibration is achieved by calibrating the working standard via repeated measurement against the international standard using a multiple correction of the measured ratios (Equation 3.4) of the reference gas and the sample gas against their calibrated ratios.

$$\frac{R_s^c}{R_s^m} = \frac{R_w^c}{R_w^m} \qquad \text{Equation 3.4}$$

where *m* = measured ratio, *c* calibrated ratio against *w* =working, *s* = sample. Furthermore to report the elemental isotope ratios (i.e. $^{13}C/^{12}C$) in this study the ion correction has to be adopted to solve for the three unknowns ($^{13}C/^{12}C$, $^{17}O/^{16}O$, $^{18}O/^{16}O$) from the molecular ^{45}R and ^{46}R ratios (SANTROCK et al., 1985).

Hydrogen isotope ratios and H_3^+ factor

An isotopic mass interference for the mass 3 complicates the δD determination of hydrogen containing compounds. An ion molecular reaction in the ion source combines the molecular H_2 gas with H_2^+ to form ·H and a H_3^+ ion that also has the mass 3 like the low abundant HD^+ ion (Equation 3.5). Consequently, following hydrogen isotopic compositions are respective components for the hydrogen gas.

$$I_2 = c_2\left[H_2^+\right]$$
$$I_3 = c_3\left[HD^+ + H_3^+\right] \qquad \text{Equation 3.5}$$

Whereas the electron impact generates HD^+ and H_2^+ ions, which are dependent on the hydrogen partial pressure, the contribution of H_3^+ is proportional to the square root of the hydrogen gas partial pressure in a two-component system (H_2 and H_2^+, Equation 3.6):

$$\frac{i3}{i2} = \frac{c_3\left[\mathrm{HD}^+\right] + c_3\left[\mathrm{H}_3^+\right]}{c_2\left[\mathrm{H}_2^+\right]^2} \qquad \text{Equation 3.6}$$

The H_3^+ ion contribution is determined with the extrapolation of the pressure dependent H_3^+ ion gradient (tan α) to the zero-point value. The H_3^+ factor (k, [1 / mA]) can be determined (Equation 3.7):

$$c_3\left[H_3^+\right] = \left(c_2\left[H_2^+\right]\right)^2 \times \tan\alpha \rightarrow \frac{i3}{i2} = \frac{c_3\left[HD^+\right] + \left(c_2\left[H_2^+\right]\right)^2 \times \tan\alpha}{c_2\left[H_2^+\right]}$$

Equation 3.7

$$= \frac{c_3\left[HD^+\right] + k\left(c_2\left[H_2^+\right]\right)^2}{c_2\left[H_2^+\right]} = K$$

A point-wise correction depending on the contribution of mass 3 to each mass 2 value seems to be the most favorable (SESSIONS et al., 2001). A value of k <10 and high stability should be achieved to reduce the effect of unusual high and time-variant H_3^+ contribution to the mass 3 ion current. In this study the experimentally k-factor was applied using Isodat 7.0 (ThermoElectron (Bremen) GmbH, Germany).

Nitrogen

For nitrogen the ion beam ratios can be directly translated into the isotope ratio following the isotope composition of molecular nitrogen ($^{15}N^{14}N$, $^{14}N_2$) (Equation 3.8):

$$\frac{I_{29/28}\text{sample}}{I_{29/28}\text{reference}} = \frac{c_{29/28}\text{sample}}{c_{29/28}\text{reference}} \times \frac{^{15}\text{Rsample}}{^{15}\text{Rreference}}$$

Equation 3.8

The simple translation into a sample isotope ratio is hampered by the different chemical origins to produce a N_2 gas for IRMS measurements.

δD values of bulk organic matter

For international comparison of the δD values of organic compounds a polyethylene foil (PET-J1) was calibrated versus VSMOW using the IAEA-CH7 (polyethylene foil) as a reference ($\delta D_{IAEA\text{-}CH7}$ = -100.3‰, $\delta D_{PET\text{-}J1}$ = -81.23‰) with a TC/IRMS system. Within 2 weeks of analysis the PET-J1 had a δD value of –86.6‰, σ_1 = 4‰, n=34.

Determination of the accuracy and reproducibility of $\delta^{13}C$ and $\delta^{15}N$ of bulk organic matter

In this study the $\delta^{13}C$ and $\delta^{15}N$ values of bulk OM were corrected for its isotope content against the internationally accepted standards (COPLEN, 1996). To reference the samples the method of WERNER and BRAND (2001) was applied by using an elemental analyzer (NA 1110, CE instruments, Milan, Italy) as a combustion unit to convert N and C containing samples to a gas phase (EA-IRMS). Each $\delta^{13}C$ and $\delta^{15}N$ value has been determined separately to avoid a co-elution and tailing of the N_2 peak into the CO_2 peak. For carbon two chemically and in terms of their isotopic content stable compounds were used as isotopic reference standard (acetanilide,

Ali-j1 to 3, $\delta^{13}C_{Ali\text{-}j1}$ = -33.98‰, $\delta^{13}C_{Ali\text{-}j2}$ = -33.98‰, $\delta^{13}C_{Ali\text{-}j3}$ = -29.81‰) and one for quality assurance (caffeine, Caf-j1). The $\delta^{13}C$ value of Ali-j1 to Ali-j3 have been determined directly versus the VPDB scale using the NBS-22 oil ($\delta^{13}C_{\text{-NBS 22}}$ = -29.78‰) and the USGS24 graphite ($\delta^{13}C_{\text{ USGS24}}$ = -16.1‰) leading to an overall standard deviation of Ali-j during 2 years of measurement of 0.03‰ for organic carbon and 0.08‰ for nitrogen.

3.5.2 Carbon and hydrogen isotope determination of biomarkers

To determine the isotope ratio of individual organic compounds an IRMS was coupled via a combustion furnace for either oxidative conversion to CO_2 or with a pyrolytic furnace at 1450 °C to H_2 gas. Figure 2.1 shows The IRMS analytical system (Delta^{PLUS}XL, ThermoElectron (Bremen) GmbH, was simultaneously coupled to an ion-trap mass spectrometer (ThermoElectron (Egelsbach)) for peak identification. Substances were injected in split-less mode at 80 °C (hold time 1 min.) and separated in a fused-silica chromatographic column. (DB1-MS: 60 m, 0.32 µm i.d., 0.5 µm thickness) with a constant He flow (2 ml / min.) using an electronic pressure controller (EPC) at the injector head. The compounds were eluted under isothermal condition at 80°C for 5 min., temperature increase at 3 °C / min. to 320 °C and hold for 40 min. to the isotope ratio and organic mass spectrometers. The substances are transferred with a constant split of 1 / 9 to the organic mass spectrometer. Again at the open-split of the Combustion III interface the gas stream was diluted with Helium in a ¼-ratio get a high signal stability of the IRMS.

Tuning of the IRMS for hydrogen isotope analysis

A voltage of ~3 kV and an electronic emission current of 1.5 mA was adjusted. High extraction potential to the electronic potential of the ionization chamber avoided the additional formation of H_3^+ ions. An energy filter in front of the mass 3 Faraday collector reduces the overlapping of He^{2+} ion peak on the mass 3 signal in the Faraday cup of the IRMS. A high extraction potential of the x-deflection reduces the production of H_3^+ ions because of a lower residence time of H_2^+ ions in the ionization chamber.

In accordance to their boiling points the eluted substances are introduced into a aluminum oxide reactor tube (Friatec, Mannheim, Germany), which consists of high-temperature α-Al_2O_3 (320 mm, i.d. 0.5 mm). For combustion of the substances at 1212K to CO_2 the tube (0.5 mm) is filled with a twisted Cu- and a catalyzing Ni wire (MERRITT et al., 1995). In an empty Al_2O_3 tube high temperature conversion at >1673.15 K leads to quantitative hydrogen gas formation (BURGOYNE and HAYES, 1998; SOFER and SCHIEFELBEIN, 1986). During the course of this study the inner diameter of the oven inlet was changed from 0.5 to 0.8mm to enhance the pyrolytic process of H_2 production due to a gas volume increase inside the oven chamber. The overall

conversion rate of ~30nmolH_2 / µl the hydrogen gas can be calculated from the amount of alkane standard mix.

3.5.3 External standardization in compound specific isotope analysis

For standardization in continuous flow IRMS a standard reference gas is injected. It is important to refer to an external or an internal integrated standard sample like a compound within a GC run to be able to report for the accuracy of the sample isotope signal of individual compounds in longer time-scales (JASPER, 2001). In this study an external standardization procedure with normal hydrocarbons was applied, each determined by off-line method and subjected to different correction procedures on pulsed reference gas peak to test the accuracy of the best fit (Table 3.3). In each run three reference gas pulses were injected in the beginning and the end of the sample and standard runs. The relative isotope values of organic standards and samples were normalized against the off-line determined δD values of the respective standard according to Equation 3.9.

$$\delta_{correfgas} = \delta_{uncorrefgas} + \frac{\delta_{standard} - \delta_{sample}}{\left(1 + \delta_{sample}\right)/1000} \qquad \text{Equation 3.9}$$

where: $\delta_{standard}$ = off-line determined relative isotope abundance, δ_{sample} = relative isotope abundance of a sample, δ_{refgas} = relative isotope value of reference gas for isotope correction or of the respective uncorrected value (uncorrected reference gas).

For individual background correction the ion current was set to 5 s before peak detection and for dynamic baseline correction to a mean moving average of 75 points. For low pass filtering Tau (τ) was set to 1 resulting in a cut-off frequency of 20 Hz (sampling rate of 5s). Peak and background detection for carbon and hydrogen was made on mass 2 or mass 44 traces, respectively. Timeshift correction after (RICCI et al., 1994), max. peak resolution >50%. The IsodatNT 1.5 software package (ThermoElectron (Bremen) GmbH) was used with such different automatic background correction procedures.

Individual background detection on the 2nd of the respective first standard gas pulses (ind1)

Individual background detection on the 2nd of the respective first and last three standard gas pulses (ind2)

Dynamic background detection on the 2nd of the respective first standard gas pulses (dyn1)

Dynamic background detection on the 2nd of the respective first and last three standard gas pulses (dyn2)

Low pass filter on the 2nd of the respective first and last three standard gas pulses (LPF).

Table 3.3. δD vs. V-SMOW and $\delta^{13}C$ of standard substances and reagents for derivatization. [a] triplicate, [b] doublets, [c] quadruples.

substance	formula	TC-IRMS δD in [‰]	Mn reduction δD in [‰]	EA-IRMS $\delta^{13}C$ in [‰]
n-*alkanes*				
n-C_{10} alkane	$C_{10}H_{22}$	-130.2±0.2	-	-
n-C_{11} alkane	$C_{11}H_{24}$	-161.3±7.9	-	-
n-C_{12} alkane	$C_{12}H_{26}$	-127.5±0.8	-127.4±0.5[a]	-34.19±0.06[a]
n-C_{13} alkane	$C_{13}H_{28}$	-33.3±0.7	-	-
n-C_{14} alkane	$C_{14}H_{30}$	-79.7±3.2	-	-28.58±0.05[a]
n-C_{15} alkane	$C_{15}H_{30}$	-136.8±3.0	-	-
n-C_{16} alkane	$C_{16}H_{34}$	-140.1±4.2	-	-34.62±0.04[a]
n-C_{17} alkane	$C_{17}H_{36}$	-157.6±1.0	-	-
n-C_{18} alkane	$C_{18}H_{38}$	-107.3±1.8[a]	-109.8±3.7[a]	-31.92±0.08[a]
n-C_{19} alkane	$C_{19}H_{40}$	-138.6±2.0[a]	-134.3±2.1[a]	-34.40±0.03[a]
n-C_{20} alkane	$C_{20}H_{42}$	-62.3±2.9[a]	-62.8±2.4[a]	-34.25±0.05[a]
n-C_{21} alkane	$C_{21}H_{44}$	-220.1±0.6[a]	-	-30.49±0.06[a]
n-C_{22} alkane	$C_{22}H_{46}$	-89.5±0.6[a]	-	-34.95±0.01[a]
n-C_{23} alkane	$C_{23}H_{48}$	-55.7±2.2[a]	-	-32.99±0.02[a]
n-C_{24} alkane	$C_{24}H_{50}$	-83.0±2.9[a]	-	-34.90±0.01[a]
n-C_{25} alkane	$C_{25}H_{52}$	-266.9±3.5[a]	-	-30.04±0.02[a]
n-C_{26} alkane	$C_{26}H_{54}$	-65.8±2.2[a]	-	-34.52±0.08[a]
n-C_{27} alkane	$C_{27}H_{56}$	-	-	-31.29±0.03[a]
n-C_{28} alkane	$C_{28}H_{58}$	-71.0±2.8[a]	-	-33.45±0.09[a]
n-C_{29} alkane	$C_{29}H_{60}$	-	-	-30.57±0.08[a]
n-C_{30} alkane	$C_{30}H_{62}$	+103.7	-	-
n-C_{31} alkane	$C_{31}H_{64}$	-	-	-
n-C_{32} alkane	$C_{32}H_{66}$	-225.6	-	-32.11±0.06[a]
aromatics			-	-
1, 3, 5-triazine	$C_3H_3N_3$	-	-	-50.09±0.08[a]
1,2,3-trimethoxy-benzene	$C_9H_{12}O_3$	-156.7±1.1[a]	-	-
1,4-cyclohexandione	$C_6H_8O_2$	-175.5±0.7[a]	-	-
1-benzothiophene	C_8H_6S	61.2±3.0 [a]	-	-28.68±0.02[a]
benzyliden-acetophenone	$C_{15}H_{12}O$	-88.0±2.8 [a]	-	-
benzophenone	$C_{13}H_{10}O$	-44.4±1.2 [a]	-	-28.51±0.03[a]
Pyrazine	$C_4H_4N_2$	-	-	-30.14±0.01[b]
squalane	$C_{30}H_{64}$	-187.1±4.6[a]	-	-
normal fatty acids				-
mysteric acid	$C_{14}H_{28}O_2$	-241±14.2 [a]	-	-
palmitic acid	$C_{16}H_{32}O_2$	-228.6±0.9[a]	-	-
stearic acid	$C_{18}H_{36}O_2$	-226.3±6.3[a]	-	-
arachidic acid	$C_{20}H_{40}O_2$	-214.7±4.5[c]	-	-
hexacosane acid	$C_{26}H_{52}O_2$	-160.8±3.3[a]	-	-
octacosaneacid	$C_{28}H_{56}O_2$	-105.5±5.2[a]	-	-
fatty acid methyl esters				-
palmiticacid	$C_{17}H_{34}O_2$	-231.6±6.7[a]	-	-
arachidicacid	$C_{23}H_{46}O_2$	-157.8±4.5[a]	-	-
pentacyclic terpenoides				-
cholesterol	$C_{27}H_{46}O$	-240.4±4.3[b]	-	-
beta-sitosterin	$C_{29}H_{50}O$	-252.6±1.6[a]	-	-
derivitizing reagents				-
BSTFA	$C_8H_{18}F_3NOSi_2$	-265.2[a]	-	-
acetamide	C_2H_5NO	-188.8[a]	-	-

4 Development of isotope analysis of biomarkers in sediments

4.1 Development of compound specific hydrogen isotope analysis

For the evaluation of the system stability and accuracy approx. 1500 single standard measurements were accomplished in compound-specific hydrogen analysis to follow the physical and chemical effects that influence the transformation to hydrogen gas during pyrolysis and the ionization capacity and properties of the IRMS ion source.

4.1.1 Ion Source stability and linearity for reporting hydrogen isotope ratios

Stability and linearity (i.e. H_3^+ factor determination) were checked with ten reference gas pulses with 0.622 nA to 8.109 nA in 500 to 1000 pA steps. The relative stability of the ion source was 0.4‰ (± 0.7, n = 76) including an outlier rejection of values deviating from a three times larger standard deviation (σ_1) (Figure 4.1). The correlation of the means is significant at $p > 0.05$ except for the sample at 1.0 nA (Mann-Whitney U test). Within the analytical range the difference of 0.06‰ per 1 nA accounts for a relative stable ionization of the ion source.

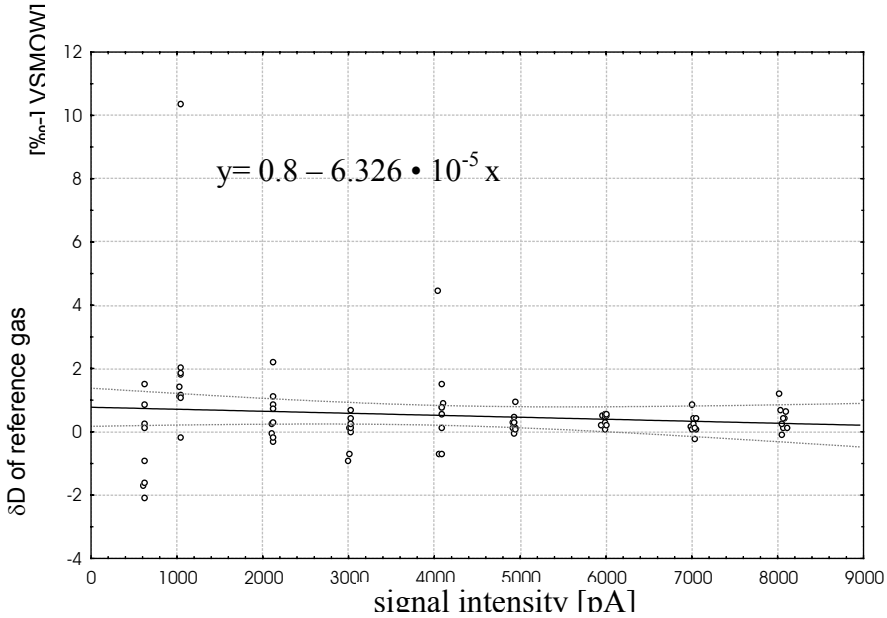

Figure 4.1. Relative stability of the IRMS ion source. δD value of reference gas set to zero ("zero enrichment test").

To determine the ion source linearity increasing doublet gas pulses of the same hydrogen gas pressure between 842 pA and 3900 pA were transferred into the ion source and the contribution of H_3^+ ions was determined applying point-wise peak detection (pers. comm. W. Brand, SESSIONS et al., 2001). Normally the background signal (no external gas pressure in the ion source) is in the range of 0.15 nA to 0.2 nA. At the beginning of the 2001 measuring campaign

the dilution with He at the reference open-split was changed from 1 bar He to 1.5 bar to refine the background stability of the mass 3 signal in the ion source resulting from a higher efficiency of Nafion^{TM} water trap. Different He gas pressures in 0.1 bar steps followed the change of the mass 3 / 2 ratio where no significant change in the ratio at 1.5 bar was indicated. During this study the linearity measurements reveal an excellent k-value of 7.7 ± 0.83 (ppm·mV^{-1}). During sample measurements in 2000 and 2001 the k-value was at 7.2 ± 0.24 and 7.75 ± 0.83, respectively. A better standard deviation of the k-value during the 2000 campaign does not automatically imply a better stability of the sample δD values, because of differences in the He flow of sample and standard open-split systems (Figure 2.1).

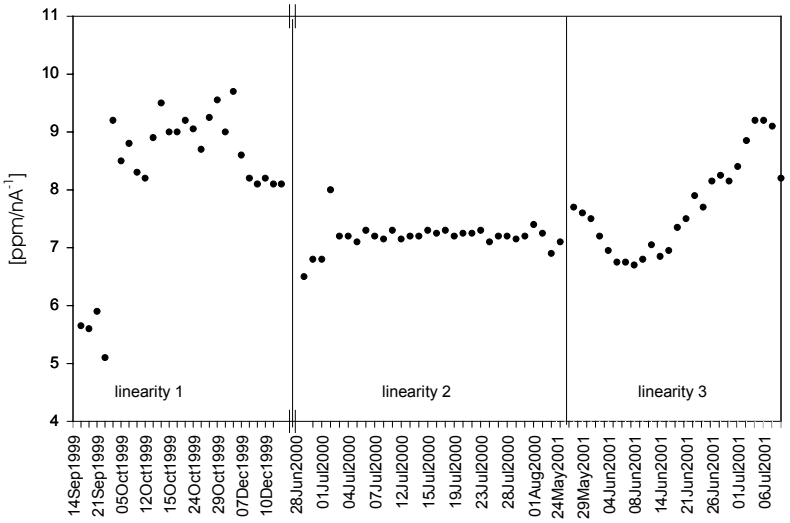

Figure 4.2. Linearity and k-factor determination during 1999, 2000 and 2001.

SESSIONS et al. (2001) revealed for the influence of k determinations on the δD values that the magnitude of errors for the value of k = 8 is approximately at 2.5‰ depending on the difference between sample and standard peak heights. Therefore, the concentration dependent H_3^+ contribution on the mass 3 with a k-factor of 7.75 reflects a high stability.

4.1.2 Formation of hydrogen gas by pyrolysis

During pyrolysis of organic compounds major constituents of the resulting gas molecules are CO, CO_2, H_2O, N_2, H_2 and in excess the production of carburized carbon (i.e. elemental C). The elemental carbon remains at lower temperature areas of the inner wall of the Al_2O_3 reactor and serves as a reaction catalyst during pyrolysis.

Below 1400 °C of furnace temperature incomplete pyrolysis might evolve methane, which acts as proton donor in the ion source leading to an additional production of H^+ ions (Equation 4.1).

$$CH_4 \rightarrow CH_3^+ + H^+ \qquad \text{Equation 4.1}$$

The H^+ ion will produce additional H_3^+ ions, which will interfere with the DH signal of the pyrolysed substances and therefore influences the *i*3 / *i*2 ratio.

Injecting of an alkane mixture (*n*-C_{12}, *n*-C_{14}, *n*-C_{16}, *n*-C_{18}, *n*-C_{19}, *n*-C_{20}) of 300ng for each alkane with an addition of 2µl *CH_4* at the end of the chromatogram the mass 15 signal[1] between temperature ranges from 1410 °C to 1450 °C in 10 °C intervals of the compounds were recorded by the CO_2 faraday detector configuration (Figure 3.1). The scattered mass 15 was not correlated to the retention time of the peaks retention time. No peak of the mass 15 could be assigned to the alkane and methane peaks assuming a total transfer of all compounds to H_2 gas (Figure 4.3, a & b). In general the mass 15 signal increased with higher pyrolytic temperature. This was related to the increase of mass 15 in the background, and not to the increased production of methane from compounds. However the mass 16 / 15 ratio was used to approximate the influence of additional gaseous oxygen (O^+ = mass 16) in the respective temperature intervals (Figure 4.3, c & d). Peaks were detected with two-point polynomial smoothing at a 0.35 time width and a point-wise baseline correction (300 points) using Origin 5.0™ software. Because one can assume that the contribution of ^{13}C was not increased significantly due to same isotope ratios of the compounds, the enrichment of the mass 16 might be related to the contribution of O^+ confirmed by the general increase of the baseline mass 15. In the opposite case the 16 / 15 ratio should have been decreased. Therefore, the increased methane concentration led to an approx. 1.75 fold higher mass 16 signal than would be added from methane of the 300 ng alkane mixture.

An approximately 60 times higher molecular hydrogen amount from the methane (3746 nmol H_2) than from an alkane (*n*-C_{12} = 64.63 nmol H_2) could be ionized in the ion source effectively. This means that at a temperature range between 1410 °C and 1450 °C the contribution of H^+ ions from 18 µg alkane can be neglected as a major proton donor in the ion source. The mass 16 / 15 ratio should have no major effect on the contribution of H^+ in the ion source, therefore the pyrolysis temperature was set to 1410 °C derived from the mass 15 signal where no additional methane could be detected whether from the high concentrated methane nor from the alkane mixture. In comparison to the alkane hydrogen yield for isotope ratio determination a minimum of 36ppB CH_4 can be applied for hydrogen isotope determination of methane on the column with a flow at 300 mbar × min^{-1}. Additionally the δD value of methane (–138‰ ± 2.2) was determined in a normal hydrogen isotope IRMS configuration in that temperature range, which confirms the complete pyrolysis at these temperatures.

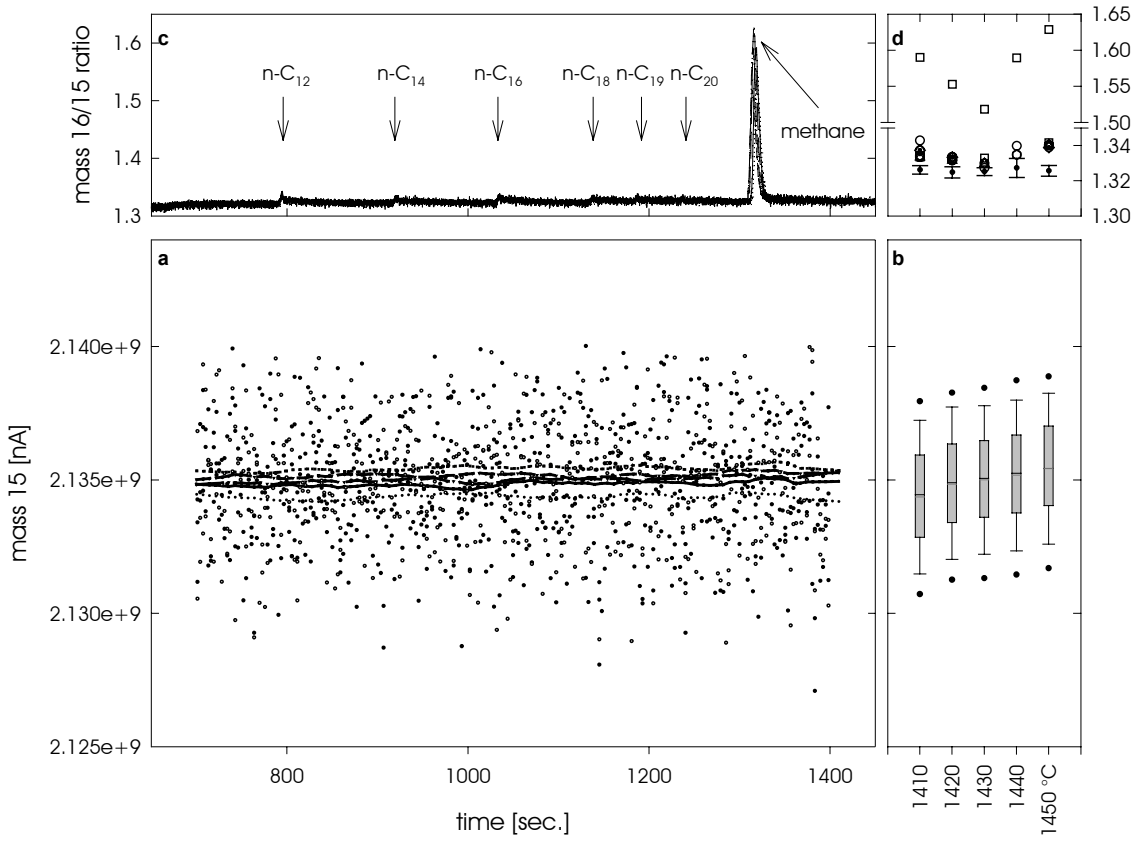

Figure 4.3. Mass 15 and ratio trace of mass 16 / 15. a) Mass 15 trace of alkane mix (*n*-C_{12}, *n*-C_{14}, *n*-C_{16}, *n*-C_{18}, *n*-C_{19}, *n*-C_{20}, and methane) in different GC runs at 1410 °C, 1420 °C, 1430 °C, 1440 °C, 1450 °C. Lines represent the smoothed mass 15 values by negative exponential smoothing at different temperatures. b) Mean (black line), median (dark grey) with whiskers at the 5 and 95 percentiles. c) 16 / 15 ratio trace of the GC runs at respective temperature levels d) 16 / 15 ratio of specific *n*-alkanes, black dots describe the mean of the baseline ratio. Note the scale difference at plot d).

To test additionally a significant availability of methane after pyrolysis causing the above mentioned chemical reaction a chromatographic gas molecular sieve (Megabore, 5Å) was held under liquid nitrogen conditions to freeze gas molecules in the stable phase of the molecular sieve. Comparison of alkane standard δD mean values before and after application showed no significant improvement of the standard deviation. This supports the complete transfer of methane and the robustness of the developed method.

4.1.3 Precision and accuracy of hydrogen isotope analysis

The precision and accuracy of the compound-specific isotope analysis and the standardization to the international scale was accomplished by the use of a standard mixture of organic substances. At the moment no international standards are available for the determination of the compound-specific isotope ratios in a GC system and therefore no direct determination of the precision and accuracy of an international isotope standard is possible. Therefore, these standards are referred to international hydrogen isotope standard waters (Standard Mean Ocean Water, VSMOW, 0‰

by determine the isotope ratio against a polyethylene foil (secondary isotope standard, IAEA-CH7) in a TC-IRMS system. The IAEA-CH7 is calibrated by the International Atomic Energy Agency to the SMOW/SLAP scale (δD value = -100.3 ‰ vs. VSMOW). Three independent replicates of an alkane (*n*-C_{15} to *n*-C_{30}, 25 ng, 50 ng, 100 ng, 150 ng, 200 ng) and squalane (300 ng) mixture, named Mix E, were used for normalized standardization (Equation 4.2) in the GC-TC-IRMS system.

$$\delta D_{SAcorrected} = \left(\frac{\delta D_{SA} + 1000}{\delta D_{WSTD} + 1000} - 1 \right) \times 1000 + \delta D_{ISTD} \qquad \text{Equation 4.2}$$

where δD_{WSTD} is the known δD value of the working standard / H_2 reference gas; δD_{SA} the δD value of the measured sample or the used δD value of the H_2 reference gas, δD_{ISTD} the δD value of the international calibrated standard or the calibrated working standard. If no direct determination of an international standard is possible, an uncertainty exists for the calibrated working standard, because the isotope ratio of this standard itself is measured and may contain systematic mistakes. Comparing the independently determined δD values of Mix E in a GC-TC-IRMS system and in a TC-IRMS system, the accuracy and precision of the δD values of the calibrated standards are evaluated. Factors influencing the accuracy and precision are the efficiency of the pyrolysis of the compounds to H_2, performance and conditions of the Al_2O_3 reactor and the linearity of the measuring range.

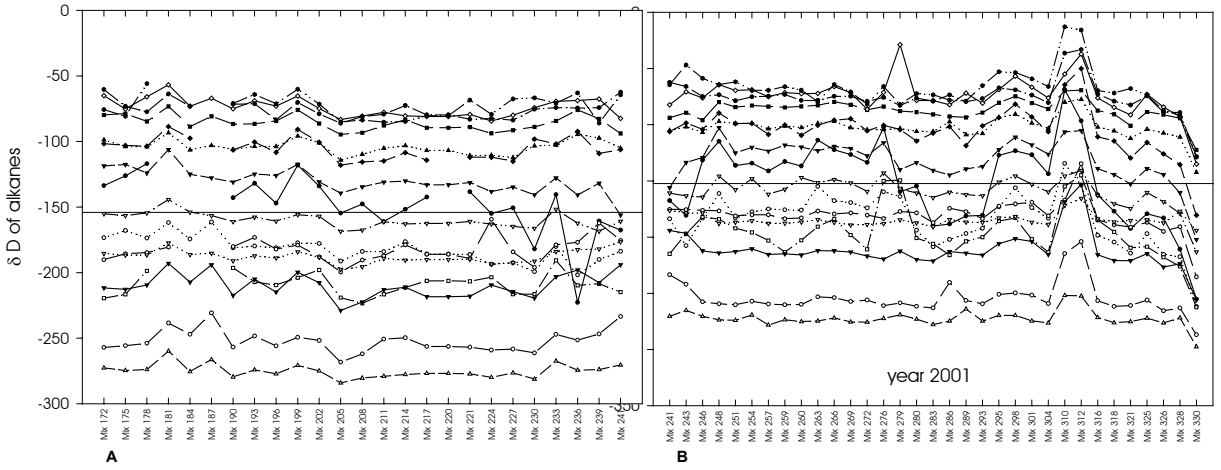

Figure 4.4. Uncorrected δD values of alkane MIX E (shown is the mean δD value of all standards). A: year 2000 and B year 2001. The δD value of H2 reference gas was set to –220‰.

The raw isotope values of the MixE standard reflect the dependency of the system over the reactor lifetime (Figure 4.4). At the end of the reactor life time the diffusion of atmospheric water, nitrogen and oxygen through microscopically visible micro cracks (not shown) strongly affects the measured δD values. Additionally, high boiling point *n*-alkanes need a high GC

elution temperature of 320 °C. This temperature together with the 1450 °C of the furnace also affects the temperature stability (280 °C) of the Vespel™ ferrule, which connects the GC fused silica into the furnace reactor and may lead to additional background.

Using the H_2 reference value of –220‰ during the year 2000 and 2001 the general performance of the Mix E standard can be shown. Consequently, before and after each triplicate analysis of the δD values of compounds in a sample the δD values of the standards were determined in triplicates. The δD values of the standards were used to calibrate the δD value of the reference gas values of the sample runs. Effects during the two periods were more depleted δD values of Mix E standards during the year 2000, less depleted δD values from Mix E 304 to Mix E 316 and more depleted δD values from Mix E 328 to Mix E 331.

All standards were more depleted in Deuterium in the year 2000 compared to 2001. Different ion source conditions may have influenced the production of H_3^+ ions and the δD values of the reference gas are less depleted in Deuterium. The H_3^+ factor was in the year 2000 with $K = 7.2 \pm 0.1$ more stable than during the year 2001 with $K = 7.71 \pm 0.8$. Consequently, the production of H_3^+ ions affected the δD value of the reference gas to less Deuterium depleted values.

During the measurement of the δD values of the Mix E 304 to the Mix E 316 a highly Deuterium enriched extract of a meteorite sample was analyzed (Figure 4.4). The memory of the Deuterium enriched meteorite has affected the δD values of the reference gas. The main constituents of this meteorite extract were short-chain normal fatty acids. Because no derivatisation of the fatty acids was used the compounds might have been released very slowly from the analytical column and exchanged with the δD of the reference gas and standard components. A derivatisation with BSTFA (N, O-bis-trimethylsilyl-trifluoroacetamide) of the meteorite extract compounds caused the δD values of the Mix E 328 to Mix E 331 standards to be more depleted in Deuterium. The fluorine silyls of the BSTFA (δD value of BSTFA = –235‰) were changing obviously the δD values of standards (Figure 4.4). The analysis of the δD values of compounds derivatized with BSTFA was to short to address the reasons for this memory effect on the δD values of standards.

The performance of the δD values of standards with this high variability explains that the δD values of sample compounds must be normalized to a standard mixture after each triplicate determination. The different concentrated alkane mixture was used to determine the measurement range of compound-specific hydrogen isotope analysis. In the year 2000 measurement an alkane mixture (Table 3.3) with additional aromatic and branched compounds was used in comparison to a alkane mixture with calibrated δD values provided by Arndt Schimmelmann, University of Indiana, Bloomington, USA. The linearity of the measurement range was determined with these two different standard mixtures. This mixture of *n*-C_{18}, *n*-C_{19},

n-C_{20}, *n*-C_{21}, *n*-C_{25} alkanes was injected with 25 ng, 50 ng, 100 ng, 200 ng, 300 ng, and 500 ng alkane on the column. In the year 2001 the alkane MIX E was used for secondary standardization.

The δD values of standards determined by GC-TC-IRMS were pooled and outlier rejected by an outlier coefficient of 1.5 times of the 25 and 75% from the mean. The δD values of the standards determined with GC-TC were calibrated with δD values of standards determined by TC-IRMS. The ΔδD is the difference between the mean δD values of the standards determined by TC-IRMS and GC-TC-IRMS. To account for the standard deviation of the δD values of *n*-alkanes of the TC-IRMS and GC-IRMS the weighed standard deviation $\sqrt{(\sum \sigma_{TC-IRMS})^2 + (\sum \sigma_{GC-TC-IRMS})^2}$ was used (Figure 4.5). The weighed mean standard deviation for 2000 and 2001 averages at 6.6 ‰ (n = 95) and 5.8‰ (n = 82), respectively. This accounts for a better stability of the system during the year 2001. No statistically significance exists between the ΔδD values of standards to the ion current (student-t, $p < 0.5$). All shown *n*-alkanes are measured in a range between 50 ng / 1µl and 500 ng / 1µl on the column (500 nA and 4000 nA).

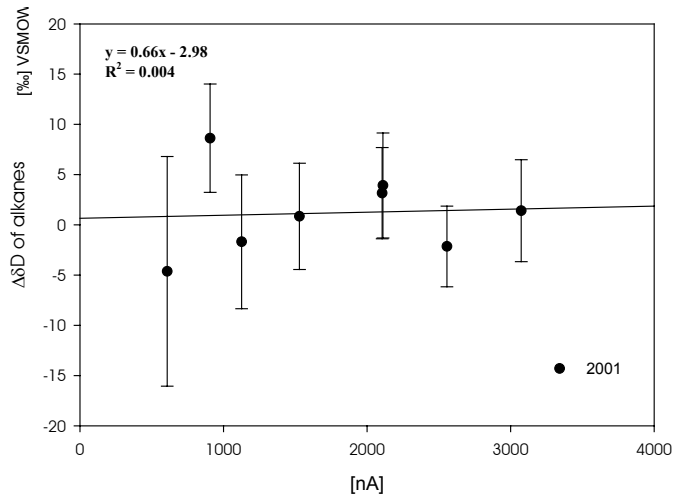

Figure 4.5. δD values of standards during 2001. Standard deviations are weighed standard deviations between TC-IRMS and GC-TC-IRMS methods (n = 234).

The δD values of *n*-alkanes determined by GC-TC-IRMS correlates to the δD values of *n*-alkanes with gradients between 0.986‰ and 1.02‰ and with interceptions at –2.9‰ and +2.6‰, respectively (Figure 4.6.). The δD values of *n*-alkanes from the GC-TC-IRMS were reproducible to the δD values of standards of the TC-IRMS. Consequently, the accuracy of the δD values of standards with a GC-TC-IRMS seems to be similar to the TC-IRMS.

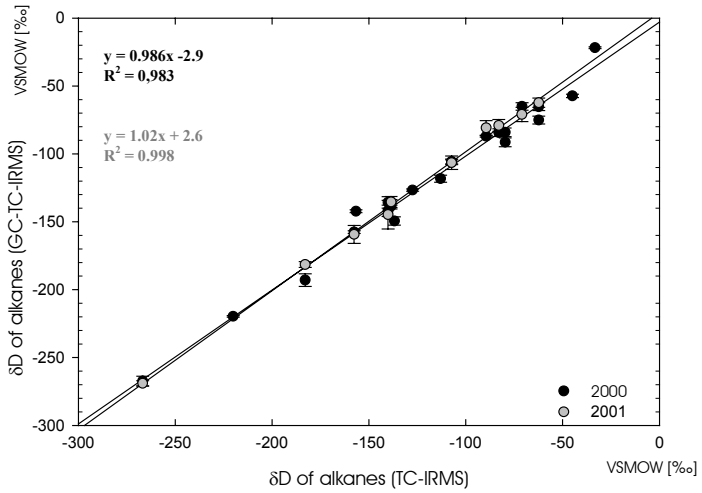

Figure 4.6. Comparison of mean δD of *n*-alkanes between TC-IRMS and GC-TC-IRMS systems.

The δD values of *n*-alkanes of a sample run were corrected by a linear correction between the δD values of previous and subsequent standard reference gas peaks (Equation 2.9). The effect of this correction procedure of the δD value of the sample alkane with the same standard alkane and only one external standard δD value of alkane (*n*-C_{28} alkane) was tested on a sample batch of 10 independent sample runs (Figure 4.7). The difference from zero of the intercept of the regression line is related to the normalization procedure of the *n*-alkanes. For the peak-to-peak procedure a simple difference between standard and sample alkane was used ($\Delta\delta D = \delta D_{sample\ alkane} - \delta D_{standard\ alkane}$). The values are 5.7‰ more enriched than the samples corrected by the general normalization procedure using the *n*-C_{28} alkane. This explains the statistically non-significant similarity of the two dependent variables (Mann-Whitney U test, $p < 0.00001$). A normalization of standards (not shown), where it was tested with simple difference, led to a general more enriched δD value (3.8‰). Therefore, it is mandatory to use the same normalization procedure in hydrogen isotope analysis. Conclusively, the correction with single standard is not changing the δD value of *n*-alkanes significantly with an accuracy of the weighed mean standard deviation between 5.2‰ and 6.7‰.

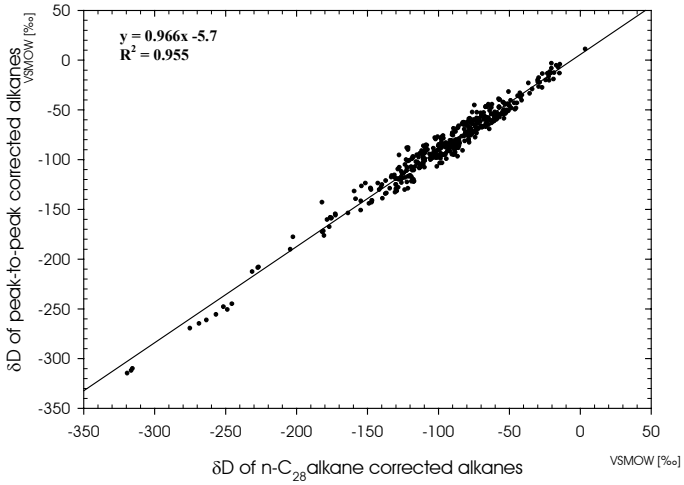

Figure 4.7. δD values of samples corrected with the δD value of a standard *n*-C_{28} alkane and of sample *n*-alkanes corrected each with the same δD value of standard *n*-alkane.

The individual and the dynamic background algorithms was applied by setting the middle peak of the three reference gas pulses at the beginning and the end of the chromatogram as a standard. The isotope ratio determination was additionally applied with and without using the last reference gas pulses as a standard. (Figure 4.8; see chapter 1). The individual background subtracts the background value found before peak detection of the mass 2 and uses the baseline signal as a background value.

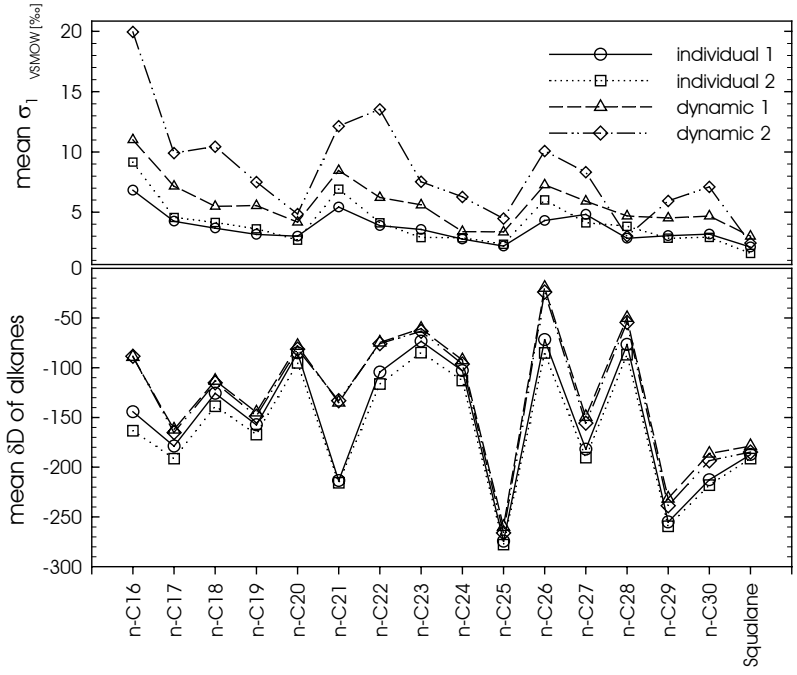

Figure 4.8. Evaluation of the best-fit background detection algorithm to determine the δD value of standards (81 mean δD values (n = 3) were used for determination of the respective standard).

The dynamic background uses a 75 point average before and at the end of the peak. The dynamic background procedure calculated enriched δD values of standards compared to the individual

background (mean for all compounds ΔδD values = 22‰). This is more pronounced at lower concentrations of the compounds (*n*-C_{16}, *n*-C_{21}, *n*-C_{26}) shown by larger difference of the δD value and higher standard deviations (mean δD for dyn 2 = 5.65‰, ind1 = 3.69‰). Differences between the standard deviations of the individual and the dynamical procedures are statistically significant (except for *n*-C_{20}, *n*-C_{25}, *n*-C_{28}). The individual background detection should be used for the evaluation of δD values of standard compounds (n = 81).

The same procedure was tested on 'real' samples (Figure 4.9). Mean values are representative for the *n*-alkanes between *n*-C_{14} and *n*-C_{21} to compare compounds of the short chain alkane fraction. In comparison to the investigation on the δD of standards the δD values of sample compounds were more similar. The differences of the correction algorithms are in the range between –87‰ (dyn1) and –96‰ (ind2) for all *n*-C_{14} and *n*-C_{21} alkanes. The comparison of standard deviations is more fluctuating depending on the sample composition, thus exceeding more than 10‰ for dynamic background detection. The low pass filter has the lowest mean standard deviation (4.9‰) and throughout the sample seems to show the lowest standard deviation compared to the individual and dynamic background detections. However, the differences of the standard deviations of the different methods are not significant.

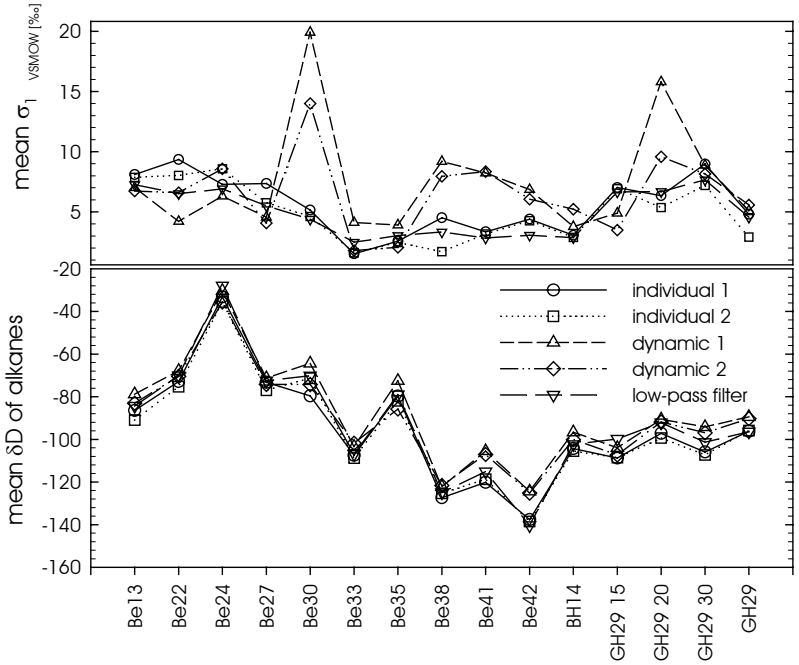

Figure 4.9. Evaluation of the best-fit algorithm to determine the δD value of samples (n = 3 for each sample).

Individual background detection was used for analysis of δD values of all sample runs. The accuracy of the δD value of sample compounds and the best-fitted algorithm can be statistically proven by a larger sample amount as used here, n = 3. The low pass filter and the individual background detection have to be tested for its statistical robustness with a standard sample. This

will attain the influences of systematic errors on the δD value of sample compounds like extraction procedure, flash chromatography and ion source effects.

4.1.4 Hydrogen isotope effects in sample preparation

4.1.4.1 Lipid extraction

Three independent PS sediments of the same sample batch were extracted one time with accelerated solvent extraction for 15, 20, and 30 min. using individual background detection (Figure 4.10). The influence of extraction time on the δD value of hydrocarbons can be evaluated.

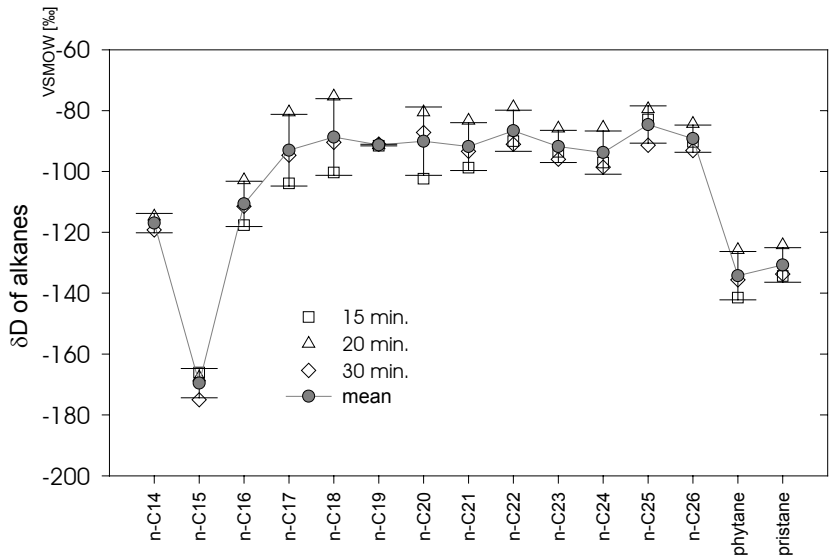

Figure 4.10. Mean δD values of n-alkanes from the same independently accelerated solvent-extracted PS sample at different duration but at same pressure and temperature, The mean and standard deviation bars represent the δD values of the n-alkanes from all independent samples.

The δD values of hydrocarbons were similar for one extraction time setting. An effect would occur, if diffusion differences of compounds or polarity differences in the extraction vessel of the ASE were prominent. These effects should occur at same temperature and pressure conditions. Similar δD values of the *n*-C_{19} alkane of 91.8‰ ± 0.6‰ for each different extraction time cannot be explained by better determination due to higher ion current or lower content of compounds in the hump of the gas chromatogram. Additionally, no differences in the deviation from the mean can be followed due to different chain-length or a significant shift of the δD value at the low-molecular weight hydrocarbons.

The δD value of the *n*-C_{14} alkane with values similar to the long-chain *n*-alkanes (*n*-C > 16) excludes the probability of an effect in the injector of the GC, where diffusion or the lower boiling point of the compounds would enrich the lighter hydrogen isotope in the remaining

compound. This first investigation of independent δD values of sample hydrocarbons shows a mean standard deviation of 6.8‰ of the three different samples only distinguished by extraction time.

4.1.4.2 Chemical clean-up procedure

n-alkanes (*n*-C_{21}, *n*-C_{23}) and heterocyclic hydrocarbons (benzylidenacetophenone, benzothiophene) were subjected to flash chromatography as matrix for chemical degradation with ruthenium tetroxide, and urea adduction with silver nitrate, their δD value determined off-line by TC/IRMS and compared to its general δD value (Figure 4.11).

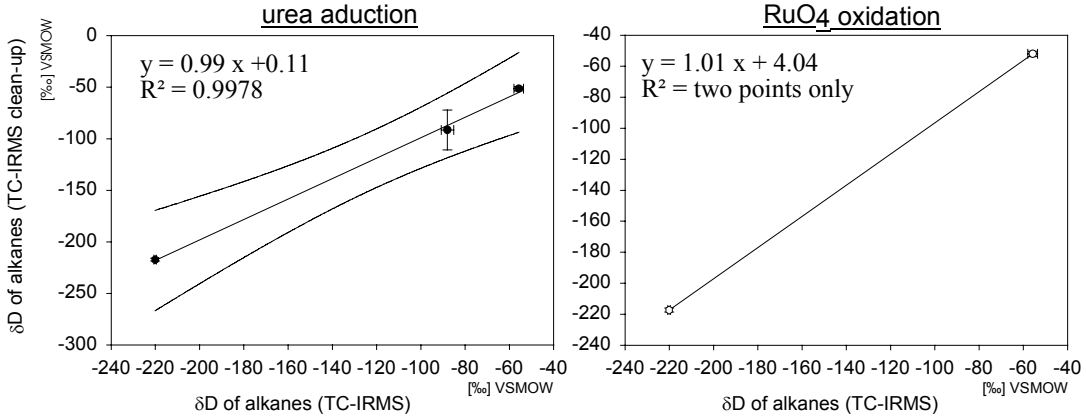

Figure 4.11. *n*-alkanes (*n*-C_{21}, *n*-C_{23}) and hetero compounds (benzylidenacetophenone) extracted under a) chemical degradation (RuO_4) and b) urea adduction (both denominated as "clean-up"). Silica gel was used as a matrix. Bands represent the 95 confidence intervals.

These procedures are commonly used to remove polycyclic compounds from the acyclic compound groups to reduce the occurrence of co-eluted compound peaks during isotope ratio determination. For the chemical degradation only *n*-alkanes were used because ruthenium tetroxide is already well known for the destruction of cyclic hydrocarbons. The mean δD values of *n*-alkanes and benzylidenacetophenone have not been affected significantly during urea adduction and chemical degradation, but chemical degradation seems to have an effect on the δD of benzylidenacetophenone indicated by the much higher standard deviation. Generally urea adduction can be used as a powerful method to reduce co-eluting hetero-components from the acyclic compound for hydrogen isotope analysis. Additionally, the results confirm the use of silical gel for separation of compounds, thus not affecting the primary δD value of compounds.

5 Correlation between hydrogen isotope ratios of lipid biomarkers and sediment maturity

5.1 Introduction

This study raises the question of how maturation processes in sediments alter the hydrogen isotope ratio (δD values) of biomarkers during geological time-scales. The δD values of biomarkers are related to the δD values of source waters and hence can reflect climate (KRISHNAMURTHY and EPSTEIN, 1985; SACHSE et al., 2004b; SAUER et al., 2001). In general, meteoric water is the primary hydrogen source for biomarkers and has a geographically influenced isotopic content. In cooler regions rain is depleted in deuterium, whereas in warmer regions it is more enriched (BUHAY, 1996; KRISHNAMURTHY et al., 1995). Additionally, different biosynthetic pathways determine the transfer function for hydrogen from source waters to different compounds (ESTEP and HOERING, 1980; LUO and STERNBERG, 1991; LUO et al., 1991; SAUER et al., 2001; SESSIONS et al., 1999; SESSIONS et al., 2002; STERNBERG, 1988; WALDRON et al., 1999). δD values of n-alkanes from recent plants vary from –187‰ to –152‰ according to different photosynthetic assimilation processes (C_3, C_4 and CAM) and plant classes (CHIKARAISHI and NARAOKA, 2003). δD values of phytol from aquatic plants and flagellates have values of –278‰ to –357‰, respectively (SESSIONS et al., 1999).

Among the different chemical compounds of organisms, aliphatic hydrocarbons are most favourable to record this primary isotope signal because they resist exchange of inorganic hydrogen into organic hydrogen (SCHIMMELMANN et al., 2001; SCHIMMELMANN et al., 1999; SESSIONS et al., 2004). The homopolar linkage of hydrogen to stable C-C bounds protects the organic hydrogen of acyclic hydrocarbons against rapid exchange reactions. The reaction time is greater than 10^8 years under natural conditions (SCHOELL, 1984c). This long reaction time enables the reconstruction of δD values of source water, since pathway-specific fractionation factors are known (ESTEP and HOERING, 1980; SESSIONS et al., 1999). Consequently, the palaeohydrology of different specific environments within the earth history can be reconstructed using the δD values of acyclic hydrocarbons (ANDERSEN et al., 2001; DAWSON et al., 2004; HUANG et al., 2002; SACHSE et al., 2004a; XIE et al., 2000).

Additionally, acyclic hydrocarbons can also be used to help reconstruct the palaeoenvironment. Short-chain alkanes (i.e. *n*-C_{17} alkane) are products from algae and bacterial biomass living in the water column. (CRANWELL et al., 1987; GELPI et al., 1970). Intermediate *n*-alkanes (*n*-C_{21} to *n*-C_{25}) are derived from aquatic macrophytes (CRANWELL et al., 1987) and long-chain alkanes originate from epicuticular wax hydrocarbons of terrestrial higher plants (*n*-C_{27} to *n*-C_{35}) (EGLINTON and HAMILTON, 1967; GIGER et al., 1980). However, some of the alkanes

(intermediate alkanes, *n*-C_{20} to *n*-C_{25}) also have different origins so that strict source assignment is not always possible (FICKEN et al., 2000; ZEGOUAGH et al., 1998).

It is generally accepted that maturation of organic matter (OM) during burial affects its isotopic composition. Besides geochemical properties, temperature and time mainly drive these isotopic shifts (SEEWALD, 2003). The reasons for the observed enrichment in D and ^{13}C of bulk OM were extensively investigated for different kerogen types using natural and artificial maturation experiments. The main factors for isotope enrichment of kerogen are a) rock-water interaction with organic bound hydrogen (MICHELS et al., 1995; SCHIMMELMANN et al., 2001; SCHIMMELMANN et al., 1999; STALKER et al., 1998) and b) the thermal and burial maturation effects due to cracking reactions, methane release, and aromatization effects (thermal decarboxylation and dehydration) (SCHOELL, 1984a; SCHOELL, 1984b). Most of these processes release D and ^{13}C depleted gaseous products like CO, H_2, CH_4 and low molecular weight aliphatic hydrocarbons C_2 to C_4. This leaves the residue from thermal cracking enriched in D and ^{13}C (REDDING et al., 1980; SACKETT, 1978). However, the effect of thermal maturation on the δD values of hydrocarbons in natural systems over geological timescales has not yet been defined.

The objective of our study was to compare maturity effects on the hydrogen isotope ratios of *n*-alkanes and acyclic isoprenoids (i.e. phytane, Ph, pristane, Pr), and to develop a correction for maturity-derived isotope effects on acyclic hydrocarbons. To avoid distortions created by isotopic fraction due to distillation effects during fluid transport, only hydrocarbons from natural closed-system deposits are suitable for investigations in the KS. Over 50% of the aliphatic content started to expulse in more mature samples of vitrinite reflectance R_m[1] > 0.8 (RULLKÖTTER et al., 1988). Therefore, two marine kerogen type II sediments that underwent thermal maturation by a) slow sedimentary burial and b) fast contact metamorphism were investigated.

5.1.1 Geological setting

The Lower Permian Basal Zechstein "Kupferschiefer" horizon (KS, Copper shale, Wuchiapingian) of the barren-zone, NE Polish Zechstein Basin (BECHTEL et al., 2000a) and the extensively studied Jurassic Posidonia shale (PS, Lower Toarcian), Northern German Basin were used for this study. Both basins should help clarify the influence of different maturation in areas with a low geothermal gradient (30°C / km) (BECHTEL et al., 2000a), such as Poland, and in a

[1] R_m: Maximum Random Vitrinite reflectance. Maturity indicator determined from the gray reflectance (546 nm) of vitrinite - a particle contained in coals (i.e. former woody tissue, bark, or leaves). The KS is absent of vitrinite, therefore the R_c can be calculated to compare with sediments with known R_m.

contact-metamorphic zone related to a magmatic intrusion during the Lower Cretaceous, Hils syncline of the "Vlotho Massiv" (RULLKÖTTER et al., 1988).

The KS consists of marine shelf deposits. The geological setting of the KS of North East Polish is described in BECHTEL et al. (2000a). The total KS deposition of less than 100,000 years has a mean sedimentation rate of 1.5 to 5 cm / 1 ky. This represents a fast transgression of marine seawater, from the boreal ocean in the NW, into the Rotliegend depositional basins of the whole Middle European continent. The KS Basin sediments were deposited under different palaeohydrological conditions in an arid to semi-arid climate zone. Additionally, the water was influenced by distinct hydrographic regimes, water depth and water supply range from lagoonal to deeper shelf areas (BECHTEL and PÜTTMANN, 1992).

At the peak of the Lower Jurassic (Lower Toarcian) transgression, the Western European area was separated into several epicontinental basins and culminated in the opening of the Northern Atlantic Ocean during the Dogger. The depositional system of the PS consists of restricted shelf sea basins with an estimated deposition period of <250,000 years (LITTKE, 1993). The organic deposition is considered uniform over a wide depositional area (RULLKÖTTER and MARZI, 1986). The basins were interconnected over palaeohighs with shallow water (LITTKE, 1993). Global anoxic events have been reported with high organic carbon accumulation (> 16%) in the PS, resulting from upwelling of bottom waters (LITTKE, 1993). Nevertheless, local or regional inputs of freshwater to the marine surface water of the restricted basins were caused by influx from the continental area related to changes in the latitudinal monsoon circulation from the Mediterranean Tethys or from distinct circulation in the northern Scandinavian area (RÖHL et al., 2001b).

The water depth in the PS of the Hils syncline was characteristic of these restrictive shelf basins. Sediments during burial the PS of the Hils syncline were exposed to a deep intrusive body (Vlotho Massif). The mean vitrinite reflectance in the investigated boreholes increases from 0.48 to 0.88% R_m over 30km from the SW to the N corresponding to a calculated $MPI1_c$[2] index of 0.4 to 1.07 (RADKE et al., 1982).

5.1.2 Samples

The analyzed samples originate from two marine sections of the Upper Permian and Lower Jurassic. 8 samples of the KS were taken from Poland and 4 samples from the Hils syncline of the Northern German Basin (Figure 5.1 a & b). The burial depth of KS samples varied from

[2] $MPI1_c$: The $MPI1_c$ is calculated from the equation of the R_m determination, if the MPI1 is not available. The MPI1 index represents the ratio of phenantrene and isomers of methylphenantrene (3-, 2-, 9-, 1-) due to specific methylisation of phenantrene at different maturation levels (RADKE et al., 1982). The indicator for maturity is the vitrinite reflectance.

1027m to 4719m (borehole depth). Samples analyzed have a MPI1 from 0.41 to 1.5, the maximum hydrocarbon generation temperature (T_{max}[3]) ranges from 419 to 441 °C, HI[4] from 371 to 432 [mgHC / gC_{org}], and Methyldibenzothiophen ratio (MDR[5]) from 2.17 to 6.84 (BECHTEL et al., 2000a). KS samples were taken exclusively from the non-mineralized (barren) zone of the KS horizon, which represents deep marine sedimentation (OSZCZEPALSKI and RYDZEWSKI, 1987). Because of the thermal anomaly during the Mesozoic and the alteration of organic matter during base metal mineralization, the Epi-Variscian zone has been excluded from further analysis in the Polish depositional area.

At the Northern German Basin, PS site samples were taken at the same horizon except for the Harderode site, where stratigraphic classification in the upper horizon made unified sampling difficult. The borehole samples were collected in a depth range from 38 m to 63 m. Intensive tectonics uplifted the sediments during burial at major fault plains and the main expulsion of oil occurred during maturation from 0.48 to 0.88 R_m (RULLKÖTTER et al., 1988). Consequently, samples were analyzed for δD of hydrocarbons in the maturation range of major oil expulsion. Samples analyzed have maturation ranges of T_{max} 421 °C to 431 °C, HI 481 to 246 [mg H / g C_{org}], and a MDR of 0.43 to 3.71. T_{max} and HI parameter were determined routinely by Rock-Eval pyrolysis of the individual samples (ESPITALIE et al., 1977).

[3] T_{max} is the determined temperature of maximum hydrocarbon generation during Rock-Eval pyrolysis (see HI[4] Index)

[4] HI index: Amount of hydrocarbons released during pyrolysis of kerogen determined with a Rock-Eval pyrolysator normalized to the organic carbon content [mgHC / gC_{org}] (TISSOT and WELTE, 1985). Instrument properties and method are described in BECHTEL et al. (2000a). A use as maturity parameter is inaccurate, because of the dependence of the hydrocarbon amount on the organic facies and preservation of organic matter.

[5] MDR: Methyldibenzothiophene ratio (RADKE, 1988) The empirical relationship to maturity is given for kerogen type I &II: $R_m = 0.4 + 0.3\ MDR - 0.094\ (MDR)^2 + 0.011\ (MDR)^3$.

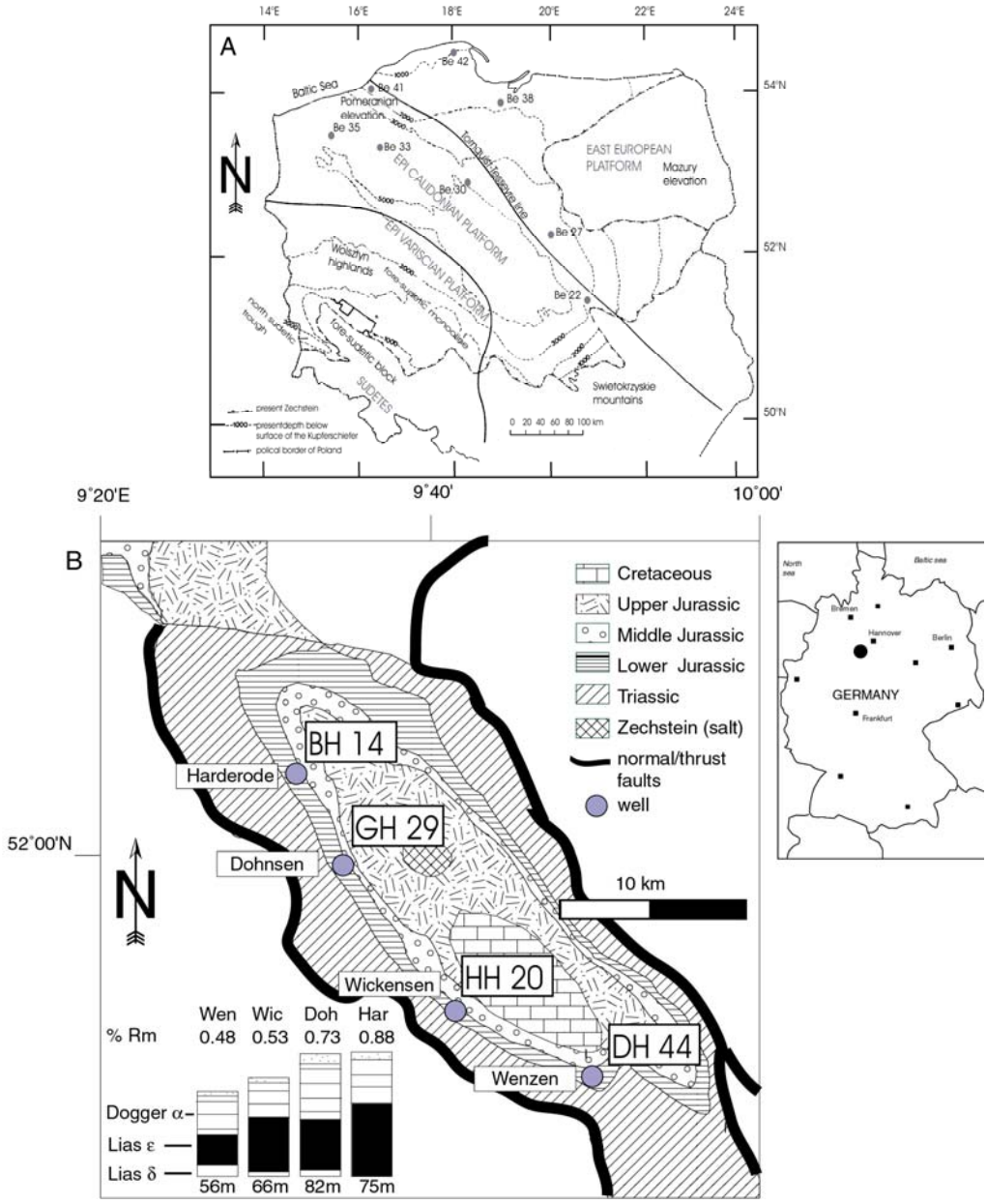

Figure 5.1. a, b. Position of boreholes. A) Sampled for Kupferschiefer within the Zechstein Basin of Poland B) Location of Posidonienschiefer boreholes in the Hilsmulde, Northern German Basin; sampling position in profile: Wenzen (No. DH44, 38.1 m), Wickensen (No. HH20, 45.1 m), Dohnsen (No. GH 29, 63.1 m), Harderode (No. BH14, 44.2 m).

5.2 Methods

Ground borehole samples were solvent extracted to yield the free lipid fraction, which was subsequently separated into aliphatic, aromatic, and polar fractions by silica chromatography (BECHTEL et al., 2000a). To determine the compound specific isotope ratios, 1 µl of the aliphatic fraction was injected in splitless mode in a GC System (hold time 5 min.). Injector temperature was held at 260 °C. Compounds were separated on a DB1-MS column (J&W Scientific) 60 m length, 0.32 µm i.d., 0.5 µm d.f.) at a constant He flow of 2 ml / min. The GC temperature was

kept for 1 min. at 80 °C, followed by a temperature gradient of 3 °C / min. to 320 °C. This temperature was held for 40 min. A constant split at the column end transferred 1 / 9 of the substance for identification into an ion-trap mass spectrometer (Thermo Electron (Egelsbach)). The remaining 8 / 9 of the column efflux were transferred to the conversion unit. In an Al_2O_3 reactor at 1420 °C, all hydrogen was pyrolyzed to H_2 and in a CuO, NiO, Pt reactor at 940 °C all carbon was oxidized to CO_2. Isotope ratios were determined in an isotope ratio mass spectrometer (Delta^{PLUS}XL, Thermo Electron (Bremen) GmbH). Hydrogen isotope ratios are reported against VSMOW.

Standards were not scaled against the slope of SMOW/SLAP according to COPLEN (1996). Calibration to the SMOW/SLAP scale was not done, because systematic differences in pyrolysis of hydrogen from water or organic standards in the silver capsules of the autosampler of the TC/EA IRMS system made comparison difficult (GEHRE et al., 2004).

The reference gas of the IRMS was calibrated against working standards, alkane mixture (*n*-C_{16} to *n*-C_{30} & squalane). Each of the used working standards was calibrated off-line by EA/TC-IRMS (Delta^{PLUS}XL, Thermo Electron (Bremen) GmbH against primary standards IAEA-CH7 (IAEA) (σ_1 = 4‰). The H_3^+ factor has been determined daily (7.75 ± 0.83, n = 25), proving stable ion source conditions. To determine the linearity of the system, working standards of alkanes (*n*-C_{16} to *n*-C_{20}, *n*-C_{21} to *n*-C_{25}, *n*-C_{26} to *n*-C_{30}; 25 ng / 1µl, 50 ng / 1µl, 100 ng / 1µl, 150 ng / 1µl, 200 ng / 1µl on column) and squalane (500 ng / 1µl) were injected in triplicate with increasing concentration between three sample runs from 50 ng / 1 µl to 300 ng / 1 µl on the column. The whole range yields a weighted mean standard deviation of 5.8‰ (n = 82) between GC-TC-IRMS and off-line TC-IRMS individual δD values of standards indicating an excellent linearity of the system. The δD values could be determined in all samples down to the *n*-C_{16} alkane, excluding those that were present in very low concentrations and thus were below the analytical limit. For calculation of the δD values Thermo Electron ISODAT NT 1.5 software was used to apply individual background correction. The internal standard deviation of all standards was 3.69‰ (n = 89).

5.3 Results

δD of alkanes and isoprenoids from the Kupferschiefer and Posidonienschiefer

The δD values of individual alkanes and isoprenoids from the KS samples range from –53‰ to –198‰ and –84‰ to –281‰, respectively. They are about +45‰ more enriched in D with increasing maturity of the samples from 0.4 to 1.5 MPI1 (see appendix Table 9.1). The mean

standard deviation of all samples is 5.5‰ for δD. However, for some peaks the standard deviations are exceptionally high, due to low shot noise ratios of the ion intensities and co-elution. Co-elution of hopanoids and the *n*-C_{34} alkane in sample No. Be42 is the reason for the low δD value of –198‰, since hopanoids are often depleted in deuterium (ANDERSEN et al., 2001). Co-eluting peaks are omitted from further investigation. The mean δD values of short-chained alkanes of >*n*-C_{11} to *n*-C_{15} range are at –112‰, and of *n*-C_{16} to *n*-C_{19} range are at –101‰ (Figure 5.2). "Intermediate" alkanes from >*n*-C_{20} to *n*-C_{25} have an isotope ratio of –92‰ and long-chain alkane groups from *n*-C_{29} to *n*-C_{35} have a mean isotope ratio of –103‰. Short-chain alkanes (> n-C_{11} to < n-C_{19}) are significantly depleted relative to the *n*-C_{20} to *n*-C_{29} alkanes. The δD values of alkanes from PS sediments vary between –76‰ and –204‰, showing mean δD values of all alkanes from individual samples between –98‰ and –167‰ (see appendix Table 9.1, Figure 5.2). The D enrichment in the alkanes is +67‰ from the immature to the mature sample. The mean standard deviation for individual alkanes is 4.8‰ for D. The exceptionally depleted δD value of the *n*-C_{18} alkane from sample HH20 with a δD value of –204‰ is not caused by co-elution; as indicated by mass spectra (see appendix Table 9.1). Possibly an alkane from another ^{2}H- or ^{13}C-depleted source contributed to this peak or the depletion results from an isotope effect on a secondary reaction, such as thermal cracking. The δD values of the *n*-C_{12} to *n*-C_{19} alkanes show a mean δD of –133‰ and for the *n*-C_{20} to *n*-C_{29} a mean isotope value of –116‰ of all PS samples. Compared to the δD values of short-chain alkanes in the KS, the δD values of short-chain alkanes in the PS are about 24‰ more depleted.

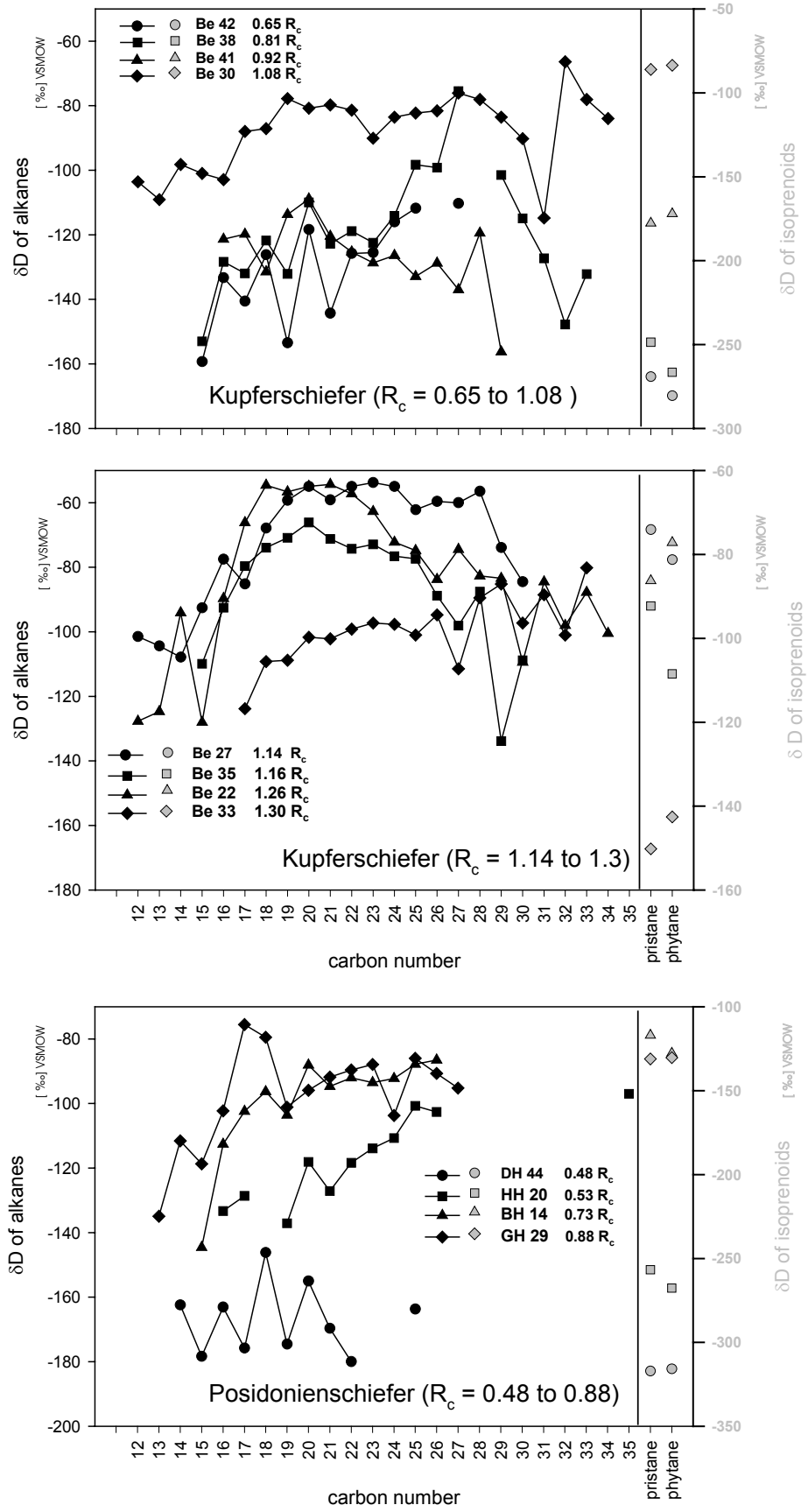

Figure 5.2. δD values of *n*-alkanes versus carbon number and δD values of pristane and phytane in Kupferschiefer and Posidonienschiefer samples. Note the scale difference in δD values for alkanes and isoprenoids. Behind sample numbers the calculated vitrinite reflectance (R_c) is given.

5.4 Discussion

5.4.1 Correlation of hydrogen isotope ratios of hydrocarbons with thermal maturation

The mean δD values of *n*-C_{16} to *n*-C_{19} alkanes have been used to investigate the influence of thermal maturity, because they represent mainly the algal biomarkers needed to reconstruct source water δD values. Furthermore they have the highest concentration in the marine sediments of the KS and PS samples. The δD values of hydrocarbons from PS and KS were correlated with maturation, indicated by the MPI1 index values (
Table **5.1**, Figure 5.3) and other maturity indices (Figure 5.4; T_{max}, HI, MDR). We chose the MPI index as the major maturity index because biomass composition does not influence this index. Primary production of algal biomass would enhance the quantity of hydrocarbons and the HI index will increase not as a matter of maturation but of biomass composition. In the KS linear regression, equations with 56 × MPI1(x)–160‰ and 179 × MPI1(x) –341‰ result from comparing the mean δD values of *n*-C_{16} to *n*-C_{19} alkanes and isoprenoids, respectively. The δD values of hydrocarbons from the PS show positive correlations of y = 104× MPI1(x) –200‰ (r^2 = 0.792, n = 4) for the *n*-C_{16} to *n*-C_{19} alkanes and y = 300 × MPI1(x) –415‰ (r^2 = 0.91, n = 4) for isoprenoids. *n*-Alkanes with less than 25 carbon atoms for the PS and less than 34 carbon atoms for KS show a positive correlation of δD values to maturity in all samples (
Table **5.1**).

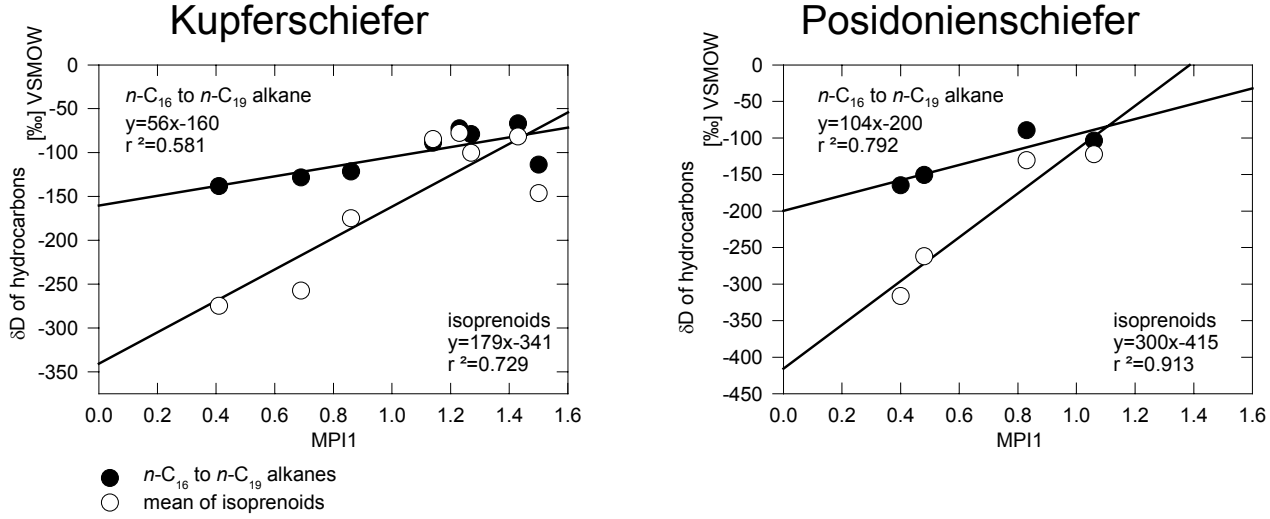

Figure 5.3. δD of hydrocarbons from Kupferschiefer deposits in the Epi-Caledonian / East European platform (circles) in relation to the MPI1 maturity index (MPI1) and δD values of hydrocarbons from Posidonienschiefer from the Vlotho Massif, Germany.

Table 5.1. Properties of linear correlation of δD values of hydrocarbon groups from (a) Kupferschiefer and (b) Posidonienschiefer samples with MPI1 index.

$\delta D_{MPI} = b \times MPI1(x) + b[0]$
where δD_{MPI} is the δD value of *n*-alkanes or isoprenoids at a specific MPI1 value. δD_{MPI} at y-intercept b[0] is the maturity corrected primary δD value of hydrocarbon

Kupferschiefer				Posidonienschiefer		
δD_{MPI}	b	b[0]	r^2	b	b[0]	r^2
all (C_{16-31})	47	-146	0.566	108	-197	0.730
C_{12}-C_{15}	57	-183	0.775	49	-183	0.445
C_{16}-C_{19}	56	-160	0.581	105	-200	0.792
C_{20}-C_{25}	55	-150	0.555	98	-185	0.652
C_{26}-C_{31}	25	-124	0.225	-	-	-
C_{32}-C_{35}	91	-224	0.692	-	-	-
isoprenoids	179	-341	0.729	300	-415	0.913

[b] and b[0] in [‰VSMOW]

Different correlations are shown in

Table **5.1** (*n*-C_{11} to *n*-C_{15} "< *n*-C_{16} alkanes", *n*-C_{16} to *n*-C_{19} (*n*-C_{16} to *n*-C_{19} alkanes", *n*-C_{20} to *n*-C_{25}, *n*-C_{26} to *n*-C_{31} "intermediate *n*-alkanes" and *n*-C_{32} to *n*-C_{35} "long-chain *n*-alkanes") and represent different biomarker groups. Short-chain alkanes are generally derived from bacterial and algae biomass (*n*-C_{16} to *n*-C_{19}), intermediate *n*-C_{20} to *n*-C_{25} alkanes from aquatic higher plants and odd alkanes with *n*-C_{27}, *n*-C_{29} and *n*-C_{31} relate to higher plants. A mixture of higher plant and marine algae alkanes are represented in the KS sediments of Northern Germany (GRICE et al., 1997).

Correlation of δD values of single n*-alkanes in Kupferschiefer and Posidonienschiefer samples*

The mean gradient of individual n-C16 to n-C19 -alkanes is 56‰ / MPI1 ± 11‰ in the KS samples and 105‰ / MPI1 ± 28‰ in the PS samples. The standard deviation within the KS samples results from the most different gradient of the individual n-C19 alkane with 75‰ / MPI1, in contrast to the 53‰ / MPI1 ± 2‰ for the n-C16 to n-C18 alkanes of the KS samples. In the PS samples the variability of different gradients of an individual alkane in each correlation is much larger than in the KS samples. All odd-carbon-numbered alkanes (n-C15, n-C17, n-C19, n-C21) and the even n-C22 alkane have the same intercept with the y-axis at –197 ± 2.3‰ and with a gradient of 96.7‰ / MPI1 ± 20‰.

Correlation of δD values of intermediate to long chain* n-*alkanes in Kupferschiefer and Posidonienschiefer samples

In the KS the gradient of the long-chain alkanes of less than 25‰ / MPI1 (*n*-C_{26} *to* *n*-C_{30}) may be explained by the effect of lower maturation, the missing δD values of long-chain alkanes in the immature samples, or the effect of evapotranspiration on the δD values of long-chain alkanes. Obviously, long-chain alkanes (> *n*-C_{20}) in sediments from the hinterland contributed to the alkanes of the KS. The leaf water of plants is enriched in D via evapotranspiration effects in relation to the soil and ground water isotope ratios (BARIAC et al., 1989). Consequently, these "higher-plant" alkanes would be enriched in D adopting the D-enrichment of leaf-water from evapotranspiration (ESTEP and HOERING, 1980). A higher hydrogen exchange reaction may be depend on the *n*-alkane chain length (see section 4.3.4). We exclude the possibility of enhanced D enrichment in the long-chain alkanes due to maturation. The contribution of organic hydrogen exchange to the deuterium enrichment should be less in long-chain alkanes than in the short-chain alkanes, because of the lower percentage of incorporated hydrogen in this process (Equation 5.1). This is not evident due to our results:

Hydrogen exchange by cracking

$$C_nH_{2n+2} \rightarrow C_{n-m}H_{(2n+2)-(m+1)} + H_{(m+1)} + C_m \quad \text{Equation 5.1}$$

where *n* is the number of carbons, *m* the number of released carbon from the primary compound. Cracking is a kinetic isotope fractionation, where one process (e.g. methane release) would cause the D enrichment in the remaining products according to Rayleigh fractionation. The cracking of larger compounds would result from rearrangement or the cracking of larger alkanes into shorter alkanes (Equation 5.1). The alkanes could be a product of theses processes and the δD values would be depend on the sum of the fractionation factors involved in these processes.

Aerobic microbial biodegradation of hydrocarbons might have been a source for deuterium enrichment in *n*-C_{15} to *n*-C_{18} alkanes (POND et al., 2002). However, a similar gradient of 48‰ / MPI1 in the *n*-C_{20} alkanes compared to the gradient of short-chain alkanes of the KS and the sample diversity from different boreholes excludes the possibility of this effect.

The mean of the δD values of the *n*-C_{32} to *n*-C_{35} alkanes show a higher gradient of D-enrichment, contradicting the argument for the reduced influence of maturation during hydrogen exchange in long-chain alkanes. Presumably, the hydrogen exchange in long-chain alkanes would lead to more negative δD values, because of the lower quantity of organic hydrogen exchanged in comparison to the short-chain alkanes.

Correlation of δD values of isoprenoids and the difference between δD values of isoprenoids and* n-*alkanes in Kupferschiefer and Posidonienschiefer samples

The difference between δD values of isoprenoids and alkanes is gradually reduced in more mature samples in both depositional areas. These results confirm that the difference between δD values of hydrocarbons and isoprenoids originates from the higher enrichment of isoprenoids in D relative to normal alkanes during maturation. The exchange of organic hydrogen is much faster in isoprenoids (i.e. phytane, Ph, pristane, Pr) than in *n*-alkanes. The known higher organic hydrogen exchange rate of hydrogen bonds to tertiary C atoms of branched hydrocarbons is the cause for these deviations (SCHIMMELMANN et al., 1999).

The intersections of the δD values of alkanes and isoprenoids in the KS fall at –160‰ and –341‰, within the range of modern δD values for these biomarkers (SESSIONS et al., 1999). In the PS lower interception values, with a mean of –200‰ for *n*-C_{16} to *n*-C_{19} alkanes and –415 ‰ for both isoprenoids, was observed (Figure 5.3, Table 3.1). The biomass of the KS and PS is of mainly marine origin, and the isotopic data is also consistent with the δD values of modern biomass from marine settings. The immature sediments in the PS have mean δD values of –165‰ for the *n*-C_{16} to *n*-C_{19} alkanes and –316.5‰ of the isoprenoids (Figure 5.3). These values are also within the expected ranges of isotopic compositions observed in modern environments of similar settings. Consequently, we conclude that the δD values of biomarkers can be corrected with maturity parameters to the original isotope ratio at the time of sedimentation, if the maturation history of the sediments is well known.

Differences in maturation effects on δD values of hydrocarbons in Kupferschiefer and Posidonienschiefer samples

Similar trends were found when the δD values of the PS samples were compared to the KS samples. Here the δD values of the short-chain alkanes correlate well between the *n*-C_{16} to *n*-C_{25} groups. With 105‰ / MPI1 for the *n*-C_{16} to *n*-C_{19} alkanes and with 300‰ / MPI1 for isoprenoids, the gradient of D-enrichment is higher than for the KS alkanes. This result demonstrates that the PS responded more to maturity than the KS. A higher maturation temperature would lead to simultaneous oil generation and migration in PS of the Vlotho Massif (RULLKÖTTER et al., 1988). The influence of high temperature on such an open-system deposit with oil migration would therefore affect the δD of hydrocarbons in the PS. In contrast to the natural effect of burial on the δD of hydrocarbons in the KS the D-depleted hydrogen release from the saturated hydrocarbon group was much faster in the PS. Given the low burial depth and younger age of the sediments (184 Ma), and consequently shorter reaction times the higher

maturation effect on δD values of *n*-alkanes in the PS may have led to the observed non-linear deuterium enrichment in the PS.

From the close correlation of the δD values of short-chain alkanes, we infer that the δD values of *n*-alkanes were influenced only by maturation. In contrast, the long-chain alkane groups have different aquatic or terrestrial biomass sources and this would interfere with the maturity influence on the δD values of alkanes. The more deuterium-enriched leaf water enriches the δD of long-chain alkanes during transpiration (CHIKARAISHI and NARAOKA, 2003; SACHSE et al., 2004b). Different biomass sources of alkanes, a different maturation effect on the δD of alkanes, or a mixture of both, would result in less pronounced correlations in the long-chain alkanes of carbon numbers greater than 25 in the KS and PS.

Correlation of δD values of n-alkanes and isoprenoids versus other maturity parameters

δD values of *n*-alkanes and isoprenoids were correlated against T_{max}, HI and MDR (Figure 5.4). BECHTEL et al. (2000a) report a correlation of T_{max} and MDR to borehole depth in KS samples from the barren zone but not for HI of sediments of the barren zone. The HI of the barren zone sediments deviate from the trend line of total HI of the northern Polish Basin to borehole depth. This indicates that a different source of biomass contributed to the hydrocarbon pool, and therefore, the HI does not only depend on maturation. The maturity parameters of a hypothetical immature sample were taken from the trend line of maturity indices against borehole depth considering the surface of the borehole (depth = 0). The δD values of *n*-C_{16} to *n*-C_{19} and isoprenoids of the immature sample were then calculated from the intercept of the trend line of δD values of compounds against the maturity parameter.

In contrast to the KS, the intercepts of the maturity parameters of the PS were evaluated from the mean of the specific maturity parameters (i.e. HI, T_{max}, R_m) within the borehole section of the samples (RADKE and WILLSCH, 1994; RULLKÖTTER et al., 1988; WILKES et al., 1998). The mean of these parameters are very similar within each Lias ε section of the borehole (Wenzen, Wickensen, Dohnsen, Harderode) of different maturity. Given the later tectonic uplift of the sediments, we regard a depth correlation to be impossible. We assume that the PS subsided quickly, resulting in an enhanced heat transfer rate.

The reconstruction of the mean δD value from maturity parameters (MPI, T_{max}, HI, MDR) of KS samples is –161 ± 7‰ for the *n*-C_{16} to *n*-C_{19} group and –346‰ ± 17‰ for the isoprenoids. The maturity parameter correlation gives a mean δD value of –162 ± 4‰ for the *n*-C_{16} to *n*-C_{19} group and –335 ± 54‰ for the isoprenoids in the PS samples. Taking into account only the δD values of HI, T_{max}, and MDR values of the PS for reconstruction, the results are –164 ± 3.5‰ for *n*-C_{16} to *n*-C_{19} group and –309 ± 9‰ for isoprenoids (Figure 5.3).

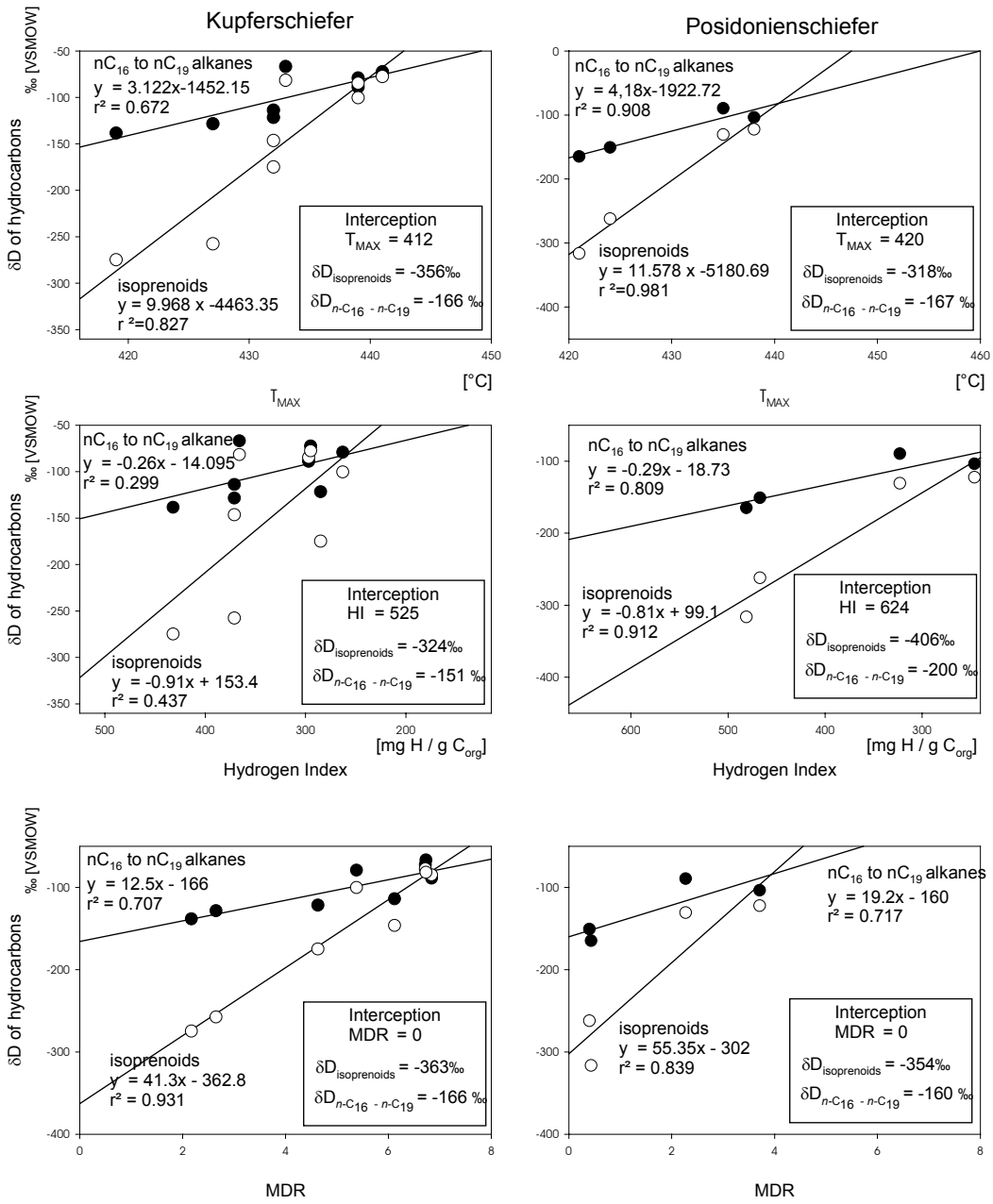

Figure 5.4. δD of hydrocarbons from Kupferschiefer deposits in the Epi-Caledonian / East European platform (circles) in relation to the MPI1 maturity index (MPI1) and δD values of hydrocarbons from Posidonienschiefer from the Vlotho Massif, Germany. MDR = O is the hypothetical non-mature sample.

In the immature, organic-rich torbanites (52 to 59% C_{org}) of Scotland and Australia, the δD values of *n*-alkanes (–140 to –230‰) and acyclic isoprenoids (–259 to –283‰) are similar to δD values of modern hydrocarbons (DAWSON et al., 2004). (DAWSON et al., 2004) based the immaturity of the type I organic matter on HI values (974 mg to 1174 mg HC / gC_{org}) and T_{max} (446 °C to 460 °C). We think that the high content of liptinite in the torbanites may be either a feature of higher resistance against hydrogen exchange in the rock matrix itself or the protection of the non-polar aliphatic hydrocarbons in the remaining organic matrix. Although the δD values

of compounds in the torbanites are very useful for palaeoclimate reconstruction, we believe that a method is needed to be able to reconstruct the primary δD values of aliphatic hydrocarbon based on a higher frequency during earth history for palaeoclimate investigations. We think our approach is important, because the availability of immature organic samples with unchanged δD values from the Palaeozoic and early Mesozoic is very limited. The ability to correct for maturity on isotope ratios of biomarkers will enlarge the number of palaeoenvironments significantly.

5.4.2 δD of isoprenoids during maturation and their synthesis

The mean δD values of phytane (Ph) and pristane (Pr) range between –275‰ in the immature and –147‰ in the mature KS samples. In the PS the range in δD values of isoprenoids is between –317‰ and –123‰ in immature and mature samples, respectively.

The mean hydrogen isotope fractionation is expressed as the mean hydrogen isotope enrichment between lipids and isoprenoids ($\varepsilon_{isoprenoids/lipids}$[6]) being –203‰ ± 67‰ between phytol – a precursor of Ph and Pr in organisms and alkanes (SESSIONS et al., 1999). $\varepsilon_{isoprenoids/alkanes}$ is –170‰ ± 13‰ in immature and –43‰ ± 26‰ in mature PS and KS samples. For the KS an $\varepsilon_{isoprenoids/alkanes}$ of –194‰ ± 29‰ can be reconstructed using the correlation of isoprenoids versus all maturity parameters. In torbanites of Scotland and SE Australia, a 60 to 80‰ difference between isoprenoids and *n*-alkanes was observed (DAWSON et al., 2004). The $\varepsilon_{isoprenoids/alkanes}$ in sediments of the Western Canadian Sedimentary Basin (WCSB) range between –56‰ and –32‰. On the one hand these differences of isoprenoids to the *n*-alkanes reflect the partial preservation of the original biosynthetic hydrogen in sediments (DAWSON et al., 2004; LI et al., 2001), on the other hand the lower D enrichment in the WSCB is comparable to that in the mature KS and PS samples suggesting an influence of maturation to the reduced difference seen in immature *n*-alkanes and isoprenoids. Enhanced hydrogen exchange in isoprenoids against that of *n*-alkanes is reflected in the δD values of more mature samples (SESSIONS et al., 2004) (see section 4.3.4).

In the sediments of the WSCB and the torbanites, the Ph is enriched in D relative to Pr by up to 24‰. In the immature KS samples, Pr is 15‰ more enriched in D than Ph. The isotopic difference indicates a different biosynthesis of the precursor or different isotope ratios of the source water from the extent biomass (DAWSON et al., 2004; LI et al., 2001). In sediments Pr can have different sources, such as, the phytol side chain of chlorophyll (TISSOT and WELTE, 1985) and bacterial tocopherol (GOOSSENS et al., 1984). Additionally, Pr can be released from

[6] Isotope enrichment factor between isoprenoids (A) and lipids (B): $\varepsilon_{A-B} = (\alpha_{A-B} - 1) \times 1000 \approx 1000 \times \ln \alpha_{A-B}$

$\alpha_{A\text{-}B}$: Isotope fractionation factor $\alpha_{A-B} = \frac{1000 + \delta_A}{1000 + \delta_B}$

polymerized compounds in the kerogen (KOOPMANS et al., 1996; KOOPMANS et al., 1999) or produced during thermal condensation (LI et al., 1995). Isotopic differences in immature samples between Pr to Ph can also be derived from the integrative addition of Pr from different sources. This effect is not preserved in the PS samples, leading us to suppose that a homogeneous supply of biomass from the same source with the same biosynthetic fractionation of Pr and Ph prevailed.

5.4.3 Possible mechanisms for observed hydrogen isotope enrichment in hydrocarbons of matured sediments

In the literature several mechanisms are described for the exchange of hydrogen in OM of sediments (ALEXANDER et al., 1982; BEHAR et al., 1995; BUTALA et al., 2000; LEWAN, 1997; MASTALERZ and SCHIMMELMANN, 2002; MICHELS et al., 1995; REDDING et al., 1980; SCHIMMELMANN et al., 2001; SCHIMMELMANN et al., 1999; SCHOELL, 1984a; SCHOELL et al., 1983). The main mechanisms proposed are: i) thermo-methanogenesis; ii) temperature-dependent thermodynamic isotope fractionation of organic compounds; iii) addition of components from the insoluble kerogen fraction to the primary pool of hydrocarbons; and iv) metallo-catalytic and / or clay catalytic hydrogen exchange with the connate or formation water ("rock water interaction").

5.4.3.1 Thermal methanogenesis

During maturation of organic compounds, the break of C-C bonds leads to free methyl radicals, which react with free hydrogen to produce methane. During low maturation, from 0.5% to 2% R_m where thermal maturation like metagenesis is less effective, 1% of the methane is released (SCHOELL, 1980). In this reaction a kinetic isotope effect with favourable linkages (where the content of isotopes of D and ^{13}C were reduced) may lead therefore to isotope enrichment.

We suppose that a consistent isotopic shift led to the D enrichment of the heavy carbon and hydrogen isotopes in the remaining alkanes. Using Rayleigh fractionation, and the hydrogen and carbon fractionation factor for the methane evolution of $\alpha-1 = 0.15$ and $\alpha-1 = 0.03$ (SACKETT, 1978) respectively, the assumed remaining isotope ratio of the carbon residue can be calculated.

Using Rayleigh fractionation processes (Equation 5.2) with two reservoirs (methane and alkanes), the respective isotopic shift during methanogenesis has been calculated (DANSGAARD, 1964):

$$R_{\text{residue}} = R_O \times f_{\text{residue}}^{(\alpha-1)} \qquad \text{Equation 5.2}$$

where R_o is the isotopic ratio of the most immature hydrocarbon and $R_{residue}$ the isotopic ratio of the remaining hydrocarbon in the specific fraction.

The turnover fraction of hydrogen and carbon of the Rayleigh fractionation model is related to the δD and $\delta^{13}C$ values of the most mature samples in the KS and PS alkanes and isoprenoids (Figure 5.5).

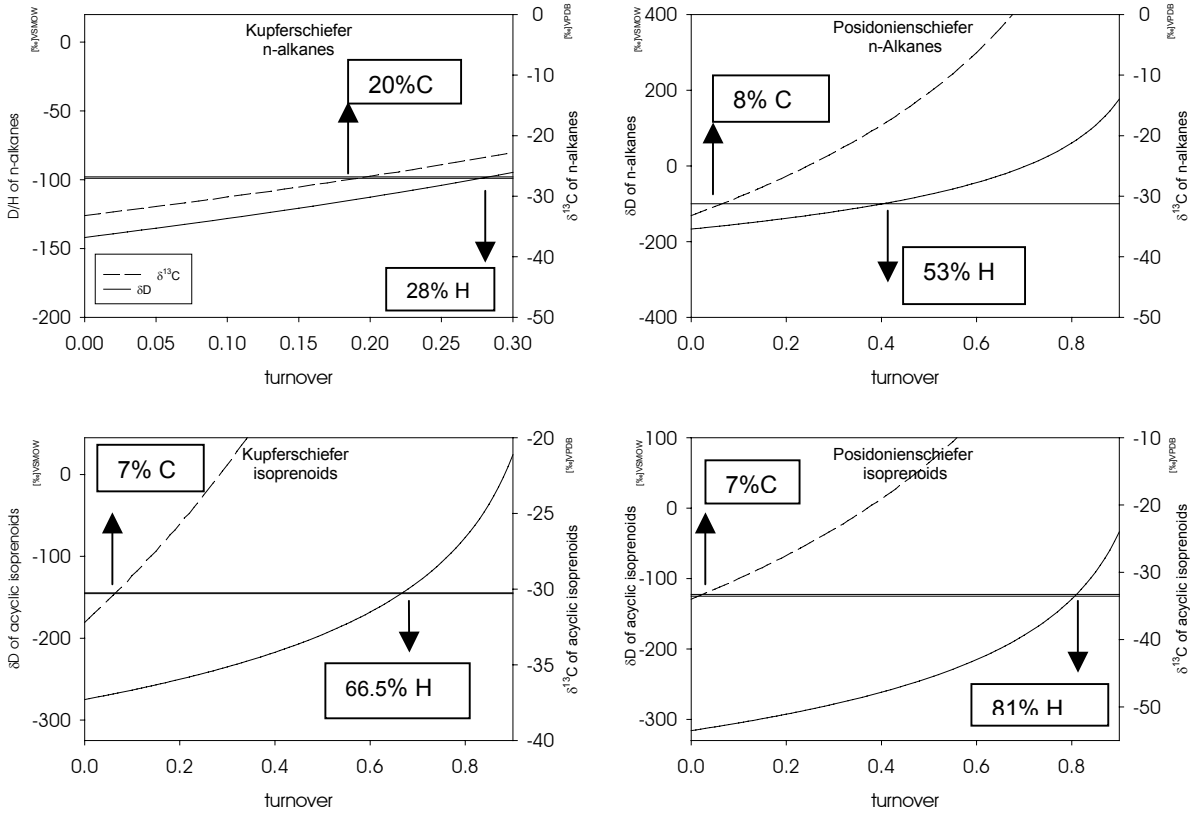

Figure 5.5. Modelled carbon and hydrogen turnover from δD and $\delta^{13}C$ values of hydrocarbons from Kupferschiefer and Posidonienschiefer deposits during thermal methanogenesis (Rayleigh fractionation). As starting values, the mean δD and $\delta^{13}C$ values of the n-C_{16} to n-C_{19} alkanes and isoprenoids from lowest matured samples were used (appendix Table 9.1). The turnover of C and H (intercept with x-axis) was determined by delta values of most matured samples. The organic hydrogen turnover rates of 53% to 81% definitely show that Rayleigh fractionation cannot be accounted for the total hydrogen exchange during maturation. For methane evolution fractionation factors of α = 0.15 for hydrogen and α = 0.03 for carbon were used (SACKETT, 1978).

Hydrogen and carbon release during methanogenesis to methane can be estimated beginning from δD values of the lowest maturity sample in the KS and PS. Except for the KS sample (20%), the turnover for carbon enrichment was less than 10% in isoprenoids and alkanes in the KS and PS samples. The release of hydrogen estimated from alkanes is lower than expected from the carbon turnover in the KS sample. In the PS 53% of H in alkanes and 81% of H in isoprenoids must have been released during methanogenesis to get the isotope enrichment in these components. Considering large differences between carbon and hydrogen turnover, and high release of hydrogen, methanogenesis cannot be regarded as the only possible isotope enrichment process. Time and temperature gradients must have contributed significantly to change organic bound hydrogen and carbon into volatile hydrocarbon gases.

5.4.3.2 Hydrogen exchange in equilibrium

In addition to the hypothesis of enhanced methanogenesis, and therefore D enrichment of the residue, a temperature-dependent thermodynamic isotope fractionation between two compounds may have been responsible for hydrogen exchange (GALIMOV, 1985)[7]. Fractionation factors α between a model normal alkane (CH_3-CH_2-CH_3) and methane are 1.032, using the ratio between thermodynamic fractionation factors (β_D) (E.M. Galimov, personal communication). Applying α to the Rayleigh fractionation for a maximum temperature of 400K, the approximately maximum D-enrichment of 60‰ in the KS would have been reached at a fraction of 60% of the primary compound degradation. Consequently, the thermodynamic isotope exchange of alkanes with methane is disregarded as a source for the D-enrichment during maturation. Exclusive thermodynamic fractionation for the exchange with water (CH_3-CH_2-CH_3/H_2O, $\beta_D = 0.940$, 400 K) would deplete the hydrocarbon components

5.4.3.3 Influence of clay minerals on the δD value of hydrocarbons

Water is generally enriched in deuterium relative to lipids by ~120‰ to 360‰ (standard mean ocean water = 0‰) and exchange reactions could explain the D-enrichment in organic compounds during maturation. ALEXANDER et al. (1984) reported a clay catalytic hydrogen exchange reaction mechanism at saturated carbons. They demonstrated in laboratory experiments that the hydrogen exchange at carbons adjacent to tertiary carbon centres is more rapid than at tertiary carbons. For clay minerals the effect of diagenetic D-enrichment is caused by similar rock-water hydrogen exchange (YEH, 1980). The δD of hydroxyl groups of clay mineral can be taken as a proxy for the palaeowater using the temperature-dependent illite-water fractionation (YEH, 1980). K/Ar ages of detrital feldspar range from 277 to 334 Ma - which is the age of the source rock of the clays - together with diagenetic neo-formed illite present in the barren zone sediments (BECHTEL et al., 2000b). The δD value of hydrogen from the hydroxyl group of illitic clays (< 2 µm) from barren KS samples ranged from –64‰ to –74‰ for the samples (BECHTEL et al., 2000b), which were investigated for the δD value of hydrocarbons, suggesting an origin from meteoric waters. If the hydrogen exchange of formation or connate water from basin brines had occurred in the illitic clays of the barren zone, the δD of illitic clays would have changed its value significantly during diagenetic equilibrium fractionation. The δD values of illitic clays

[7] $\beta_{A/B}$: Thermodynamic fractionation factor between two compounds. The temperature related equilibrium isotope fractionations α of mono-substituted forms are related to calculate the thermodynamic equilibrium fractionation factor of components ($\beta_{A/B}$). $\beta_{A/B} = \alpha A/\alpha B$.

show no significant relation to the δD values of alkanes or isoprenoids (Figure 5.6). In comparison to the D-depletion of isoprenoids in the low maturity sediments, the δD value of clays of these samples is within the range of the other clays of the barren zone. Because an exchange of hydrogen from the connate or formation water with the organic and inorganic hydrogen is expected to be reflected in the δD of both components, we assume that the D-enrichment in the hydrocarbons of the KS is not primarily affected by organic hydrogen exchange with formation or connate water.

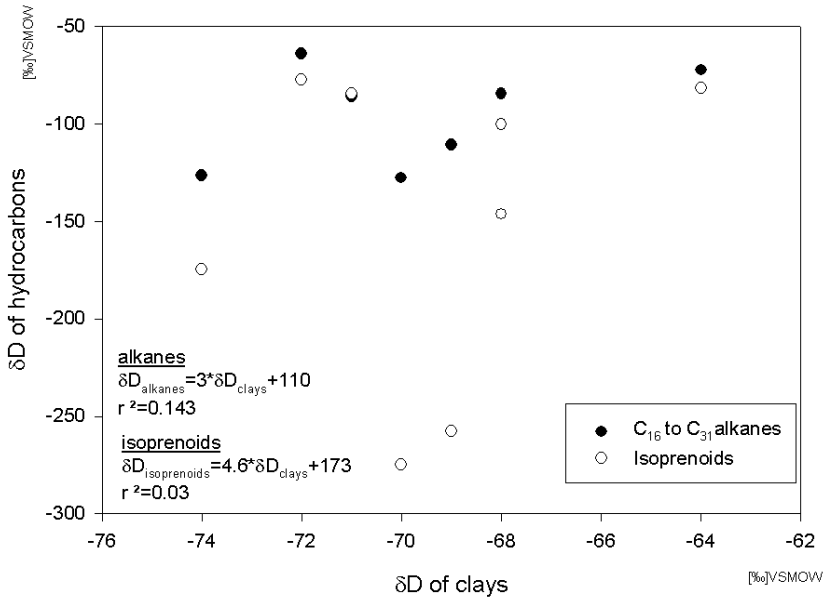

Figure 5.6. Correlation diagram between δD of hydrocarbons and δD of clay mineral hydroxyl groups of the Kupferschiefer samples. δD values of illitic clays (BECHTEL et al., 2000b).

5.4.3.4 *Influence of heat transfer on D enrichment in hydrocarbons*

Thermodynamic fractionation, reaction with water, and thermal cracking does not seem to be important for the observed large enrichment in hydrocarbons. Isotope fractionation during reaction with water can also be ruled out, because enhanced exchange with water in isoprenoids should result in more positive isotope ratios than the δD values of alkanes. From low carbon turnover in hydrocarbons, we conclude that cracking is a minor process for enrichment. Cracking would affect the isotope ratio in the same range that it influences the δD of hydrocarbons. Moreover, this would not explain the enhanced fractionation in acyclic hydrocarbons. The higher percentage of hydrogen exchange in isoprenoids could, however, be explained by higher D enrichment in this compound class due to lower bond-dissociation energy in tertiary-linked C-H bonds. Organic hydrogen bound in these tertiary positions constitutes 11% in Pr and 8.33% in Ph of the total incorporated hydrogen. The same conclusion could be drawn from the difference in C/H ratios between short- and long-chain alkanes (0.47 for *n*-C_{16}, 0.58 for *n*-C_{29}), enhancing the

influence of deuterium enrichment in the short-chain alkane range compared to the long-chain alkanes. However, this effect was not observed in the present study, although the lower enrichment gradient in the KS might be evidence for this effect. Enhanced fluid migration might explain the general linear D-enrichment of hydrocarbons due to temperature in the KS and PS. The lighter hydrogen isotope would remain by higher adsorption in the residual hydrocarbon fraction during kinetic fractionation (geochromatographic effect). One fact that seems to be evident for this process is that closed systems like the source rock deposits of the KS, where the adsorption is reduced, were not affected by enhanced D enrichment. On the other hand, we assume that heat transfer would have had an influence on the different reaction rates in isoprenoids and alkanes, and would have influenced the isotope exchange rate of these compounds (SESSIONS et al., 2004). The less enriched δD value of isoprenoids compared to alkanes would be a consequence of these different reaction rates. Enhanced heat transfer occurs if sediments are near to a heat source or during long term and deeper burial. Consequently, the different heat transfer rates in the KS and PS sediments were expressed by different and divergent isotope enrichments in alkanes and acyclic isoprenoids. The role of water is seen as the main influence, together with other inorganic catalysts, of newly generated hydrocarbons (SEEWALD, 2003). Our results rule out the influence of water on the δD of linear hydrocarbons. The different heat regimes of the KS and the PS suggest that a hydrogen exchange is significantly influenced by temperature, lithostatic conditions in the sedimentation area, and time. These factors influence the activation energy of different C-H bonds, alkanes, and isoprenoids, and can be seen as the driving forces for organic hydrogen exchange rates and the production of hydrocarbon gases (CO_2, CH_4).

5.4.4 Reconstruction of δD values of initial source water

Applying the lipid/water isotope fractionation factors ($\varepsilon_{l/w}$) of –160‰ for individual alkanes (SESSIONS et al., 1999), we reconstructed an initial δD value of *marine source water* of 0‰ for the KS Basin using the intercept with the y-axis of the short-chain alkane maturity correlation. For the least mature sample No. Be42, we calculated a δD value of –3.5‰ using the δD value of the *n*-C_{17} alkane as biomarker for aquatic biomass. $\delta^{18}O$ values of dolomite from the KS samples (BECHTEL et al., 2000a) were used to calculate the $\delta^{18}O$ of the marine source water, taking the temperature-dependent isotope equilibrium fractionation of dolomite against seawater (MATTHEWS and KATZ, 1977). An equilibrium temperature between 15 and 25 °C was used to derive the $\delta^{18}O$ of seawater with –1.8 ± 0.9‰ (15 °C) to 0.4 ± 0.9‰ (25 °C) for the KS samples, assuming constant local salinity. The typical surface water temperature in the Black Sea averages 14.5 °C to 15 °C (SWART, 1991). The reconstructed δD and $\delta^{18}O$ values of these samples imply

that the KS Basin must have been less evaporative than the recent Mediterranean Sea where δD and $\delta^{18}O$ values of +8‰ and +1.7‰ at a salinity of 38.9 are observed (GAT et al., 1996).

δD values between –20‰ and –40‰ of Permian *meteoric water* in the KS from Poland are calculated from the illite/water fractionation at ambient temperature (25°C, $\delta^{18}O$ = -3.5 to -6.5‰) (BECHTEL et al., 2000b). The δD of the illite clay reveals that δD values of Permian precipitation and the δD of marine source water are available from alkanes. The reconstruction of the $\delta D/\delta^{18}O$ relationship from illitic clays is indicative for meteoric water known from temperate climate regions and similar to the modern global meteoric water line ($\delta D = +8.17\times\delta^{18}O + 11.27$‰ VSMOW). We conclude that the KS Basin water in comparison to recent arid to semi-arid lagoonal areas was under a less arid influence. We also conclude that the basin was under less influence of evaporation and that the reconstructed oxygen and hydrogen isotope values of precipitation of the hinterland area are typical for recent rain shadow areas of mountain ranges under monsoon influence (E-W gradient in S-India ground water: $\delta^{18}O$ = –0.3 to –5‰; δD=+3.7 to –38.4‰) (DESHPANDE et al., 2003). Summer wet monsoon precipitation on the east coast of the Pangean continent had a similar effect during the Wordian (KUTZBACH and ZIEGLER, 1993; REES et al., 1999). In comparison to the influence of monsoon climate on the eastern Middle European basin surface waters, the western basin was more influenced by arid climates of the Pangean interior. Consequently, an isotopically depleted freshwater source could have supplied D-depleted KS surface water in the eastern basin.

The calculations from the reconstruction of primary source water led us to suppose that the correlation of δD of hydrocarbons from KS can be applied as a correlation function to calculate the δD value of primary biomass during deposition and the reconstructed δD of the source water (δD_c of water). Although the influence of maturation was different in distinctive thermal environments, as indicated by the rather unchanged δD values of the PS occurring at R_c[8] = 0.48%, the KS maturity indices might be useful for thermal gradients in an area with low geothermal gradients in sediments of Palaeozoic origin such as continental shields.

5.5 Conclusions

1. Compound specific hydrogen isotope values of *n*-alkanes and acyclic isoprenoids in matured sediments of the KS (Wuchiapingian) and the PS (Lower Toarcian) correlate in similar ways to several maturity parameters. These correlations allow extrapolation of the δD values of *n*-alkanes and isoprenoids to their original values.

[8] R_c: Calculated vitrinite reflectance from the correlation of MPI 1 to R_m; $Rc=0.6\times MPI1+0.4$.

2. The activation energy of different C-H bonds led to different deuterium enrichments in the two compound classes. Different timescales and temperature regimes during burial of sediments in the KS and the PS led to different hydrogen fractionations within the same compound class.

3. Applying a linear relationship to correct δD values of alkanes and acyclic isoprenoids for sediment maturity reconstitutes the biosynthetic differences (–203‰) among phytol-derived acyclic isoprenoids and normal alkanes known from modern analogues,

4. After correction, palaeohydrological information can be obtained from the δD values of the KS sedimentary biomarkers. The corrected biomarker δD values led to realistic reconstructed δD values of source water and plot in the range of marine seawater,

6 Hydrogen isotope reconstruction of the water cycle of equatorial, continental deposits of the Upper Carboniferous to the Lower Permian and in marine deposits of the Upper Permian and Middle Mesozoic (Central Europe)

6.1 Introduction

Global climate changes and environmental properties influence δD values of organic biomass deposited in near equatorial, terrestrial ecosystems during the Late Palaeozoic like the Saar-Nahe Basin (SNB), Döhlen Basin (DB), and the Lodève Basin (LB). For comparison the shallow marine Kupferschiefer (KS, Upper Permian) and Posidonienschiefer (PS, Lower Jurassic) were studied, which are also situated in the central European part of northern Pangea.

Local influence on the δD of biomass during formation of sediment depends on plant specific evolution, changes of reconstructed atmospheric properties (air mass circulation, CO_2 content, precipitation, evaporation), regional and global orographic evolution and connected sea or lake level changes. In spite of the existence of shallow shelf complexes or short-term sedimentary changes in marine environments the global or local changes of water masses or physical and chemical sediment properties of full marine areas are rather stable for a long time period compared to terrestrial palaeoenvironments. Marine, in particular offshore environments intergrate physical and biochemical signals over longer time periods than terrestrial ones.

Especially, coals and terrestrial sediments rich in organic matter have been used as a record to follow palaeohydrological changes within terrestrial environments (CECIL et al., 1985). The δD of kerogen has been used to gain information about the hydrology of lake surface waters (HASSAN and SPALDING, 2001), but investigations of short-term processes in old sediments such as variations of ground water levels, lake level changes or closure of water inlets or outlets are missing. Such processes will differentiate open or closed lakes and must have an effect on the δD of lake water. In particular, coal swamps are also influenced by very dynamic local environmental changes. In order to distinguish long-term or even global impacts from short term changes on the δD of organic matter in a coal environment the effects of meteoric waters on a single stratigraphic unit or coal seam need to be investigated.

Investigations of the δD values of biomarkers in continental deposits are a valuable tool to follow climate changes and stabilities in the biosphere and atmosphere related to the global climate interactions between tropical and polar regions and have been applied to the Palaeozoic (FLUTEAU et al., 2001; OTTO-BLIESNER, 1998; TABOR and MONTANEZ, 2002). δD of biomarkers may explain shifts in $\delta^{13}C$ and $\delta^{18}O$ values of brachiopod carbonate in marine settings

(BRUCKSCHEN et al., 1999) and $\delta^{13}C$ values of organic matter (SCHEFFLER et al., 2003) already known from investigations of marine environments. However, difficulties arise to exactly resolve the time relationship of strata from different regional sites (MENNING, 2001; MENNING et al., 2001; SCHNEIDER, 2001). Synchronous stratigraphic time markers (e.g. volcanic ash layers) are rare or even non-existent. Magnetostratigraphic / lithostratigraphic units and absolute time markers are often obscured due to local events and are difficult to correlate in a global context (STOLLHOFEN, 1999). Biostratigraphic classification becomes a difficult task because of the high acidity, high oxidation risk and low preservation potential in terrestrial environments.

6.1.1 Palaeogeography and palaeoclimate during icehouse-greenhouse conditions in the Upper Palaeozoic

During the Late Palaeozoic the Permo-Carboniferous glaciation of the southern hemisphere persisted from 330 to 275 Ma with its largest extent at the end of the Westphalian (VEEVERS and POWELL, 1987). Based on model results a maximum ice volume of four times (150×10^6 km^3) compared to the Pleistocene glacial maximum (35×10^6 km^3) has been calculated. The onset of glaciation was initiated by the continental configuration with a large landmass moving across the south pole (CROWLEY et al., 1987) accompanied by a CO_2 concentration compared to recent levels and a solar luminosity 3% to 2.25% less than today (CROWLEY and BAUM, 1992). The Devonian to Carboniferous period was characterized by a decrease in CO_2 content in the atmosphere as a consequence of colonization of the continents by land plants since the Middle Devonian and fixation of atmospheric CO_2 into terrestrial biomass. Therefore, CO_2 as forcing factor for the net radiation in the atmosphere was reduced (BERNER, 1997). The decreased solar luminosity would result in a ~ 4 °C less global mean temperature (CROWLEY, 1994). The Permo-Carboniferous glaciation terminated when the continents Laurussia, Siberia and Gondwana formed the supercontinent Pangea during Early Permian.

The characteristics of climate evolution, the associated response in global plant distribution as well as ice extension and volume have been modelled in specific icehouse and greenhouse states during the late Palaeozoic and Pangea configuration of the Mesozoic (ZIEGLER, 1990). Because of plant evolution the CO_2 content of the atmosphere decreased from the Early Carboniferous to values similar to Recent ones. During the Westphalian / Stephanian a warming phase is indicated by the occurrence of glacial marine sediments and tillites restricted to higher latitudes (FRAKES et al., 1992) and a global sea level rise (VISSER, 1997). This warming phase during Permo-Carboniferous icehouse conditions might reflect major modifications of the atmospheric circulation system with higher global mean atmospheric temperatures (BERNER, 1994). Higher atmospheric flow to the western Euramerica is taken as an indicator of cross-equatorial flow with monsoon rainfall at the western coastline of the Gondwana continent (KUTZBACH and

GALLIMORE, 1989). Changes in atmospheric circulation could be followed by increased palaeowind intensities to the inland of western Pangea (SOREGHAN et al., 2002) and increased aridity derived from isotope and mineral proxy data of pedogenic carbonates and clays (KÖRNER et al., 2003; TABOR and MONTANEZ, 2002; TABOR et al., 2002). Plant associations and plant species distribution in the equatorial Euramerica reacted to ecological shifts on the continent (CECIL et al., 1985; DIMICHELE et al., 1996; DIMICHELE and PHILLIPS, 1994; KERP, 1996; PHILLIPS and KOCH, 2002). Consequently, these processes culminated in the global extinction of Lycopsids as a major plant group during the Stephanian. (GASTALDO et al., 1996).

Discrepancies in the reconstruction of palaeogeographic position of landmasses (Figure 6.1) will exert a crucial impact on climate models (Figure 6.1). For the Late Palaeozoic palaeomaps available, a longitudinal expansion of the west Pangea coastline (GOLONKA and FORD, 2000; SCOTESE, 1997) stands in contradiction with a 3000 km displacement of Gondwana towards the east (FLUTEAU et al., 2001; TORCQ et al., 1997). The resulting discrepancies in the size of the Tethys Ocean will cause large differences in the energy budget of the Tethys seawater and its current regime. Due to the intense coupling of marine and atmospheric flow regimes large differences in continental climate evolution will result depending on the selection of the palaeogeographic reconstruction.

Palaeoaltitudes of prominent mountain chains and mean elevations in continental areas during Late Palaeozoic are elusive for the quantification of temperature and precipitation distribution on the Pangea continent. Humid and arid climate prevail on the windward or lee side of mountain chains. Additionally, tight coupling of cold upwelling systems with low humidity transport of air masses to the land and the rain-shadow effect behind a mountain range caused low humidity in lower atmospheric layers.

Driving factors for monsoon circulation are up-lift of air masses and intensification of latent heat release during passage of air over land. As a result precipitation would have been increased due to differences in the land / ocean air pressure systems (KUTZBACH and GALLIMORE, 1989; OTTO-BLIESNER, 1998; PARRISH, 1993; ROWLEY et al., 1985). The northern hemisphere monsoon circulation of Pangea from the Early Permian to the Late Permian is thought to be intensified due to enhanced cross-equatorial atmospheric transport concomitant with an intensification of the equatorial low pressure system. The increase of precipitation at the wind-associated side of the equatorial Alleghenian / Hercynian mountain chain reduced precipitation in adjacent lowlands and the lee side. The consequence of this circulation change is the pattern of wet and dry climates during Early Permian.

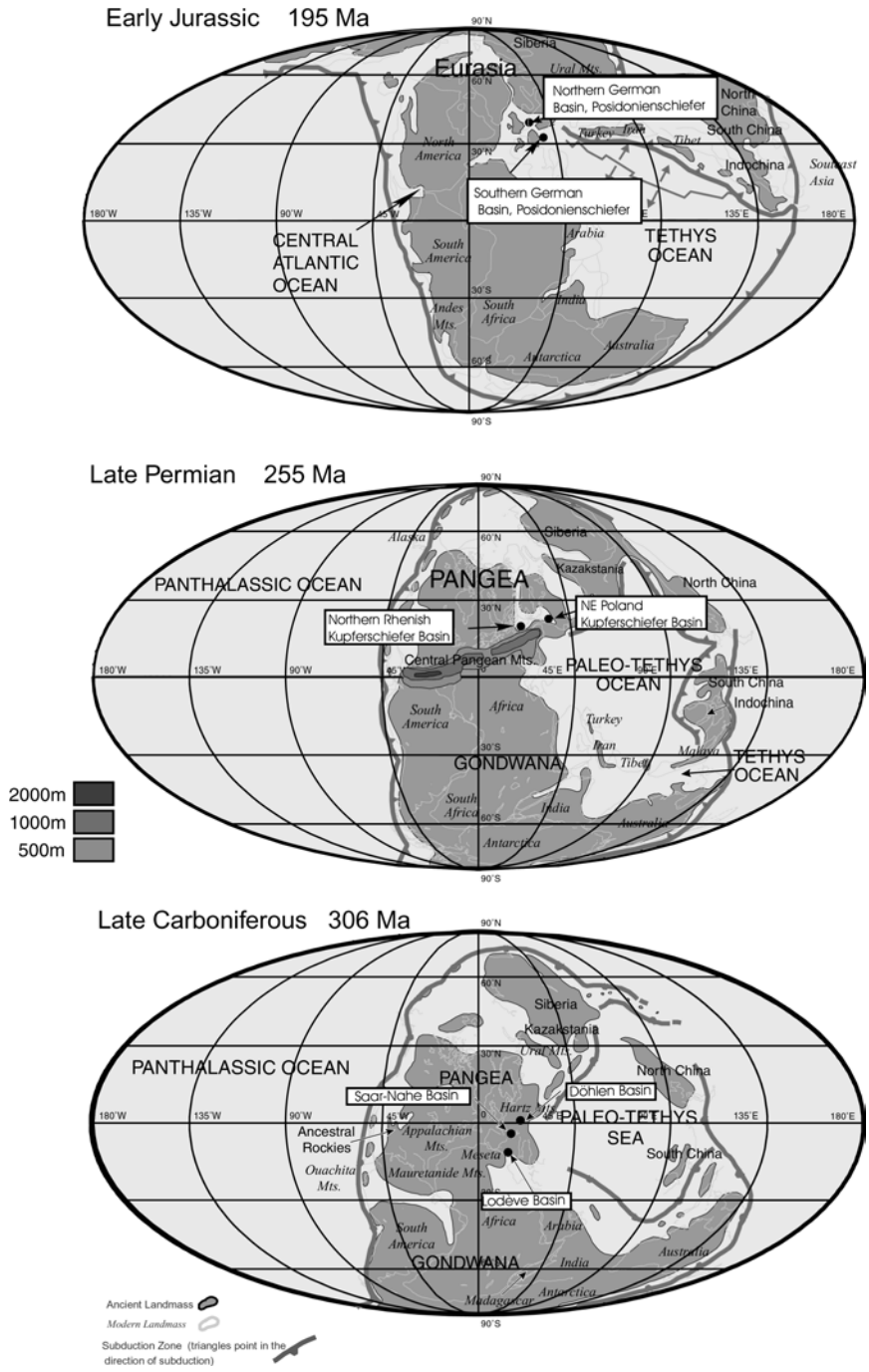

Figure 6.1. Palaeogeographic reconstructions and atmospheric circulation properties of the Late Carboniferous, Late Permian and Early Jurassic. Base maps with continental distribution and tectonic elements are from SCOTESE (1997). Late Permian Alleghenian / Hercynian mountain extension and height at Late Permian are from FLUTEAU et al. (2001). For further explanation see text.

6.1.2 Palaeogeography and palaeoclimate

6.1.2.1 *Continental climate reconstruction from Permo-Carboniferous deposits*

The approach of this study is to test whether the application of hydrogen isotopes of biomarkers in a sequence of sediments from Central European lakes and intermontane coal systems (Saar-Nahe Basin SNB, Döhlen Basin DB, Lodève Basin, LB) can be compared to other climate proxies and modells in the continental area of Euramerica (Figure 6.2, Figure 6.3). Investigations from the western Euramerica already show that a climate change from a Permo-Carboniferous icehouse into a Late Early Permian greenhouse is coincident with a shift of oxygen isotopes from hydroxyl groups of soil clays to more ^{18}O enriched values (TABOR and MONTANEZ, 2002; TABOR et al., 2002). This indicates a major drying of the equatorial belt of the Laurasia continent (Euramerica) associated with increased wind velocities and shifts in main wind directions (SOREGHAN et al., 2002). A continent wide shift from latitudinal western atmospheric circulation occurred during the Middle to Upper Permian. The shift to monsoon circulation patterns induced a change in the precipitation pattern and therefore its hydrogen isotope content. Monsoon circulation affected the amount of precipitation due to the influence of the equatorial Variscid / Hercynid mountain range, which acted as a topographical barrier to draw moisture further into the continental hinterland (HAY et al., 1990; OTTO-BLIESNER, 1998). These climatic patterns should be transferred into the δD of biomarkers from organisms that incorporated water upon biosynthesis of organic matter.

6.1.2.2 *Palaeozoic-Mesozoic marine deposits*

The Kupferschiefer of NE Polish (NPB) and the Lower Rhine Kupferschiefer Basin (LRB) is representative for a major marine ingression into a restricted shelf basin short above the base of the Upper Permian (260 Ma). Lagoonal to lower shelf water depths were characteristic for the western LRB and for the NPB (BECHTEL and PÜTTMANN, 1997; OSZCZEPALSKI and RYDZEWSKI, 1987). Additionally the two depositional areas were under different climate influence from the hinterland, with more arid influence from the continental interior of Pangea in the western part and more influence from monsoon precipitation in the eastern part of the Pangean continent. The PS must have had similar organic sedimentary properties like the KS with a high contribution of organic matter from a stratified water column. In contrast to the KS the upper water column of the PS in the North and Southwest-German Basin received variable influx from either the Mediterranean tropical Tethys or the polar Arctic Ocean (FRIMMEL et al., 2004; RÖHL et al., 2001a). Although a longitudinal seaway existed during the Lower Jurassic the area of PS

deposition was separated into two sub-basins with a connection to the Tethys Ocean over a wide carbonate shelf sea area during the Lower Jurassic (LITTKE, 1993; ZIEGLER, 1990). One objective of this study was to evaluate whether different hydrogen isotope ratios of water masses can be reconstructed via the δD of *n*-alkanes of the marine biomass. Additionally it was focused on the investigation whether local freshwater run-offs have reached the surrounding PS Sea from land areas, e.g. Rhenish Massif, the Bohemian Massif the Vindelician Highland. It can be expected that the δD of biomarkers should reflect these dissimilar water mass properties by more D-enriched values in the evaporative LRB and the less freshwater influenced PS samples.

6.2 Geological setting of the marine and continental deposits

6.2.1 Intermontane basins of Central Europe from the Late Carboniferous to the Early Permian

The equatorial continental region at the eastern Pangean side can be compared to lakes in the recent East African rift systems. Extensional tectonics activated a system of transfer faults on equatorial western Pangea (STOLLHOFEN, 1998). Consequently, on the eastern side of Pangea several intermontane basins developed in Central Europe from southern France to East Germany at approx. 10°N enclosed by or related to structural heights (i.e. SNB: Rhenish Massif "Rheinisches Schiefergebirge"). In this study, sediments of three different intermontane basins were investigated: the Westphalian D / Stephanian A sediments of the SNB (Frankfurt, Germany), the Gzhelian/Asselian sediments of the DB (Dresden, Germany) and to sediments of the same age in the Lodève Basin (SE France).

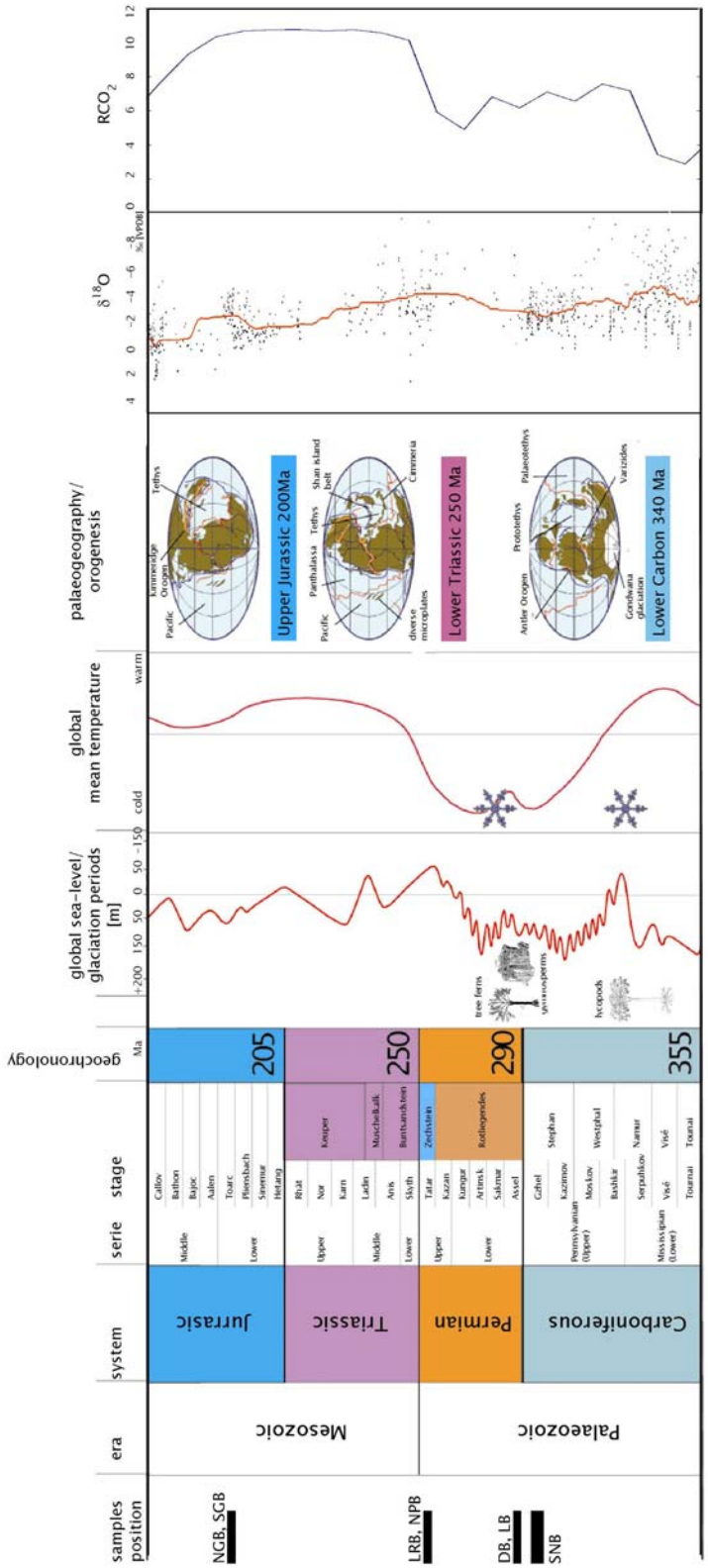

Figure 6.2. Stratigraphic distribution of samples and their relation to palaeoclimate data. Time scale (HARLAND et al., 1990), global sea-level (VAIL et al., 1991), globale mean temperature (FRAKES et al., 1992), oxygen isotope ratios of samples (VEIZER et al., 2000); RCO2 (BERNER, 1994). NGB: Northern German Posidonienschiefer Basin, SGB: Southern German PS Basin, NPB: North-East Polish Kupferschiefer Basin, DB: Döhlen Basin, LB: Lodève Basin, SNB: Saar-Nahe Basin.

6.2.1.1 Saar-Nahe Basin

The largest of the intermontane basins is the Saar-Nahe Basin situated between the Rhenohercynian and Saxothuringian zone in different tectonic stages (HENK, 1993). Deposition and facies changes in the different formations (e.g. coarse grained fluvial deposits Westphalian A; fluvial to lacustrine coal deposition, Westphalian B; braided and meandering river sedimentation, Westphalian C; fluvial-deltaic sedimentation, Westphalian D).

The present study is focused on the transition from the Westphalian D to the Stephanian A. The Westphalian D (Heiligenwald-Fm.) contains fluvio-lacustrine sediments alternating with braided fluvial deposits. The tectonic reorganization between the Westphalian D / Stephanian A led to the reorganization of the drainage pattern of the basin indicating a depocenter shift from the SE to the NW during the Stephanian (SCHÄFER, 1989). In between sedimentation ceased during phases of erosion (Cantabrian hiatus, 3.6 Ma to 2.2 Ma) postdated by the Holzer conglomerate (BURGER et al., 1997). During the Stephanian A clastic lakes with lacustrine and swamp environments developed, river sedimentation succeeded (Heusweiler Formation).

We here focus on sediments with organic contents (C_{org}) between 2.2% to 80.4% $C_{org.}$ Selected deposits are from the Westphalian D / Stephanian A transition, because major plant evolutionary steps occurred at this interval. The sediments are associated to a major first drying interval of the tropical equatorial Euramerica (CECIL, 1990; CECIL et al., 1985; DIMICHELE et al., 1996; DIMICHELE et al., 2001; DIMICHELE and PHILLIPS, 1995; DIMICHELE and PHILLIPS, 1996; DIMICHELE et al., 1985; GASTALDO et al., 1996; PHILLIPS and PEPPERS, 1984). The approach for the Saar-Nahe Basin was to investigate a sequence from the Westphalian to the Stephanian in order to understand the pattern of changes in plant associations as well as their link to tectonically driven basin development and hydrology. After Parrish (1993), availability of moisture in the lowland tropics was influenced by monsoon circulation during Late Westphalian and increased seasonality and aridity began at the Stephanian A, when the Euramerian area moved from ever-wet equatorial to subtropical position (ZIEGLER et al., 1997).

6.2.1.2 Döhlen Basin

The intermontane Döhlen Basin (Döhlen Basin; Rotliegend, Gzhelian-Sakmarian) extends over 6 × 22km and is situated southwest of Dresden, SE Germany. The investigated sediments of the Döhlen Formation (Gzhelian-Asselian), Stephanian C to Lowest Lower Rotliegend belong to the second depositional meso-cycle with sub-cycles of palustrine to lacustrine sand to siltstone fininig-upward sequences (ALEXKOWSKY et al., 1999; SCHNEIDER, 1994; SCHNEIDER et al., 1999). Each of the sequences is terminated by coal deposition. From seam 3 (0.5 m to 1.3 m thickness) the samples No. Z2 (basal seam) and No. Zauk II/b (central seam) were taken and from seam 5 (4 m to 6 m thickness), in stratigraphic order, the samples No. W874 and No. W669

(REICHEL, 1984). Organic carbon content of the samples is between 6% and 36%. Laterally changing facies patterns of organic sediments are characterized by gyttja, channel-boghead coals and sapropelites.

6.2.1.3 Lodève Basin

The intermontane LB in SE France (26 × 10km) filled by continental deposits of Lower Permian (Asselian / Sakmarian) to possibly early Upper Permian age (KÖRNER et al., 2003). From the base to the top the LB is subdivided into the Usclas St. Privat (fluvio-lacustrine, semi-humid), Tuilières-Loiras (fluvio-lacustrine, semi-humid to semiarid), Viala (alluvial, semi-arid), Rabéjac and the Salagou Formation (pediplain and playa, semi-arid) (GAND et al., 1997). The investigated organic rich black-shales (3% to 10% C_{org}), SP48 and UB X, belong to the first two Lower Permian units.

The carbonaceous, horizontally laminated sample SP48 origins from the top of the Usclas St. Privat Formation, the second sample comes from the Tuilières-Loiras Formation (Usclas du Bosc, sample UBX). During the deposition of the Uslas St. Privat Formation (Asselian / Sakmarian) a subtropical semi-humid climate prevailed with typical dominance of meso- to xerophilous conifers in the floral associations. In the Tuilières-Loiras a transition from black-shale containing fining upward sequences (gray facies) to a red facies type with hydromorphic palaeosoils took place. This indicates a transition to dryer climate situations with a near surface groundwater level in a distal flood plain environment.

6.2.2 Late Palaeozoic and Middle Mesozoic marine deposits

6.2.2.1 The Kupferschiefer

The two samples from the Upper Permian KS (Wuchiapingian) were in particular selected from the western "Lower Rhine Kupferschiefer Basin" (LRB; No. 957515) and from the North East Polish Basin (No. Be 42), because these samples were deposited in distinctive basins with shallow lagoon environment in the western basin and shallow shelf in the eastern Polish area of the basin (BECHTEL and PÜTTMANN, 1997; OSZCZEPALSKI and RYDZEWSKI, 1987).

6.2.2.2 The Posidonienschiefer

A similar approach has been applied taking two samples from the PS of the Northern German Basin (NGB, No. DH44) and the Southern German Basin (SGB, No. 950874). This should facilitate reconstruction of possible changes in the Deuterium content of water masses via the δD of *n*-alkanes.

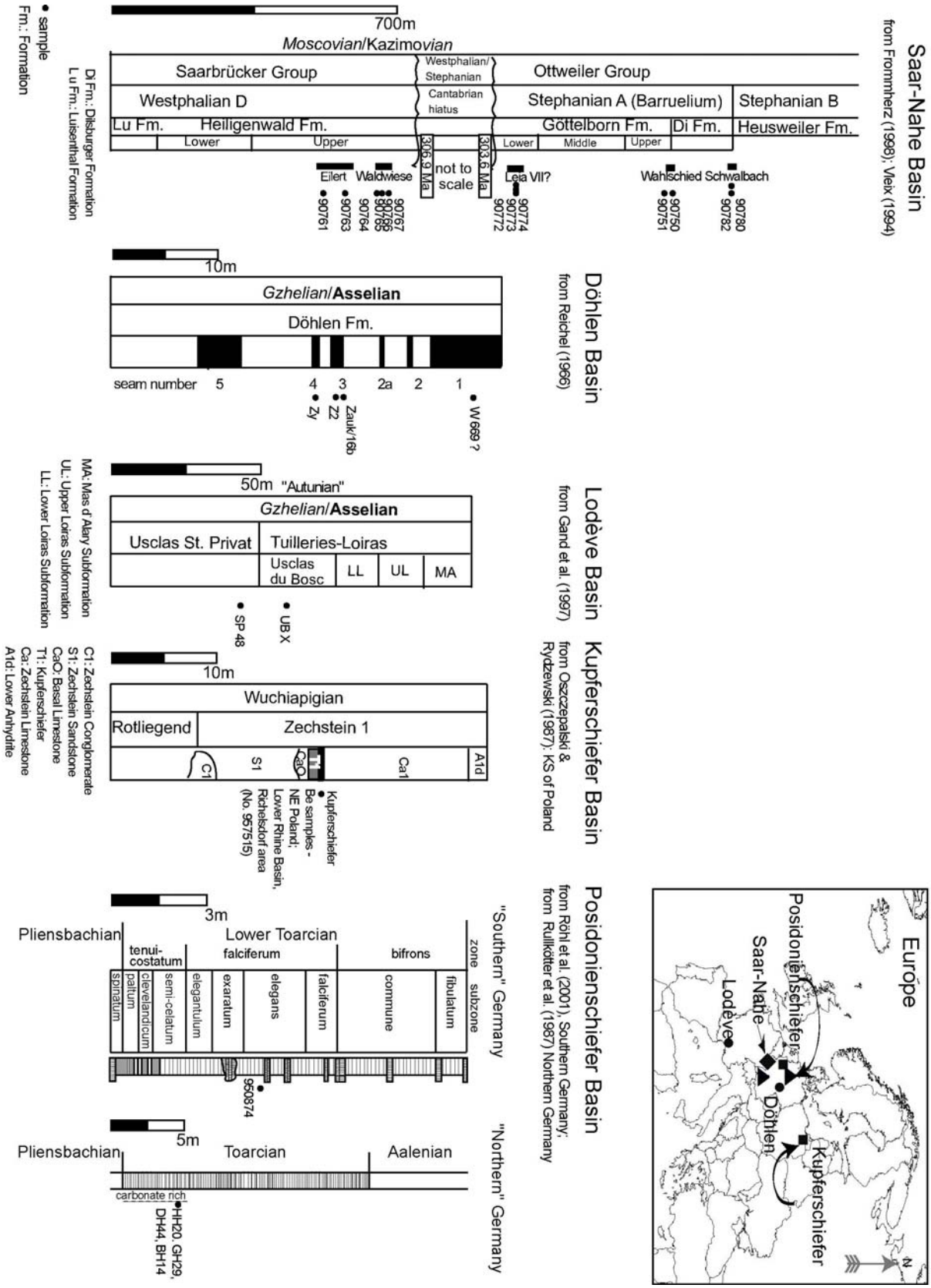

Figure 6.3. General Stratigraphy of sample sets.

6.3 Methods

6.3.1 Sample preparation

Two LB and two of the DB samples are un-weathered outcrop samples taken according to organic-geochemical standards. The SNB, KS, DB and Posidonienschiefer (PS) samples are borehole samples. Two aliquots were taken for elemental analysis (Rock-Eval analysis, N_{tot}, C_{org}, carbonate content, bulk isotope analysis of $^{13}C_{org}$ and $\delta^{15}N$) and for the organic solvent extraction of the lipid fraction. For compound specific analysis of sediments the organic solvent extract was separated into the saturated hydrocarbon fraction (45 ml hexane), aromatic hydrocarbon fraction (35 ml chloroform) and heterocomponents fraction (N, S, O components) (40 ml methanol) using pre-conditioned, pre-cleaned silica gel (KG60, 0.040-0.063 mesh-size, VWR International GmbH, Germany, VCR, Europe). No molecular sieve separation of *n*-alkanes from the lipid fraction was used to avoid the loss of *n*-alkanes greater than n-C_{18} during cleaning. Resulting amounts of the aromatic fractions were too low to be used for further compound specific isotope analysis, but used for quantification of phenantrenes in the samples.

6.3.2 Quantification of elements

The elemental analysis of organic and inorganic C, S, N has been performed by use of vario EL elemental analyzer (Elementar Analysensysteme GmbH, Hanau, Germany). After determination of the total elemental content aliquots of bulk sediment samples were treated with HCL and rinsed with distilled water until acid-base neutralization. The remaining inorganic carbon-free sediment was used for determination of bulk isotope-ratios ($\delta^{15}N$ and $\delta^{13}C_{org}$) and for measurement of the total organic C (C_{org}) and total nitrogen content (N_{tot}).

An amount of 20 mg to 200 mg bulk sediment (depending on the amount of C) was combusted with O_2 and WO_3 as chemical catalysts at 1150 °C to CO_2, H_2O, NO_x and SO_3/SO_2. Reduction to remaining reaction gases (CO_2, N_2, SO_2) was reached with elemental Cu at 830 °C in a reduction tube. Each analysis was done by triplicate and checked by inter-laboratory standardization.

Organic facies and maturity indices[9] (T_{max}, S1, S2, oxygen index (OI) and hydrogen index (HI)) of the samples were determined by Rock-Eval pyrolysis following standardized procedure (see appendix Table 9.2) (ESPITALIÉ et al., 1985). VLIEX (1994) determined the maturity index (see

[9] S1, S2, T_{MAX}, OI, HI are determined by online Rock-Eval pyrolysis of a bulk sample using a temperature gradient. S1: free hydrocarbon (HC) amount [mg HC/g], S2: pyrolysable hydrocarbons [mgHC/gC], T_{MAX}: temperature of maximum pyrolysate yield (S2 peak top), OI: [g CO_2 / g C_{org}], HI [S_2 / g C_{org}]: HI and OI are normalized to the organic carbon contents of the samples.

appendix Table 9.2), methyl phenantrene index, MPI1[10], of the SNB samples. MPI1 from KS samples are adopted from BECHTEL et al. (2000a). MPI1 values for PS samples were calculated from vitrinite reflectance data according to the relationship of MPI1 values against reflectance data (RADKE, 1988). MPI1 values of Döhlen and Lodève Basin samples were determined by GC/MS in the aromatic hydrocarbon fraction.

6.3.3 Isotope ratio determination of δD and $\delta^{13}C$ values

The lipid fraction of the bituminous solvent extract was separated in a GC coupled directly to an IRMS (Delta^{PLUS}XL, Thermo Electron (Bremen) GmbH, Germany) and an organic mass spectrometer (Thermo Electron (San José, USA)). The details of the GC separation to determine $\delta^{13}C$ and δD values of compounds and to establish the analytical range for hydrogen isotope measurement is published elsewhere (RADKE et al., in press). For carbon and hydrogen isotopes of hydrocarbons, the non-polar fraction was resolved in three replicates for isotope ratio reporting of data bracketed with three standard mix runs.

The H_2 pressure dependent H_3^+ formation is corrected using point-wise peak detection of the masses 2 and 3. A H_3^+ factor of 7.71±0.8pA^{-1} (n=25, 42 days) reflects high stability during sample analysis and has been determined daily. $\delta^{13}C$ and δD values of hydrocarbons and H_3^+ factors were measured using individual background detection (IsodatNT^{TM}, ver. 1.75, Thermo Electron (Bremen) GmbH). The δD values of *n*-alkanes (*n*-C_{10} to *n*-C_{30} alkane) and squalane (*i*-C_{25}) standards were standardized against VSMOW in an elemental analyzer coupled to an IRMS system (Delta^{PLUS}XL). For gas chromatographic hydrogen isotope analysis compounds were pyrolysed at 1450°C in an empty Al_2O_3 reactor (HILKERT et al., 1999).

For the external calibration of $\delta^{13}C$ values of compounds the $\delta^{13}C$ value of caffeine (Alj-1) was calibrated against VPDB in an elemental analyzer IRMS (WERNER and BRAND, 2001). In gas chromatographic carbon isotope analysis (GC-C-IRMS) the carbon of compounds was combusted to CO_2 at 940 °C in an Al_2O_3 reactor filled with CuO_2 / Pt / Ni. After combustion, additional oxides (i.e. NO_x, N_xO) were reduced to N_2 with elemental copper. $\delta^{13}C$ values of the CO_2 reference gas in GC-C-IRMS were calibrated against the external calibrated $\delta^{13}C$ value of caffeine. δD values of standard substance were reported in RADKE et al. (in press) and for $\delta^{13}C$ values of standards in KRACHT and GLEIXNER (2000).

[10] MPI: Methylphenantrene index is the ratio of phenanthrene and isomers of methylphenanthrene (3-, 2-, 9-, 1-) related to methylisation of phenanthrene at different maturation levels (Radke et. al.,1982).

6.3.4 Maturity correction and hydrogen isotope ratio modelling of source water

For hydrogen exchange of *n*-alkanes and acyclic isoprenoids (RADKE et al., in press) found a correlation of different thermally matured sediments to maturity indices. We use in the present study the correlation of the δD values of *n*-alkanes in the Kupferschiefer (KS) sediments against the MPI1 values to correct for the influence of maturation on δD values of *n*-alkanes in the investigated sediment sections. The correlation of the δD values of hydrocarbons from KS samples seems to be most favorable because together with T_{max} these values are only maturity dependent and the maturation gradient of investigated sediments is similar to the North East Polish KS samples.

In modern sediments, the δD of lipids is dependent on the biosynthesis and supposedly on environmental factors (SESSIONS et al., 1999). The δD values of *n*-alkanes from aquatic (*n*-C_{17}) and terrestrial (*n*-C_{27}, *n*-C_{29}, *n*-C_{31}) biomass correlate against the δD of source water (HUANG et al., 2004; SACHSE et al., 2004b). The hydrogen enrichment factor of *n*-alkanes against water was used to reconstruct the δD of the source water by use of the δD values of biomass specific biomarkers. For reconstruction of the δD values of aquatic sediments (i.e. lake or marine water) we used the δD values of *n*-C_{17} to *n*-C_{19} alkanes and for terrestrial biomass the δD values of *n*-C_{27} to and *n*-C_{29} alkanes were used.

6.4 Results

6.4.1 δD values of *n*-alkanes in Late Palaeozoic and Early Jurassic sediments in relation to environmental parameters

The δD values of *n*-alkanes in the different samples from Palaeozoic marine and lacustrine deposits range from -61‰ to –216‰ (appendix Table 9.3) in individual *n*-alkanes. The mean standard deviation of three replicates is 6‰ for the investigated samples. In some single compounds it reaches 37‰, although from the MS spectra no contaminants are indicated. The mean δD values of all *n*-alkanes in one sample (n-C_{11} to n-C_{34}) range from –77‰ to –136‰ in the lacustrine samples and from –99‰ to –162‰ in the marine sediments. In general the short chain *n*-alkanes are on average depleted by –9‰ compared to the mean of long-chain *n*-alkanes. In some of the Stephanian A samples the Deuterium depletion of the short-chain *n*-alkanes exceeds 20‰ compared to the long-chain *n*-alkanes. The Deuterium enrichment in long chain *n*-alkanes ranges between 3‰ and 34‰ compared to the δD of short chain *n*-alkanes.

The organic carbon content (C_{org}) of lacustrine samples ranges between 2% and 78%. The C_{org} in the aquatic sediments of the LB to the PS sediments varies from 0.8 to 16%. The SNB sediments contain no carbonates. The carbonate content in the LB sediments and the marine sediments of

KS and PS is in the range from of 3% to 16% of carbonate. The carbonate content of 28% in sample No. W874 of the DB Formation is exceptionally high whereas it is much lower in the other sediments with a maximum of 1.5% in sample No. W669. C/N ratios vary between 16.1 to 75.1 in the SNB. The lowest C/N ratio in this basin occurs in sample No. 90774, which derives from the lacustrine Leia horizons of the Early Stephanian A in the SNB. The DB sediments have significant lower C/N ratios from 24 to 42 in relationship to the SNB sediments. Similar to the DB are the C/N ratios of the aquatic sediments, which range from 31 to 56. The lake sediments of the LB have a mean C/N ratio of 54 and therefore attribute the organic matter to a terrestrial source, in which the C/N ratios are higher because of a smaller contribution of protein-rich organic matter.

The $\delta^{13}C_{org}$ value of the SNB has a range from –25.7‰ to –22.9‰. The average value is -24.3±0.8‰ and no significant trend from the Westphalian to the Stephanian exists. The DB Formation has a similar mean $\delta^{13}C_{org}$ of –22.5 ± 0.7‰. In the LB and the PS Basin the maximum $\delta^{13}C_{org}$ values of –19‰ are attributed to a contribution of carbon 13 during sample preparation. $\delta^{13}C_{org}$ varies from –28.7 to –24.2‰ in the LRB and from –26.7‰ to –28.2 ‰ in the KS of Poland (BECHTEL et al., 2000a; BECHTEL and PÜTTMANN, 1992). Similar to the KS are the $\delta^{13}C_{org}$ values with a minimum of –29.2‰ in the PS. The $\delta^{15}N$ values of total nitrogen are <5‰ in samples from the SNB, the DB and the PS. No $\delta^{15}N$ values exist for the KS because only organic solvent extracts were available. Most of the preserved nitrogen tends to originate from terrigenous organic matter in the samples, therefore $\delta^{15}N$ values >10‰ of the Lodève samples are probably related to enhanced recycling of organic matter.

6.4.1.1 Lateral and intra-coal seam variations of δD values from hydrocarbons in the Saar-Nahe Basin and Döhlen Basin

Above the Cantabrian hiatus represented by the Holzer Conglomerate the δD values in the Stephanian A *n*-alkanes are again more depleted in Deuterium (all *n*-alkanes ΔδD = –11.7‰) as in the sample at the base of the Westphalian D. The samples are, however, more enriched to the end of the Stephanian sedimentary succession in comparison to the base of the Westphalian D (all *n*-alkanes ΔδD=+28‰). The $\delta^{13}C$ values of hydrocarbons (mean $\delta^{13}C$ = –30.94 ± 2.95, n = 10) do not differ significantly in the SNB. The bulk C_{org} is 6.1‰ enriched in ^{13}C relative to the *n*-alkanes.

The variation of δD values of *n*-alkanes in the SNB within a single coal seam, the transition from lacustrine sedimentation into coal deposition and from coal deposition into lacustrine sedimentation can be regarded comparing the maturity corrected δD values of the samples (Figure 6.4). The variability of the mean δD of *n*-alkanes is regarded by the root mean square

standard deviation (σ_1 / sqr (n)) within one group of *n*-alkanes (i.e. *n*-C_{16} to *n*-$C_{19,}$ *n*-C_{26} to *n*-C_{31}). The differences of δD values between the short-chain and long-chain *n*-alkane groups can be derived. Short chain *n*-alkanes, serving as biomarkers of algae in lakes, represent the δD of lake water and the long-chain *n*-alkanes, as epicuticular waxes of higher plant leaves, the δD of the leaf water in higher plants.

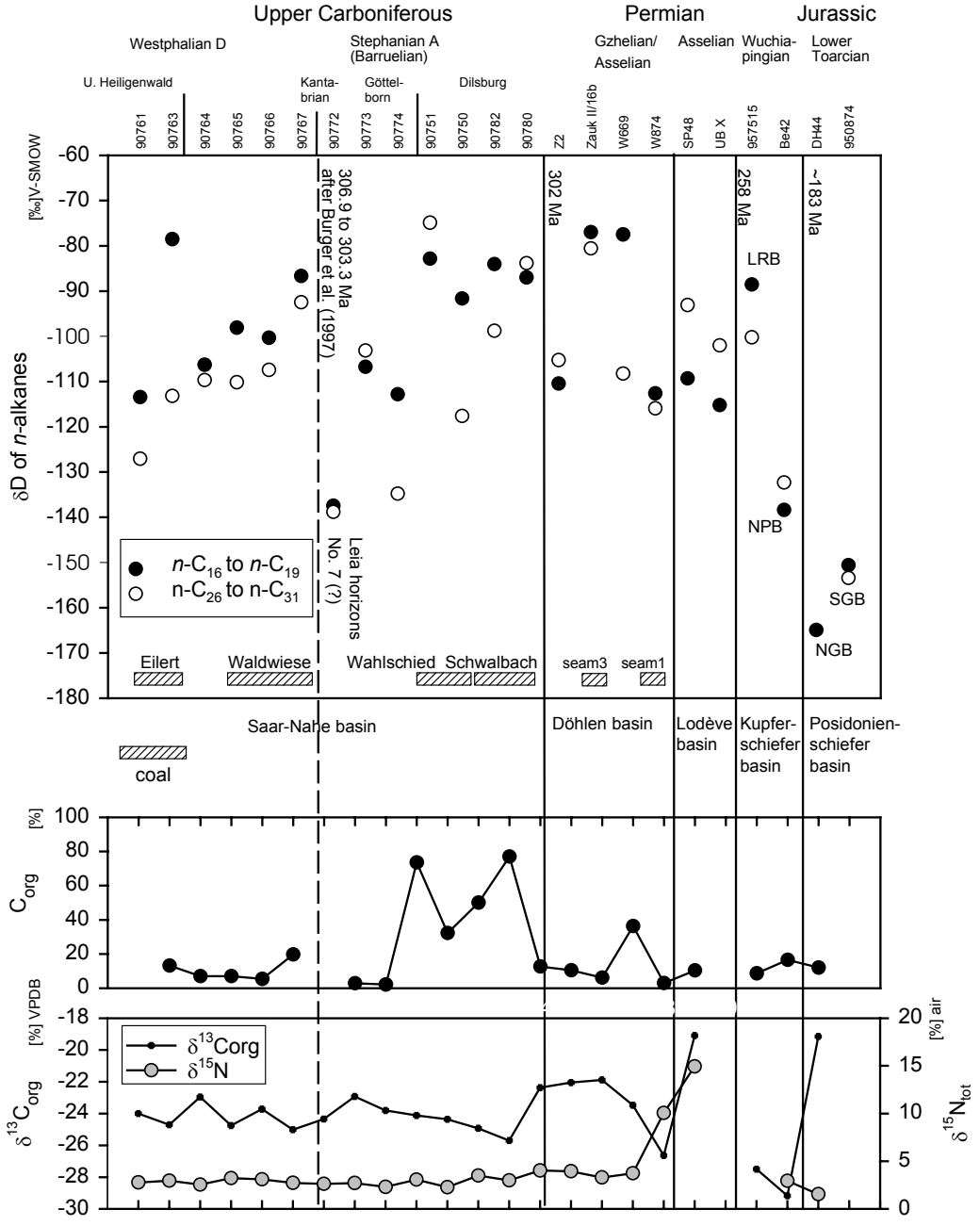

Figure 6.4. δD values of the mean of *n*-alkanes and isoprenoids (pristane, phytane) against sample number. C_{org} content of aquatic sediments from the Upper Permian Kupferschiefer and the Lower Jurassic Posidonienschiefer. $\delta^{13}C_{org}$ and $\delta^{15}N$ of the same sediments. No data available for long-chain *n*-alkanes in NGB sample.

The thickness of single coal seams varies from 1 to 2 m (SNB: Westphalian Eilert and Waldwiese seams, Stephanian Wahlschied and Schwalbach seams, DB: seam No.1 and No.3). Except for the Schwalbach seam, in all coals a trend to Deuterium enrichment is indicated in the long-chain *n*-alkanes in the solvent extracts of the coal seam samples. In the Schwalbach and Hirzweiler coal seam samples, a trend towards depletion in Deuterium within the short-chain *n*-alkanes was determined in comparison to Deuterium enrichment in the sample from the Wemmetsweiler coal seam. Other horizons represent clay-rich sediments deposited at larger distance from coals. The first three Stephanian A sediments refer to sedimentation of lake deposits at the beginning of the Stephanian (Leia 1 to 7 horizons). In continental lakes, the contribution of higher plants biomarkers is commonly well preserved and must be viewed as a rather regional signal represent input from the entire catchment area. Sediment stratigraphic work classifies the Leia horizons as the first occurrence of lake deposits within the Stephanian. These horizons belong to the lake level lowstand deposition of 3rd order cycle in the early Stephanian (STOLLHOFEN, 1998).

The last two borehole samples (Hirzweiler) are 30 km NW of the sampling locations. The comparison of δD values of hydrocarbons to the nearest Wahlschied coal deposits has no significant difference. Plant spore associations of the SNB coal deposits already have shown a very small species variation within the same coal seam over tens of kms (FROMMHERZ, 1998).

The mean δD values of *n*-alkanes in the DB range from –77‰ to –113‰ for short-chain *n*-alkanes and from –81‰ to –116‰ for long-chain *n*-alkanes. Two divergent trends of δD values of short-chain and long-chain *n*-alkanes were determined in the two coal seams. For seam 3 the δD value of short-chain *n*-alkanes rise about +33.5‰ within seam 3. This is in contrast to seam 1, in which the δD values of short-chain *n*-alkanes decrease with –35‰. The decrease of δD values in long-chain *n*-alkanes in seam 3 amounts to 25‰, but opposite to the short-chain *n*-alkanes in the two coals the depletion totals to –8‰.

In the LB the δD values *n*-alkanes are between –109 and –115‰ for short-chain *n*-alkanes and between –93‰ and –102‰ for long-chain *n*-alkanes. The mean δD value of short *n*-alkanes of both samples is about 14‰ more depleted than that of the long-chain alkane ($\sigma_1 = 2.1$‰). No trend towards Deuterium depleted or enriched values could be detected in the different *n*-alkanes of the two sediments.

6.4.1.2 *δD values of n-alkanes in marine sediments*

The mean δD values of the short-chain and long-chain *n*-alkanes range in the KS from –88‰ to –138‰ and from –100‰ to –132‰, respectively. In the PS the range of the δD values is from -165‰ to –151‰ for short-chain *n*-alkanes and from –198‰ to –154‰ for long-chain *n*-alkanes

(Figure 6.4). The δD values of *n*-alkanes in the western KS are significantly higher than the east with a mean δD difference of –41‰ (σ_1 = 13‰). From the Northern to the Southern German PS Basin the δD values of *n*-alkanes become more enriched in Deuterium with +14‰ for short-chain *n*-alkanes and to +44‰ for the long-chain *n*-alkanes.

The δD values of *n*-alkanes were corrected for maturity influences using the linear correlation of δD values of hydrocarbons to the MPI of KS sediments (RADKE et al., in press). To derive the δD values of reconstructed source water the enrichment fractionation ($\varepsilon_{alkane/water}$) of –158‰ from the *n*-$C_{17}$ short-chain alkane of algae in aquatic biomass (SESSIONS et al., 1999) and the $\varepsilon_{alkane/water}$ of –130.2‰ (SACHSE et al., 2004b) from the *n*-C_{29} long-chain alkane from epicuticular waxes in higher plant biomass were used.

6.5 Discussion

6.5.1 General distribution of δD values of *n*-alkanes in Late Palaeozoic and Early Mesozoic sediments

The δD values of *n*-alkanes in the Westphalian deposits have a characteristic bell shape, with a lower deuterium enrichment of 15‰ in the low and high molecular alkane fractions (mean of δD values *n*-C_{12} to *n*-C_{15} alkanes and *n*-C_{26} to *n*-C_{31} alkanes) against the intermediate alkane fraction (mean of δD *n*-C_{16} to *n*-C_{25}). In some samples larger deviations of single δD values from the general trend in specific δD_c values of *n*-alkanes fractions are possible (see appendix Table 9.3) *n*-C_{15}: No. 90763; *n*-C_{20}: No. 90766; *n*-C_{25}: No. 90766; *n*-C_{26}: No. 90761, No. 90765; *n*-C_{27}: No. 90774). In all other sediments the Deuterium enrichment in specific alkane fractions is less pronounced. Through C2 chain prolongation in a multi-enzyme complex *n*-alkanes and fatty acids are produced successively from Acetyl CoA until reaching the palmitic acid (C_{16}). Generally, long chain *n*-alkanes are produced via addition of acyclic compounds. This difference of δD values between long and short chain lipids from one organism may result from the synthesis of *n*-alkanes in different cell compartments. The additional Deuterium depletion in the long-chain alkane fraction might be related to the climate conditions on land. The depleted δD value of the long-chain *n*-alkanes may indicate an origin from Deuterium depleted source water for the growing plants (see below).

Saw tooth shape of the δD values is represented in the sediments of marine or aqueous origin (KS, PS) with depletion in Deuterium in the odd, lower molecular weight *n*-alkanes. An exception is made for the PS (No. 950874), which is Deuterium depleted in the even, higher molecular weight *n*-alkanes. The saw tooth shape is not characteristic for the whole alkane range, but for a specific fraction of the low molecular weight *n*-alkanes (No. DH44, No. Be 42). In

these samples a maximum variability of approximately 20‰ is prominent in the short / chain *n*-alkane fraction and of approximately 60‰ in the long / chain *n*-alkanes of the KS (No. 957515) and 25‰ in the PS (No. 950874).

In Torbanites the saw tooth pattern of relatively negative δD values in even *n*-alkanes of the *n*-C_{20} to *n*-C_{30} range is ascribed to the source of the primary biomass from *Botryococcus braunii* (DAWSON et al., 2004). Additionally, the more positive δD values of odd *n*-alkanes have been attributed to the higher land plants, because of the effect of transpiration on the δD of epicuticular *n*-alkanes from terrestrial biomass. The pattern with more positive δD values in the odd, lower molecular weight *n*-alkanes in the KS and PS samples are opposite to that observed in the Torbanites. On the other hand the δD values of even, lower and higher molecular weight *n*-alkanes are relatively constant. Therefore, it can be concluded that both alkane groups derive mainly from the same source of biomass. The relatively higher depletion in Deuterium in the odd, higher molecular weight *n*-alkanes is related to δD values of meteoric water, which was depleted in Deuterium in comparison to the δD values of the source water of the aquatic biomass.

An extraordinary high D enrichment occurs in the SNB No. 90751 and No. 90763 with raw δD values of *n*-alkanes from –42‰ to –60‰. In the DB samples the largest Deuterium enrichment occurs in sample No. Zauk II/b with –14‰ in the intermediate *n*-alkane fraction. In the higher molecular weight range *n*-alkanes the Deuterium enrichment of these samples is balanced to depleted δD values. An explanation might be the type and the source of the organic matter. This is indicated by the high oxygen index (see appendix Table 9.2) in the Döhlen sediments, which is the highest (OI=55.3 ± 7.8) in comparison to all other sediments (OI=7.2±3.7), that is attributed to the type of organic matter of the terrestrial kerogen type III organic matter.

6.5.1.1 Reconstructed δD values of source water n-alkanes in coals of the Saar-Nahe Basin and Döhlen Basin

The reconstructed δD values of source water (δD_c) from maturity corrected δD values of *n*-alkanes within one coal seam and adjacent samples are discussed for the processes of Deuterium enrichment or depletion in lake water or terrestrial meteoric water in context with own geochemical data and supplementary data taken from VLIEX (1994). The characteristic changes in the δD_c values are: a) Deuterium enriched to Deuterium depleted δD_c values of source water in one coal seam; b) Deuterium depleted to deuterium enriched δD_c values of source water in one coal seam; and c) the change of δD_c values during the transition of sedimentation from coal to organic-rich sediments (Figure 6.5). Spatial and temporal changes in the water cycle can be resolved by the smaller scale sampling procedure. The δD_c values of the source waters depend

on the sediment facies, because the δD of the source water was influenced by physical changes in the environment in which the biomass was produced (evaporation, shift in ground water level, transpiration). The transitions in the sediment facies from terrestrial coal deposits to clastic organic rich deposition or vice versa, or in the same coal seam show that the δD_c values of source water do not depend on global climatic changes but on temporal and spatial physical changes of in the environment of deposition such as evapotranspiration influencing the δD of leaf water used for biomarker synthesis and degradation of biomarkers after sedimentation.

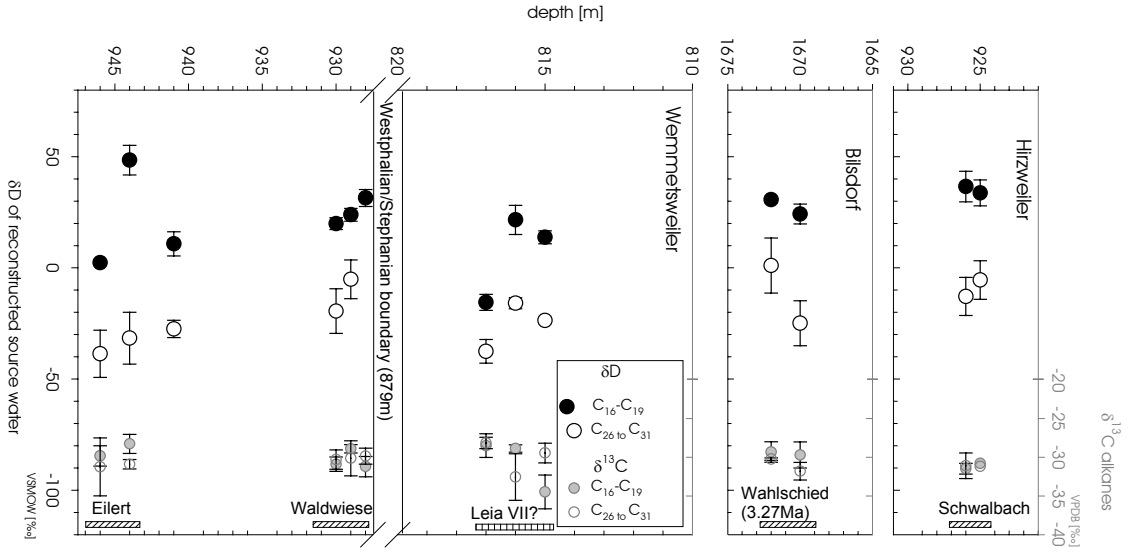

Figure 6.5. Reconstruction of δD of source water (δD_c) from the Saar-Nahe Basin samples against borehole depth. For reconstruction procedure see text in methods. SNB samples were corrected for the depth distance of two neighboring coal seams (Wahlschied and Schwalbach) to reach a comprehensive depth range of the three different borehole depths. The individual borehole depth was correlated with seam Wahlschied, which appears in each borehole This enables an approximate realistic depth of the samples. Shown is the corrected mean depth approached from these coal seam depths of VLIEX (1994) and ENGEL (1985). Radiogen age determinations after BURGER et al. (1997) and LIPPOLT and HESS (1989), stage boundaries after GERMAN-STRATIGRAPHIC-COMMISSION (2002). Organic-rich, non-coal sediments of the Wemmetsweiler belong to the Leia VII horizon (see text).

Deuterium enrichment in reconstructed source water to the top in one coal seam

The abrupt changes in the δD values of the *n*-alkanes in single coal seams (Eilert, Waldwiese, Schwalbach of the SNB samples, seam 3 of the Döhlen Basin samples) are regarded as the effects of the hydrological conditions on δD values of biomass in its palaeoenvironment. The change of the δD values and conclusively the hydrological conditions seem to superimpose the plant community changes in the lake environment. Lake desiccation during the final stage of coal cyclothem evolution leads to a relative D-enrichment in the reconstructed source water in a range of 12‰ to 45‰. This led to extreme δD_c values of palaeolake water of +65‰ due to high evaporation or long residence time of the water in an intermontane lake environment (No. ZaukII/B, No. Z2).

The large positive excursion of the δD_c values of palaeolake water with +48‰ deviated from the top of seam Eilert can only be explained by a high evaporation on the lake water surface. The

δD_c values of meteoric water on land remains at –38‰ and a significant contribution of Deuterium enriched meteoric water has to be excluded. Biomarkers from the higher plants were presumably synthesized in relatively disconnected water source areas, because their isotopic signature differs significantly from that of lake water.

This would mean that the plant source could be related to water sources further away from the lake water. The effect of evaporation due to transpiration on the leaf surface has a far more distinct influence on the δD of epicuticular leaf waxes (CHIKARAISHI and NARAOKA, 2003) and the δD of leafwater itself (BARIAC et al., 1989; FLANAGAN et al., 1991). Unfortunately, the evaluation of $\varepsilon_{alkane/water}$ is recently only known for temperate climate zones. Nevertheless, the δD_c of water can be related to the δD_c of the plants source water, the atmospheric water as primary source or groundwater and river water. The later will not differ significantly, if no Deuterium enrichment due to evaporation of water occurred (LEANEY et al., 1985; YANG and HUANG, 2003).

Deuterium depletion in reconstructed source water to the top in one coal seam

Deuterium depletion towards the top in one coal seam is only evident in the δD_c of palaeolake water from the Wahlschied and the Hirzweiler coals in the SNB and from the Seam No.1 in the Döhlen Formation. In the δD_c values of source water from land, Deuterium depletion is present in the Schwalbach coal seam and in seam No.1. Although the changes of the mean δD_c values of both water resources are not significantly different except for the δD_c value of land water resources of the Wahlschied coal, it can be inferred that the more extreme changes in δD_c value of the land water had a smaller effect on the δD_c value of the palaeolake water during their deposition. This may indicate that changes in the δD value of meteoric water or evaporation occurred over a relatively short time span. Longer residence time of water in these lakes, caused by longer periods of warmer temperatures in the tropics would enrich the Deuterium content in the lake water due to continuous evaporation at the lake surface and enhanced recycling of water into the atmosphere.

Deuterium content of organic-rich sediments

Organic rich sediments analyzed in this study were deposited adjacent to the Upper Westphalian D Eilert coal seam and the clastic lake sediments in the Stephanian A.

Close to the Eilert seam organic-rich sediments (No. 90764) with lower D-enrichment are preserved. These show lower D-enrichment against the sediment at the top of the Eilert coal seam with δD_c values of +38‰ in the lake water and +27‰ in the meteoric water. Both δD_c values are congruent to the general gradient of Deuterium enrichment in the Westphalian sediments. The enrichment may comprise up to +31‰ in δD_c values of palaeolake water and to

-5‰ in δD_c values of meteoric water. This explains that the highly enriched δD_c value of the Eilert seam was established by a spatial and temporarily restricted event. The Deuterium enrichment of *n*-alkanes in aquatic biomass may indicate its episodic production under short-lived evaporative conditions. The D depleted biomass from plants was derived from groundwater sources or from autochthonous biomass. The autochthonous biomass had δD values of source water comparable to the δD value of local meteoric water without evaporative influence.

The Leia horizons (I to VII) are preserved clastic, light grayish-to-grayish shallow lacustrine shales throughout the Göttelborn and Dilsburg Formation. The non-coal sediments are allocated to the Leia horizon VII, because these were directly deposited after the coal seam André (826 m) that follows the Holzer Conglomerates (879 m) (ENGEL, 1985). The variations of δD_c values are comparable to the progression of δD_c values from the seam Eilert but with the same amplitude from –15‰ to +22‰ in the palaeolake values and –37‰ to –23‰ in the terrestrial data. This affirms that the δD_c values are not significantly deviating from the δD_c values from coaly environments.

Surprisingly the δD_c values of samples following the the Cantabrian hiatus (i.e. Holzer Conglomerates, ~ 306.9 to 303.3 Ma.) start at the same level as the isotope ratios of the Eilert seam, which occurred at a relatively short time before the transition to this hiatus. This hiatus coincides with a tectonic reorganization and therefore a complete reconstruction of the drainage pattern. The western outlet system with its sediment transport from the Rhenohercynian zone shifted to a drainage system with a source area in the southern Moldanubian Zone (SCHÄFER, 1986). The Deuterium depletion in the first sample may point to this reorganization and the start of a new lake depositional environment.

Although only three samples (No. 90772, No. 90773, No. 90774) were investigated, the data confirm the variability of δD_c values in the shallow lakes (–16‰ to –14‰) and the hydrology of the terrestrial surrounding (–38‰ to –23‰). A tight coupling of the different environments is indicated considering the maximum difference between the δD_c values of 37‰ in the sample No. 90772. Apparently, the Deuterium enrichment in the lake water was connected to the hydrologic system on land. Moreover, it may be concluded that isotope changes in the meteoric water (e.g. river water, ground water) were not influenced by a remote source region with a distinctive isotope ratio of meteoric water. As an example the Colorado River, U.S.A., flowing through arid regions has still the imprinted Deuterium depleted isotope ratios from its headwaters (FRIEDMAN et al., 1992).

6.5.2 Reconstruction of the δD_c value of source water in individual sedimentary sections

6.5.2.1 *Reconstruction of the source water in the Saar-Nahe Basin and Döhlen Basin*

The δD_c values from the aquatic and land plant biomarkers increase through the entire sequence of the Westphalian / Stephanian. This evidently indicates that the locations Wemmetsweiler, Bilsdorf, and Hirzweiler show spatially consistent δD_c values in the Saar-Nahe Basin. Therefore, the δD_c signature of sediments represents a regional to global palaeohydrological pattern.

The $\delta^{13}C_{org}$ value of the bulk organic matter and the $\delta^{13}C$ value of individual *n*-alkanes deviate by approximately 6‰ independently regardless of the chain length (mean $\delta^{13}C$ value of all *n*-alkanes = –30.4‰ ± 1.4‰). The $\delta^{13}C$ value of the individual *n*-alkanes is in the range of terrestrial organic matter (MEYERS, 1997). A $\Delta\delta^{13}C$ of bulk organic matter offset to *n*-alkanes is commonly found with *n*-alkanes depleted in the range from 2‰ to 10‰ (COLLISTER et al., 1994; LOCKHEART et al., 1997; PAGANI et al., 2000). The higher ^{13}C content in C_{org} enriched samples is due to a contribution of other, ^{13}C enriched compounds presumably incorporated in the polar lipid or kerogen fraction.

Neither $\delta^{15}N$ values, $\delta^{13}C$ values of bulk OM, nor $\delta^{13}C$ values of *n*-alkanes show a significant correlation to the δD values of *n*-alkanes or δD_c values (Figure 6.4, Figure 6.5). Consequently, properties of the other components of the palaeobiogeochemical cycles were not affecting the hydrogen fractionation during biosynthesis of the biomarkers. $\delta^{13}C$ values of the plant synthesized compounds is externally driven by the atmospheric CO_2 concentration ($c[CO_2]$) or during photosynthesis ($p[CO_2]$) and by the stomata conductivity (FARQUHAR et al., 1989). Additionally, the fractionation of plant organic matter to ^{13}C-enriched OM is generated during carbohydrate synthesis (O'LEARY, 1988); for a review see (HAYES, 2001; IVLEV, 2001). Shortly, low $p[CO_2]$ inside the leaf is plant-physiologically driven (C3-, CAM-, C4-metabolism) and influenced by the global $p[CO_2]$ of the atmosphere. High stomatal $p[CO_2]$ increases carbon fractionation, thus yielding depleted products. Consequently, biomarker $\delta^{13}C$ values become more negative. Apart from temperature and CO_2 as climate factors land plants are affected by water use efficiency (LANGE et al., 1988). Changes in humidity may therefore have played a role in changing the carbon isotope signature of plant biomarkers (LOCKHEART et al., 1997). Additionally, $\delta^{13}C$ of land plants depends on growth rate and phytogeographic distribution of plants with different fractionation properties.

The relative differences between the δD_c values of lake water and meteoric water in the SNB and the DB show distinctive offsets of 38‰ versus 58‰, respectively. Differences in palaeohumidity

between the two intermontane basins have contributed to the ^{13}C enrichment in the bulk organic matter of the DB. A dryer atmosphere in the DB area could have influenced the CO_2 assimilation by restricting stomatal conductance. Lower $p[CO_2]$ will have decreased carbon isotope fractionation leading to enhanced ^{13}C uptake into biomass. Enhanced evaporation of lake surface water may have enriched Deuterium in surface water to a larger degree in the DB versus the SNB. This is supported by the δD_c values of the meteoric water in the DB, which is similar to the δD_c values of meteoric water of the SNB and the similar $\delta^{13}C$ values of bulk OM.

The increase of pollen and biomarkers from xerophytic gymnosperms and pteridosperms (VLIEX et al., 1994) is related to the equatorial climate evolution of the Westphalian / Stephanian (GASTALDO et al., 1996). The δD_c values shows no dependence on the palynological and biomarker data in the SNB. This simplistic evidence demonstrates that the two most common ecological structures of plant associations, i.e. marsh vegetation and upland forest, did not affect the environment-dependent hydrogen fractionation of biomarkers. Therefore, the palecological distinction between ombotrophic (rainwater fed peatland) versus rheotrophic (groundwater connected) peatlands during the Carboniferous (DIMICHELE and PHILLIPS, 1994) cannot be followed by the δD_c data.

6.5.2.2 Reconstruction of the source water in the Lodève Basin

Preservation of lipids in carbonaceous, organic rich lacustrine sediments of the Lodève Basin (LB) for hydrogen isotope analysis was only possible for the lower Usclas St. Privat Formation (UP.-Fm.). In the upper section oxidation of organic matter of lacustrine and pedogenic origin hampered any isotope determination.

In the lacustrine black-shales of the LB the $\Delta\delta D_c$ value between the different water sources is 11‰. This is much lower compared to the fully terrestrial samples from the SNB and the DB. Additionally, the source water δD_c of land plants agrees well with an UP-Fm. deposited in an environment with rivers and lakes bound to incised valleys that cut into a low topography landscape (CHATEAUNEUF and FARJANEL, 1989). The δD_c value of "river-lake" water and plant source water had very similar values. Averages of δD_c values of +11.1‰ and -0.4‰ indicate lower evaporation of lake surface water than in the intermontane basins of Cental Europe, where maximum δD_c values of –38‰ were reached. Evidence that tight coupling between land plants and aquatic biomass existed is confirmed by source waters with the same δD_c value. From palaeobotanical investigations it is concluded that plants were growing along riverbanks in moderately humid to dry environments. A Recent example of this transition between river and terminal lake is the Okavango River delta of semi-arid northern Botswana. The river emanates from humid areas but undergoes progressive evaporation during its passage through the delta

(DINÇER et al., 1979). The δD values of groundwater in the river aquifer of the delta and the channels are approximately –15‰ versus 5‰ in the swamp water. The mean δD value of –44‰ for groundwater outside the delta reflects the local meteoric recharge. Therefore, the δD_c value of LB water may be confined by the local meteoric isotope signal.

6.5.3 Global climatic shift at the equatorial coastline of eastern Pangea

The palaeolake systems of the eastern Pangean continent (Southern France, the SNB and the Döhlen Basin) allow first interpretation of climatic changes in equatorial Pangea from the Upper Carboniferous to the Lower Permian. Enriched δD_c values of lake water with a maximum +48‰ in the SNB and +65‰ the DB reflect extreme evaporation periods during the sedimentation of the organic deposits and a long residence time of the water in the basin (Figure 6.6 & Figure 6.7).

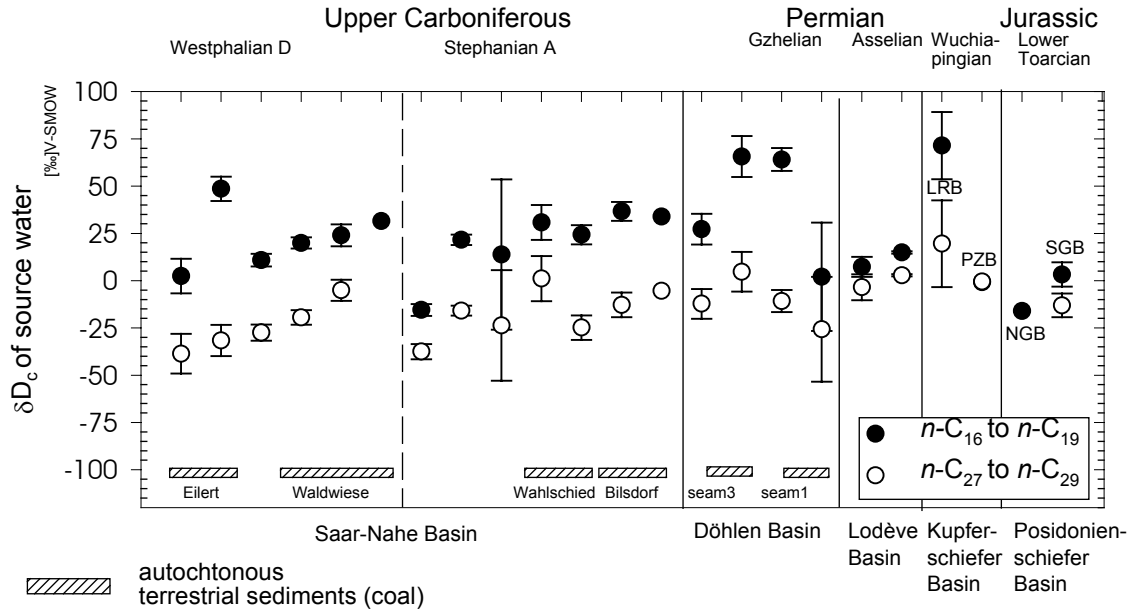

Figure 6.6. Reconstructed δD values of source water (δD_c) of the terrestrial Upper Palaeozoic sediments and of the marine Mesozoic sediments. The δD_c of surface water was reconstructed from the δD of *n*-alkane biomarkers of aquatic biomass (*n*-C_{16} to *n*-C_{19}). The δD_c of meteoric water was reconstructed from the δD of *n*-alkane biomarkers of higher plants (*n*-C_{27} to *n*-C_{29}).

But generally the integrated δD_c values of lake water increase from the Westphalian D to the Stephanian A from +15.6‰ +27.8‰. For meteoric waters the δD_c value rise from -32.9‰ to –17.7‰ (Figure 6.7). This shift can be attributed to a global change of the hydrological cycle between the Westphalian and Stephanian. The mean difference between these two water sources is very constant at approximately 45‰. In temperate climate zones the difference averages 30‰. From the δD difference of 15‰ in water between the dry tropical and the temperate climate, it can be assumed that evaporation significantly changed the isotope ratio of the lake water. A rise in temperature or change of atmospheric circulation attributed to this shifts since both water

pools were affected by Deuterium enrichment. An increase of precipitation can be induced with cooler tropical temperature, because of weakened monsoon precipitation but increased continuous rain in the tropical region. Further evidence of a temperature increase and increase of monsoonal atmospheric circulation is the increased deuterium enrichment in the source water due to the onset of monsoon precipitation in the Early Permian. This cumulated in the total disappearance of stable lakes and the transition to playa environments in the LB and the entire European Permian basins as well (KÖRNER et al., 2003; SCHNEIDER, 2001)

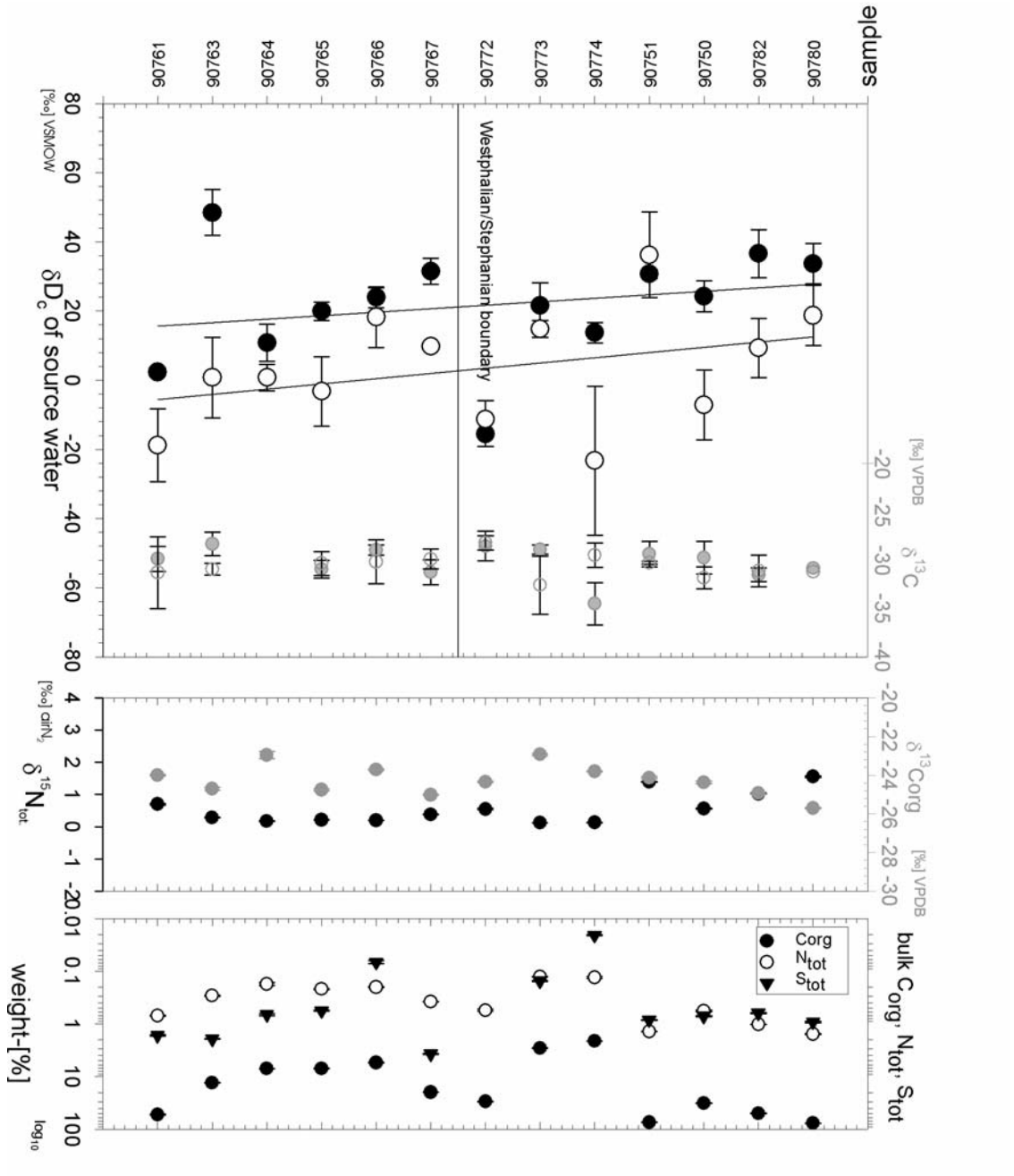

Figure 6.7. The δD_c of the Saar-Nahe Basin. The line in the upper graph shows the trend of δD_c values of precipitation on land using the δD values of long-chain alkane biomarkers and of lake water using the δD of short chain n-alkanes. Elemental data ($C_{org,}$ N_{tot}, S_{tot}), $\delta^{13}C_{org}$ and δN_{tot} are plotted to show that none of these parameters influenced the δD values of *n*-alkanes.

High enrichments of δD of lake water were not uncommon and well known for recent east African rift-system lakes. Lake Tanganyika has a δD value of +28‰, which is ascribed to previous dryer climate (Figure 6.8) (GONFIANTINI, 1986; GONFIANTINI et al., 1979). Ethiopian lake Danakil shows mean surface water δD values of +27.3 to +29.4 ‰ (GONFIANTINI et al., 1973). The δD_c values offer opportunities to compare the changes in the eastern Euramerica continent to changes in the western Euramerican for the Latest Westphalian to early Permian equatorial climate system (TABOR and MONTANEZ, 2002) (Figure 6.8).

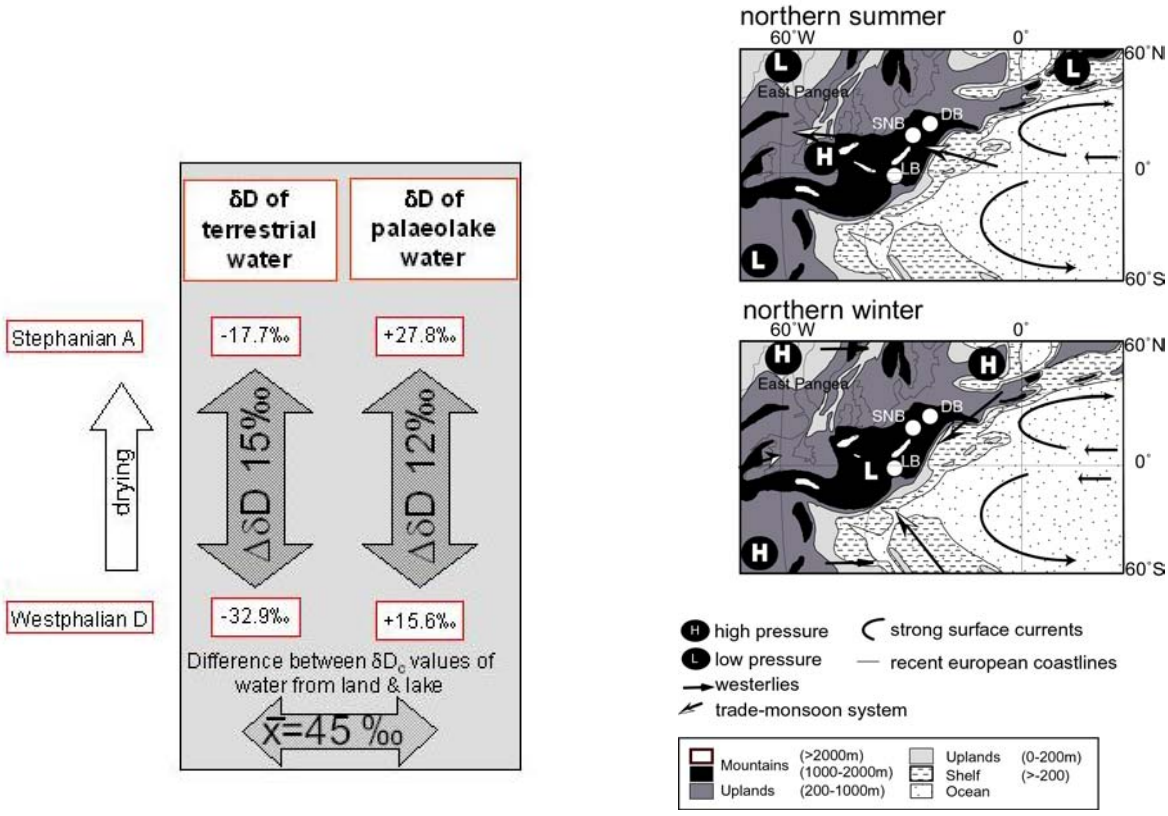

Figure 6.8. a) Shift of δD_c values in waters from the Westphalian to the Stephanian. **b)** Geographic and atmospheric monsoon circulation during the Late Palaeozoic on the east coast of Pangea. Increased humidity transport over land explains the lower δD_c values during Westphalian D. LB: Lodève Basin, SNB: Saar-Nahe Basin, DB: Döhlen Basin (approximate palaeogeographic location). Palaeomap: (ZIEGLER et al., 1997).

The teleconnection argues for a monsoon circulation over both equatorial regions. Increased rain shadow effects in the SNB and DB during the Late Carboniferous and Early Permian led to the conclusion that hydrological conditions were changed due to enhanced evaporation and increased aridity. Increased moisture was transported from the Palaeotethys ocean into the palaeolake area of eastern Pangea at the base of the investigated Westphalian D and after the Kantabrian hiatus. The base for data is too spare to draw conclusions from the effect of the warming phase during the Permo-Carboniferous glaciation on the δD_c values in this

palaeoequatorial region. Changes in δD_c values might simply be related to changes in direction and intensity of atmospheric flow. Though enhanced global cooling intensifies the strength of air flow because of temperature difference between low and high latitude areas. The tropical climate region changed from ever-wet to dryer conditions (PARRISH, 1993), consequently, the δD_c value of precipitation and source water was enriched in Deuterium.

6.5.4 Reconstruction of the source water in the Kupferschiefer Basin

The KS sample from the LRB (Rheinberg) had experienced only maturation by burial depth. δD values of extracted bitumen had a narrow variation from –137‰ to –125‰ (BECHTEL and PÜTTMANN, 1992). In comparison the KS sample in this study had a δD value of –88‰ indicating the source of less Deuterium enriched compounds in the other soluble fractions. The sample represents the palaeogeographical setting of a small lagoon separated from the main southern Permian basin. This embayment experienced increasing salinity during deposition of the KS indicated by the distribution of methylated chromanes, which serve as molecular palaeosalinity indicators (SCHWARK and PÜTTMANN, 1990). This is also confirmed by the highly enriched δD_c values of the surface water with +75‰. Similar Deuterium enrichments of up to +68‰ in the surface waters are indicated in a lagoon of the Zechstein in Central Europe (SACHSE et al., 2004a).

Even the δD_c values of the land plant lipids are very high with +20‰ compared to the δD_c values of the NPB with –3.5‰ of seawater and –0.5‰ for meteoric water on land. During northern winter the atmospheric flow is characterised by dry-air crossing over the continental area of Pangea. During summer monsoonal circulation prevails. On the one hand the area of the LRB is protected from humidity by a mountain chain, which explains the Deuterium enrichment in the lagoonal surface water (Figure 6.9). On the other hand surface water currents of the arctic boreal area influenced the NPB surface water. Between –20 to –40‰ were reconstructed for meteoric water from the δD of hydroxyl from illitic clay (BECHTEL et al., 2000b). This would support the theory of salinity stratification due to freshwater water run-off into the basin leading to high nutrient inputs (PANCOST et al., 2002; TURNER and MAGARITZ, 1981).

Prevailing wind directions were from the SE to the NW reconstructed from Dune structures of the underlying Permian sandstones (BRONGERSMA-SANDERS, 1965). Additionally, the western basins were more under the influence of the arid interior of the continent than the eastern continental border of the Pangean continent as shown by palaeoclimate modelling of the Upper Rotliegend (Wordian) (PARRISH, 1993; ZIEGLER et al., 1997). Although the interpretation is supported by a small data set of only two examples, δD signatures of lipid biomarkers independently confirm that the western basin was under more arid influence. Continental run-off

delivered by monsoon precipitation might have supplied the necessary fresh water and nutrients to the basin for the extreme OM enrichment in the Kupferschiefer of the Early Upper Permian.

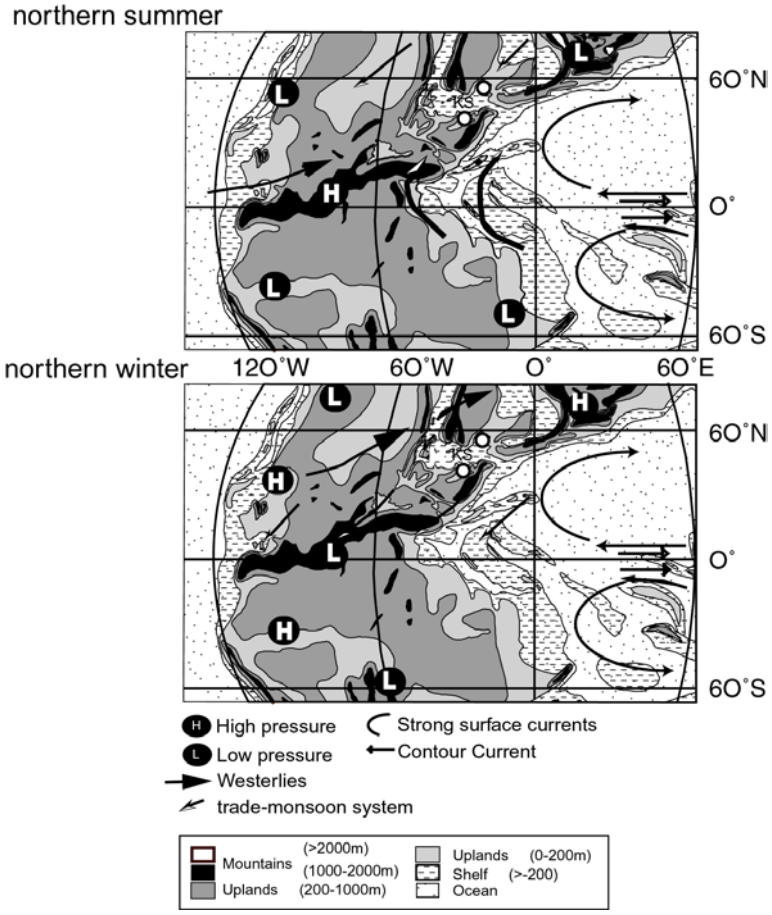

Figure 6.9. Surface and atmospheric pressure systems. These determined the δD_c of surface water and meteoric water on land. In northern summer the atmospheric flow is strongly influenced by SE trade wind (Monsoon). In northern winter the area of the lagoon system (LRB) is influenced by dry atmospheric flow from the continent increasing evaporation over the water surface. Palaeomap and Climate: (ZIEGLER et al., 1997).

6.5.5 Reconstruction of the source water in the Posidonienschiefer Basin

During the Early Toarcian an oceanic anoxic event led to a north to south trend of decreasing amount of sedimentary organic carbon from the boreal to southern pelagic Tethys (BUCEFALO PALLIANI et al., 2002; LITTKE, 1993). The higher organic matter burial is attributed to a more extensive oxygen minimum zone in the north due to more stagnant water column conditions during a relative sea level high-stand (SCHMID-RÖHL et al., 2002). Several explanations exist for coeval high rates organic carbon burial and widespread $\delta^{13}C$ excursion to more positive values in the carbonaceous material and positive values in carbonates and organic matter during the *Falciferum exaratum* subzone. KÜSPERT (1982) introduced the CO_2 recycling hypothesis with uptake of ^{13}C enriched organic matter from the calcareous nanoplankton, which was supported by JENKYNS (1985); JENKYNS and CLAYTON (1986); JENKYNS and CLAYTON (1997). An additional concept is the "estuarine recycling model" with salinity stratification producing an up

welling of nutrient-rich, ^{13}C depleted, anoxic bottom into the surface water with concomitant fixation in coccolith and photosynthate occurred. An alternative hypothesis is the massive release of isotopically depleted methane into the atmosphere (HESSELBO et al., 2000).

SCHMID-RÖHL et al. (2002) have shown $\delta^{18}O$ values of reconstructed source water between –6.7‰ to –5‰ which would transfer to 36 °C to 46°C of surface water temperature. Therefore, depleted $\delta^{18}O$ of carbonates were explained by elevated temperature (25 °C to 30 °C) and enhanced fresh water supply from the continental areas according to mega-monsoon circulation during supercontinent accumulation (PARRISH, 1993; PARRISH and CURTIS, 1982) (Figure 6.10).

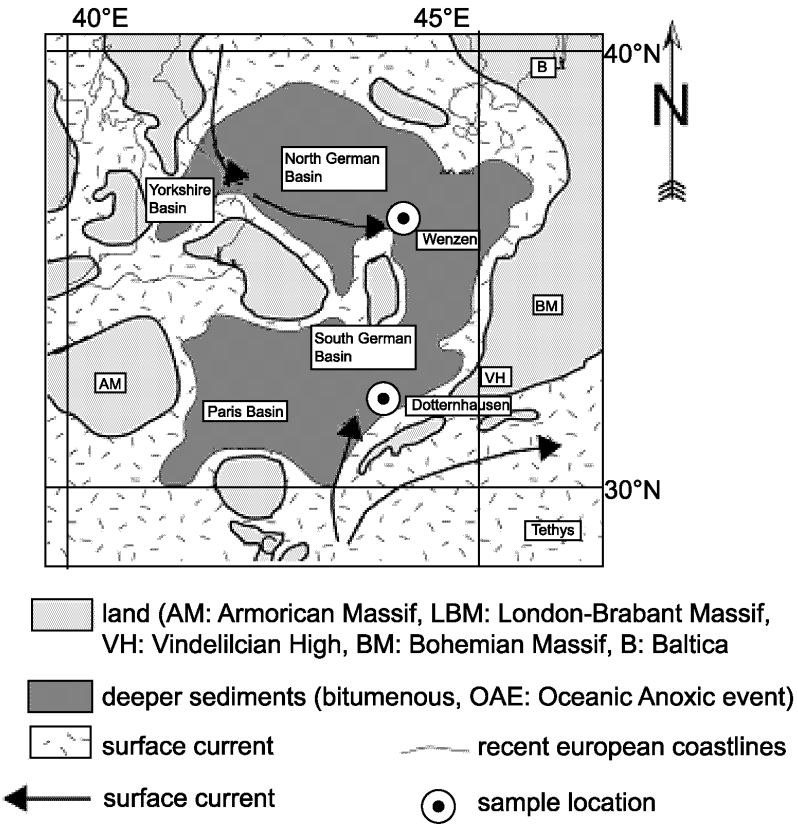

Figure 6.10. Palaeogeographic distribution of landmasses and inferred marine surface water currents during the Lower Toarcian of Central Europe resultant from reconstruction of δD_c of water. Palaeomap: (ZIEGLER et al., 1997).

The δD_c values of –8.2‰ for the PS surface water in the NGB show a picture similar to the two KS waters. Again, the δD_c value is 10‰ more depleted in the north than in the south. The δD_c values of PS surface waters in the southern basin are 3.3‰ less enriched than the lagoon water of the LRB of the KS. These results strongly suggest the influence of freshwater stratification in the water column as a basin wide property in the north (Figure 6.10). Enhanced nutrient supply in that region is strongly supported by δD_c values of –48‰ in the continental water. The δD values are similar to meteoric waters of humid to temperate climate zones. The deuterium enriched surface waters in the PS of the SGB suggest the influence of warm surface currents from the NE

Tethys into the southern epicontinental sea or enhanced influence of evaporation induced by less water mass exchange during sea-level lowstand. The δD_c value of the continental meteoric water with –13.1‰ of the PS sediments seem to represent a monsoon region like the recent Indian continent (+3.7‰ to –38.4‰).

6.6 Conclusions for the reconstruction of δD_c of source water in Upper Carboniferous to Middle Mesozoic marine and continental deposits

The maturity correction of δD values of *n*-alkanes from the Palaeozoic to Mesozoic continental shield sediments confirms the results of maturity correlation of δD values of *n*-alkanes from the KS deposits in the NE Poland. The reconstruction of δD values of water from δD values of *n*-alkanes in Palaeozoic and Mesozoic sediments is with –23‰ to +61‰ in the range of modern continental and marine waters.

The δD_c values of surface water in palaeolakes of the Saar-Nahe Basin increase from –33‰ during the Westphalian D to –18‰ in the lower Stephanian A. This quantifies for the first time the drying of the equatorial tropics during the Late Carboniferous on the eastern Euramerican continent. Additionally the evolution of tree ferns coincides with this drying. The decrease of δD_c values of the palaeolake water shows that this drying was interrupted by an increase of humidity after the Kantabrian hiatus.

The constant difference of δD_c values of +45‰ between palaeolake water and plant source water from the Westphalian D to the Stephanian A and the Deuterium enrichment of +28‰ in the palaeolake water confirms that the precipitation and the palaelake water reservoir were tightly coupled under constant Deuterium enrichment in the lake water.

The δD_c values of Döhlen Basin and Lodève Basin source waters reflect enhanced evaporation in small palaeolake basins with high Deuterium enrichment of up to +65‰. The small difference of a 14‰ lower Deuterium enrichment in the higher plant biomass from the Lodève Basin is evidently concomitant with other scientific results, which interpretate the lower Lodève organic deposits as originated from incisive river beds within a semi-arid climate zone. Higher plants associations were tightly connected to hydrogen isotope signal of the river water.

The main effects controlling anoxic sedimentation are enhanced productivity due to nutrient recycling or external nutrient supply and enhanced preservation rates due to anoxicity. Nutrient supply from continents into marginal subbasins of the Permian Kupferschiefer and Jurassic PS Seas by continental run-off might have favored primary productivity. Establishment of a freshwater surface layer led to intensively stratified water bodies thus favoring preservation of organic biomass in sediments. Both processes are supported in the present study by Deuterium depleted surface waters in the marginal basin settings studied.

7 General conclusions and summary

The objective of this thesis is to assess the δD values of *n*-alkanes as a new proxy for hydrogen isotope reconstruction of the water cycle in palaeoclimate research. In this thesis the transition of the Westphalian / Stephanian boundary sets for the first time a reference point for the Palaeozoic continental palaeoclimate reconstruction with δD values of *n*-alkanes (see below). This transition is of major interest because at this time the evolution of land plants to first gymnosperms and dry-resistant tree ferns seems to be concomitant with a warming phase during the Permo-Carboniferous glaciation.

At first the implementation of the measurement system of compound-specific hydrogen isotope determination (GC-TC-IRMS) and isotope standardization (accuracy, precision) are essential for the reliability of the reported data. The reconstruction of the δD value of source water in the Palaeozoic with the δD value of *n*-alkanes as a proxy can only be consolidated if the primary δD value of the *n*-alkanes in sediments is either preserved or the varying effects on the change of the δD of *n*-alkanes during burial can be quantified. These were predominantly quantified by using two exemplary sediments varying in their degree of maturation. The Permian Kupferschiefer of North East Poland with a maturation gradient representative for sediments preserved in continental shields and the Lower Toarcian Posidonienschiefer of the Vlotho Massif (NW Germany), which exemplifies sediments buried under higher thermal stress (e.g. contact metamorphism, fast burial).

With the quantified maturity effect from the KS sediments on the δD value of *n*-alkanes in sediments and the proxy relationship of the δD value of *n*-alkanes to recent source water, the δD value of source water is modelled in Palaeozoic and Mesozoic sediments. A calculated Deuterium enrichment of approximately 20‰ of the eastern Pangean continent during the Westphalian / Stephanian and source water reconstructions from other equatorial eastern Pangean sediments quantify for the first time atmospheric changes in the global and large-scale regional water budget.

7.1 Implementation of the GC-TC-MS/IRMS System for compound specific hydrogen analysis in palaeoclimate reconstruction

Precision and reproducibility of the δD values from hydrocarbon standards and sample compounds have been determined together with evaluation of effects of matrix clean-up methods (e.g. silver nitrate adduction, ruthenium oxidation) and solvent extraction on the preservation of primary δD value of organic compounds in sediment samples and standards.

A good reproducibility of the δD value from standard alkane mixture have been achieved due to the low contribution of H_3^+ ions (7.75 ± 0.83 pA^{-1}) in the ion source of the IRMS. This H_3^+ factor confirms the high stability of the IRMS system. Additionally, a significant contribution of CH_4 from thermal conversion of organic compounds would lead to a similar contribution of H_3^+ ions because of its role as proton donor during electron bombardment in the ion source. Recording of the mass 15 during changes of the conversion temperature from 1400 °C to 1450 °C (ΔT = 10°C) could show the even minor influence of CH_4 in the lower temperature field resulting in a longer lifetime of the Al_2O_3 and connectors of the oven inlet.

The H_3^+ factor has been determined on a daily basis and used for the correction of δD-values of the following sample runs and alkane standard mixture. The standard mixture contains a triplicate of five different concentrated alkanes from *n*-C_{15} to n-C_{32} alkanes (25, 50, 100, 150, 200 ng / µl) with squalane (*i*-C_{25}, 300 ng / µl) as additional standard. δD values of the standard mixture used by GC-TC-IRMS compared to δD values of the same compounds independently determined by TC-EA-IRMS have a weight mean standard deviation of of 5.8‰. This indicates a high reproducability of the reported δD values of *n*-alkanes.

To avoid co-elution of substances with alkanes and isoprenoids within the aliphatic fraction co-eluting compounds can be removed by oxidation of aromatic compounds using RuO_2 or by $AgNO_3$ adduction. Both procedures were applied to *n*-alkanes and aromatic compounds leading to a non-significant change of the δD values of *n*-alkanes. Whereas the discrimination of the δD-values of N, S, O compounds to lower values seems to reflect a kinetic isotope effect due to preferential oxidation of the depleted heteropolar linkage. Therefore the $AgNO_3$ adduction and the RuO_2 method can be used to avoid co-elution of background compounds with hydrocarbons within the GC System.

A Posidonienschiefer sediment was one-time sequentially extracted (10, 20, 30 min.) to prove the reproducibility of the δD values of hydrocarbons in three statistically independent samples. The δD value of the *n*-alkanes from the three extracts had a standard deviatioin (σ1) of 6.8‰. An

extraction time of 20 min. should be applied to get an integrated amount of compounds without isotope effect on the δD values of individual hydrocarbons.

7.2 Influence of thermal maturity on the δD value of hydrocarbons in sediments

The δD and $\delta^{13}C$ values of *n*-alkanes and of acyclic isoprenoids (pristane, phytane) were correlated to maturity indices (e.g. MPI1, R_M, HI, TMAX, MDR). The δD values of the compounds in the Lower Permian Kupferschiefer of North East Polish Basin (NPB) and the Lower Toarcian Posidonenschiefer of the North West German Posidonienschiefer Basin (NGB) correlate differently with sediment maturity. The NPB sediment range from a vitrinite reflectance of > 0.6% to 1.45% R_M compared to NGB sediments from the Vlotho Massif in a range from 0.45 to 0.85 R_M. The maturation history of the PS is characterized by thermal maturation by an intrusive body compared to maturation under temperature gradients in a continental shield. The δD values of the extracted hydrocarbons positively correlate with thermal maturity in the barren zone of the NPB deposits (y = 56‰ × MPI1(x) – 160‰ [VSMOW]) and in the NPB (y = 104‰ × MPI1(x) – 200‰ [VSMOW]). The δD value of isoprenoids is more affected (y=179‰ × MPI1(x) – 341‰ [VSMOW]) in the KS; (y=300‰ × MPI1(x) – 415‰ [VSMOW]) in PS).

The absence of fractionation of δD values between *n*-alkanes and acyclic isoprenoids in mature sediments can be explained by the larger D-enrichments of initially lighter acyclic isoprenoids during sustained maturation. The $\delta^{13}C$ values are not significantly isotopically changed in the Kupferschiefer deposits indicating that no cracking processes changed the δD values of hydrocarbons significantly. Rayleigh fractionation modelling showed that the Deuterium enrichment in hydrocarbons could be attributed with less than 8% to thermal methanogenesis. Thermodynamic fractionation and exchange with sedimentary water was also excluded due to low exchange rates and no significant correlation of the δD values of hydrocarbons in the sediments. It can be considered that activation energy contributes to the Deuterium enrichment in the alkanes and isoprenoids as dependent from the burial time and temperature of sediments.

The correlation of δD values of hydrocarbons to maturity convincingly shows the absence of fractionation of D/H between *n*-alkanes and acyclic isoprenoids in mature sediments. This explains the larger Deuterium-enrichments of initially lighter acyclic isoprenoids during sustained maturation. Consequently, the results shall enable δD values from biomarkers from sediments of known maturity to be corrected back to their initial values, allowing them to be used to make climatic and biosynthetic reconstructions at the time of deposition.

7.3 Reconstruction of δD values of source water from δD values *n*-alkanes in Palaeozoic and Mesozoic sediments

In the framework of the SPP 1054 ("Evolution des Systemes Erde während des jüngeren Paläozoikums im Spiegel der Sediment-Geochemie"), sediments from the Permo-Carboniferous and additionally the Mesozoic were taken and corrected for the maturity influence on their primary δD values of *n*-alkanes using the correlation of δD values of *n*-alkanes versus MPI1. The calculated δD values of maturity corrected *n*-alkanes were used to reconstruct the δD values of source water (δD_c) from isotope fractionation factors of *n*-alkanes in higher plants and aquatic biomass. The first results of δD_c values in the Palaeozoic sediments will provide a reference point for further scientific work.

7.3.1 The reconstruction of equatorial source waters in marginal Central Pangea during the Westphalian / Stephanian warming phase

The δD_c values of palaeolake water and source water from higher plants provide the ability to reconstruct continental hydrogen isotope signals from organic biomass in the Palaeozoic. The reconstruction of δD values of lake and plant source waters from biomarkers is a great advantage compared to the reconstruction of δD values of water from clay minerals in non-calcarous sediments. The comparison enables the reconstruction of evapotranspiration within the same sediment section, when both the aquatic and plant *n*-alkanes have their origin in the same area and were produced during the same time. The reconstruction of δD_c values is considered herein as an integration over a longer time interval, but is still of importance for the reconstruction of the water cycle in the palaeoclimate record.

The SNB in the Middle European continental area is a perfect reference point because of the large sedimentological and organic-geochemical research in that area. In general, the global trend is recorded in the complete section of the Westphalian D / Stephanian A of the SNB. The Deuterium enrichment has a difference of 33‰ in the δD_c values of Westphalian (–33‰) to Stephanian palaeolake water (–18‰). The δD_c of meteoric water shifts from +16‰ at the Westphalian D to +28‰ during Stephanian A. The less difference between Stephanian and Westphalian meteoric waters (+13‰) indicates an enhanced recycling of lake water from the Westphalian to the Stephanian. The larger difference in the isotope ratio of the lake water might be evident for an enhanced evaporation of the lake water.

The SNB sediments are characterized by coal deposition and organic-rich shale sedimentation. This facies difference is concomitant with positive or negative differences in the δD_c values from the primary *n*-alkanes and independent from the location of their deposition either in the lake or

on land. Additionally, this variability of δD_c values is also reflected in the same coal seam of a borehole. This indicates the high spatial difference of δD_c values of source water in one palaeoenvironment. The palaeoenvironment diversifies in facies with higher evaporative swamp areas or areas with more open water in the lake. Even the source of the biomarker might be autochtoneous or differences in isotope ratios of the ground water were possible.

The hypothesis of being able to reconstruct the palaeohydrological conditions with δD values of *n*-alkanes is supported by the comparison of reconstructed δD values of source water to the isotope ratio of palaeolake water in the tropics of the east African rift system. Recent Lake Tanganyika has δD values of +28‰ resultant from the high evaporative recycling of surface waters and the general δD value of rain water (-12‰ [SMOW], Kericho, Kenya).

First dry resistant gymnosperms evolved during the Westphalian D in the Pangean continental area. In the SNB, sediment biomarker of the dry resistant tree ferns confirm that the same climate related evolution of plants is also prominent at the eastern Pangean continental side. The abrupt isotope shift to values of -30‰ after the Westphalian / Stephanian boundary can be reflected as a change in source water directions feeding the lake and less evaporation of surface lake water. The global trend of drying in that area indicated by isotope enrichment in the source water supports that more xerophytic plants replaced other plant groups (i.e. Lycopods).

7.3.2 Lower Permian of the Lodève and the Döhlen Basin

The LB and the DB shifted during the Permo-Carboniferous into palaeolatitudes of the subarid climate zone (10 °C to 15 °C). The influence of monsoonal atmospheric circulation patterns began to be prominent. δD_c values from maturity corrected *n*-alkanes are 11‰ less enriched in the LB indicating this climatic difference to the palaeogeographic position of the SNB samples. Indication of riverbank environments from sedimentological evidence (river levees) is supported by the direct coupling of isotope ratios of aquatic source water and plant source water in the LB.

The difference between the lake and precipitation is about 20‰ larger in the DB than in the SNB. Enhanced evaporation of lake surface water may have enriched Deuterium in surface water to a larger degree in the DB versus the SNB. This is supported by the δD_c values of the meteoric water in the DB, which is similar to the δD_c of meteoric water of the SNB.

7.3.3 δD_c values in source water of Permian and Mesozoic marine sediments – the Kupferschiefer and the Posidonienschiefer Basins

δD_c values of source water from marine settings and the hinterland climate region were investigated in the Kupferschiefer Basin of the Lower Rhine area (LRB) and the North East Polish Kupferschiefer Basin (NPB). Two sediment samples were considered to explain the

general depletion in the δD_c values of the surface water and the influence of arid climate in the hinterland. The aridity decreased from +75‰ in the LRB to +8‰ in the more easterly KS Basin. A similar north-to-south trend of a 10‰ D-enrichment emerges in the surface waters of the PS Basin. In both sediments, the Kupferschiefer and the Posidonienschiefer Basin black-shale sedimentation was favored by high organic matter deposition or higher preservation. The depletion of the δD_c values in the more easterly KS Basin and the more northern PS Basin indicates that the influence of freshwater supply might enhance the supply of nutrients in the surface water, and thus the productivity. In general the δD_c value of palaeowaters is a tool to quantify the atmospheric and oceanic circulation, the nutrient cycling of marine and freshwater systems and the palaeohydrology of marine and terrestrial palaeoenviroments.

8 Literature

Alexander R., Kagi R. I., and Larcher A. V. (1982) Clay catalysis of aromatic hydrogen-exchange reactions. *Geochim. Cosmochim. Acta* **46**(2), 219-222.

Alexander R., Kagi R. I., and Larcher A. V. (1984) Clay catalysis of alkyl hydrogen exchange reactions-reaction mechanisms. *Org. Geochem.* **6**, 755-760.

Alexkowsky W., Koch E. A., Kurze M., Schneider J. W., Tröger K. A., and Wolf L. (1999) Erläuterungen zu Blatt K 5048 Kreischa. In *Geologische Karte des Freistaates Sachsen 1:25000* (ed. J. Goebel, H. Joisten, K. Kardel, G. Palme, L. Pfeiffer, R. Pohlenz, T. Seifert, H. Weber, C. D. Werner, W. Wilke, B. Witthauer, and W. Witthauer), pp. 37-61. Sächs. L. Umwelt u. Geologie - Ber. Boden u. Geologie.

Allison G. B., Gat J. R., and Leaney F. W. J. (1985) The relationship between deuterium and oxygen-18 delta values in leaf water. *Chem. Geol.* **58**, 145-156.

Andersen N., Paul H. A., Bernasconi S. M., McKenzie J. A., Behrens A., Schaeffer P., and Albrecht P. (2001) Large and rapid climate variability during the Messinian salinity crisis: Evidence from deuterium concentrations of individual biomarkers. *Geology* **29**(9), 799-802.

Barbour M. M., Roden J. S., Farquhar G. D., and Ehleringer J. R. (2004) Expressing leaf water and cellulose oxygen isotope ratios as enrichment above source water reveals evidence of a Peclet effect. *Oecologia* **138**(3), 426-435.

Bariac T., Rambal S., Jusserand C., and Berger A. (1989) Evaluating water fluxes of field-grown alfalfa from diurnal observations of natural isotope concentrations, energy budget and ecophysiological parameters. *Agr. Forest Meteorol.* **48**(3-4), 263-283.

Barrick R. C., Hedges J. I., and Peterson M. L. (1980) Hydrocarbon geochemistry of the Pudget Sound region. 1. sedimentary acyclic hydrocarbons. *Geochim. Cosmochim. Acta* **44**(9), 1349-1362.

Bechtel A., Gratzer R., Püttmann W., and Oszczepalski S. (2000a) Geochemical and isotopic composition of organic matter in the Kupferschiefer of the Polish Zechstein basin: relation to maturity and base metal mineralization. *Int. J. Earth Sci.* **89**(1), 72-89.

Bechtel A. and Püttmann W. (1992) Combined isotopic and biomarker investigations of temperature-dependent and facies-dependent variations in the Kupferschiefer of the Lower Rhine Basin, Northwestern Germany. *Chem. Geol.* **102**(1-4), 23-40.

Bechtel A. and Püttmann W. (1997) Palaeoceanography of the early Zechstein sea during Kupferschiefer deposition in the Lower Rhine Basin (Germany); a reappraisal from stable isotope and organic geochemical investigations. *Paleogeogr. Paleoclimatol. Paleoecol.* **136**(1-4), 331-358.

Bechtel A., Shieh Y. N., Elliott W. C., Oszczepalski S., and Hoernes S. (2000b) Mineralogy, crystallinity and stable isotopic composition of illitic clays within the Polish Zechstein basin: implications for the genesis of Kupferschiefer mineralization. *Chem. Geol.* **163**(1-4), 189-205.

Behar F., Vandenbroucke M., Teermann S. C., Hatcher P. G., Leblond C., and Lerat O. (1995) Experimental simulation of gas generation from coals and a marine kerogen. *Chem. Geol.* **126**(3-4), 247-260.

Berner R. A. (1994) 3GEOCARB II: A revised model of atmospheric CO_2 over phanerozoic time. *Am. J. Sci.* **294**, 56-91.

Berner R. A. (1997) Paleoclimate - The rise of plants and their effect on weathering and atmospheric CO_2. *Science* **276**(5312), 544-546.

Boucher R. J., Standen G., and Eglinton G. (1991) Molecular characterization of kerogens by mild selective chemical degradation - Ruthenium tetroxide oxidation. *Fuel* **70**(6), 695-702.

Brand W. A. (2004) Mass spectrometer hardware for analyzing stable isotope ratios. In *Handbook of Stable Isotope Analytical Techniques*, Vol. Part I (ed. P. A. de Groot), pp. 836-858. Elsevier.

Brongersma-Sanders M. (1965) Metals of the Kupferschiefer supplied by normal sea water. *Geol. Rundsch.* **55**, 365-375.

Broutin J., Cabanis B., Chateauneuf J. J., and Deroin J. P. (1994) Biostratigraphy, magmatism, and tectonics of the SW European realm during the Permian times with paleogeographic consequences. *Bull. Soc. Geol. Fr.* **165**(2), 163-179.

Bruckschen P., Oesmann S., and Veizer J. (1999) Isotope stratigraphy of the European Carboniferous: proxy signals for ocean chemistry, climate and tectonics. *Chem. Geol.* **161**(1-3), 127-163.

Bucefalo Palliani R., Mattioli E., and Riding J. B. (2002) The response of marine phytoplankton and sedimentary organic matter to the early Toarcian (Lower Jurassic) oceanic anoxic event in northern England. *Marine Micropaleontology* **46**(1-2), 223-245.

Buhay W. M. (1996) Evaluating kinetic fractionation factors used for ecologic and paleoclimatic reconstructions from oxygen and hydrogen isotope ratios in plant water and cellulose. *Geochim. Cosmochim. Acta* **60**(12), 2209-2218.

Burger K., Hess J. C., and Lippolt H. J. (1997) Tephrochronologie mit Kaolin-Tonsteinen: Mittel zur Korrelation paralischer und limnischer Ablagerungen des Oberkarbon. In *Geologisches Jahrbuch, Reihe A*, Vol. 147, pp. 37.

Burgoyne T. W. and Hayes J. M. (1998) Quantitative production of H_2 by pyrolysis of gas chromatographic effluents. *Anal. Chem.* **70**, 5136-5141.

Butala S. J. M., Medina J. C., Taylor T. Q., Bartholomew C. H., and Lee M. L. (2000) Mechanisms and kinetics of reactions leading to natural gas formation during coal maturation. *Energy Fuels* **14**(2), 235-259.

Cecil C. B. (1990) Paleoclimate controls on stratigraphic repetion of chemical and siliciclastic rocks. *Geology* **18**, 533-536.

Cecil C. B., Stanton R. W., Neuzil S. G., Dulong F. T., Ruppert L. F., and Pierce B. S. (1985) Paleoclimate controls on late Paleozoic sedimentation and peat formation in the central Appalachian Basin (U.S.A.). In *Paleoclimatic controls on coal resources of the Pennsylvanian System of North America.*, Vol. 5 (ed. Phillips, Tom, L ; Cecil, and Blaine), pp. 195-230. Elsevier.

Chateauneuf J. J. and Farjanel G. (1989) Synthèse géologique des bassins permiens Français. *Mémoires du B.R.G.M.* **128**, 288.
Chikaraishi Y. and Naraoka H. (2003) Compound-specific δD-δ^{13}C analysis of *n*-alkanes extracted from terrestrial and aquatic plants. *Phytochemistry* **63**(3), 361-371.
Chikariaishi Y. and Naraoka H. (2005) δ^{13}C and δD identification of sources of lipid biomarkers in sediments of Lake Haruna (Japan). *Geochimica et Cosmochima Acta* **69**(13), 3285-3297.
Chikariaishi Y., Naraoka H., and Poulson S. R. (2004) Carbon and hydrogen isotopic fractionation during lipid biosynthesis in a higher plant (Cryptomeria japonica). *Phytochemistry* **65**(3), 323-330.
Cogne J. P., Brun J. P., and Vandendriessche J. (1990) Paleomagnetic evidence for rotation during Stephano-Permian extension in Southern Massif-Central (France). *Earth Planet. Sci. Lett.* **101**(2-4), 272-280.
Cogne J. P., Vandendriessche J., and Brun J. P. (1993) Syn-extension rotations in the Permian St-Affrique Basin (Massif-Central, France) - Paleomagnetic constraints. *Earth Planet. Sci. Lett.* **115**(1-4), 29-42.
Collister J. W., Rieley G., Stern B., Eglinton G., and Fry B. (1994) Compound-specific delta-C-13 analyses of leaf lipids from plants with differing carbon-dioxide metabolisms. *Org. Geochem.* **21**(6-7), 619-627.
Coplen T. B. (1996) New guidelines for reporting stable hydrogen, carbon, and oxygen isotope-ratio data. *Geochim. Cosmochim. Acta* **60**(17), 3359-3360.
Craig H. (1961) Isotopic variations in meteoric waters. *Science* **133**(346), 1702-1703.
Cranwell P. A., Eglinton G., and Robinson N. (1987) Lipids of aquatic organisms as potential contributors to lacustrine sediments. 2. *Org. Geochem.* **11**(6), 513-527.
Crowley T. J. (1994) Pangean climates. In *Pangea; paleoclimate, tectonics, and sedimentation during accretion, zenith and breakup of a supercontinent.*, Vol. 288 (ed. G. D. Klein), pp. 25-39. Geological Society of America.
Crowley T. J. and Baum S. K. (1992) Modeling Late Paleozoic Glaciation. *Geology* **20**(6), 507-510.
Crowley T. J., Mengel J. G., and Short D. A. (1987) Gondwanalands Seasonal Cycle. *Nature* **329**(6142), 803-807.
Dansgaard W. (1964) Stable isotopes in precipitation. *Tellus* **16**, 436-468.
Dawson D., Grice K., Wanga S., Alexander R., and Radke J. (2004) Stable hydrogen isotopic composition of biomarkers in torbanites from different palaeogeographical locations: D/H as a palaeoclimate indicator. *Org. Geochem.* **35**(2), 189-197.
Deshpande R. D., Bhattacharya S. K., Jani R. A., and Gupta S. K. (2003) Distribution of oxygen and hydrogen isotopes in shallow groundwaters from Southern India: lnfluence of a dual monsoon system. *J. Hydrol.* **271**(1-4), 226-239.
DiMichele W. A., Pfefferkorn H., and Phillips T. L. (1996) Persistence of Late Carboniferous tropical vegetation during glacially driven climatic and sea-level fluctuations. *Paleogeogr. Paleoclimatol. Paleoecol.* **125**(1-4), 105-128.
DiMichele W. A., Pfefferkorn H. W., and Gastaldo R. A. (2001) Response of Late Carboniferous and Early Permian plant communities to climate change. *Annu. Rev. Earth Planet. Sci.* **29**, 461-487.
DiMichele W. A. and Phillips T. L. (1994) Paleobotanical and paleoecological constraints on models of peat formation in the Late Carboniferous of Euramerica. *Paleogeogr. Paleoclimatol. Paleoecol.* **106**(1-4), 39-90.
DiMichele W. A. and Phillips T. L. (1995) The response of hierarchially structured ecosystems to long-term climatic change; a case study using tropical peat swamps of Pennsylvanian age. In *Effects of past global change on life.* (ed. S. M. Stanley), pp. 134-155. National Academy Press.
DiMichele W. A. and Phillips T. L. (1996) Clades, ecological amplitudes, a ecomorphs: phylogenetic effects and persistence of primitive plant communities on the Pennsylvanian-age tropical wetlands. *Paleogeogr. Paleoclimatol. Paleoecol.* **127**, 83-105.
DiMichele W. A., Phillips T. L., and Peppers R. A. (1985) The influence of climate and depositional environment on the distribution and evolution of Pennsylvanian coal-swamp plants. In *Geological factors and the evolution of plants.* (ed. Tiffney and Bruce), pp. 223-256. Yale Univ. Press.
Dinçer T., Hutton L. G., and Kupe B. B. J. (1979) Study of using stable isotopes, flow distribution, surface-groundwater relations and evaporation in the Okavango Swamp, Botswana (IAEA-SM-/52). *International Symposium on Isotope Hydrology*, 3-26.
dosSantos P. R., RochaCampos A. C., and Canuto J. R. (1996) Patterns of late Palaeozoic deglaciation in the Parana Basin, Brazil. *Paleogeogr. Paleoclimatol. Paleoecol.* **125**(1-4), 165-184.
Eglinton G. and Hamilton R. J. (1967) Leaf epicuticular waxes. *Science* **156**(3780), 1322-1323.
Ellis L. and Fincannon A. L. (1998) Analytical improvements in irm-GC/MS analyses: Advanced techniques in tube furnace design and sample preparation. *Org. Geochem.* **29**(5-7), 1101-1117.
Engel H. (1985) Zur Tektogenese des Saarbrücker Hauptsattels und der südlichen Randüberschiebung. In *Beiträge zur Tiefentektonik westdeutscher Steinkohlenlagerstätten* (ed. G. Drozdzewski, H. Engel, R. Wolf, R. Wrede, and V. Wrede), pp. 217-239. Geologisches Landesamt Westfalen.
Erez J. and Luz B. (1983) Experimental paleotemperature equation for planktonic foraminifera. *Geochim. Cosmochim. Acta* **47**, 1025-1031.
Espitalié J., Deroo G., and Marquis F. (1985) Rock Eval pyrolysis and its applications. *Rev. Inst. Francais. Pétr.* **Part I, Part II, Part III (40, 40, 41)**, 653-678, 755-784, 73-89.
Espitalie J., Laporte J. L., Madec M., Marquis F., Leplat P., Paulet J., and Boutefeu A. (1977) Rapid Method for Source Rocks Characterization and for Determination of Petroleum Potential and Degree of Evolution. *Revue De L Institut Francais Du Petrole* **32**(1), 23-42.
Estep M. E. and Hoering T. C. (1980) Biogeochemistry of the stable hydrogen isotopes. *Geochim. Cosmochim. Acta* **44**, 1197-1206.
Estep M. F. (1984) Carbon and hydrogen isotopic compositions of algae and bacteria from hydrothermal environments, Yellowstone National Park. *Geochim. Cosmochim. Acta* **48**, 591-599.
Farquhar G. D., Ehleringer J. R., and Hubick K. T. (1989) Carbon isotope discrimination and photosynthesis. *Annu. Rev. Plant Physiol. Plant Molec. Biol.* **40**, 503-537.

Ficken K. J., Li B., Swain D. L., and Eglinton G. (2000) An n-alkane proxy for the sedimentary input of submerged/floating freshwater aquatic macrophytes. *Org. Geochem.* **31**(7-8), 745-749.

Flanagan L. B., Comstock J. P., and Ehleringer J. R. (1991) Comparison of modeled and observed environmental-influences on the stable oxygen and hydrogen isotope composition of leaf water in *Phaseolus vulgaris* L. *Plant Physiol.* **96**(2), 588-596.

Fluteau F., Besse J., Broutin J., and Ramstein G. (2001) The Late Permian climate. What can be inferred from climate modelling concerning Pangea scenarios and Hercynian range altitude? *Paleogeogr. Paleoclimatol. Paleoecol.* **167**(1-2), 39-71.

Frakes L. A., Francis J. E., and Syktus J. I. (1992) *Climate modes of the Phanerozoic : the history of the earth's climate over the past 600 million years*. Cambridge University Press.

Friedman I., Redfield A. C., Schoen B., and Harris J. (1964) The variation of the deuterium content of natural waters in the hydrologic cycle. *Rev. Geophys.* **2**(1), 177-224.

Friedman I., Smith G. I., Gleason J. D., Warden A., and Harris J. M. (1992) Stable isotope composition of waters in southeastern California: Part I. *J. of Geophys. Res.* **93**(D5), 5795-5812.

Frimmel A., Oschmann W., and Schwark L. (2004) Chemostratigraphy of the Posidonia Black Shale, SW-Germany: I - Influence of Sea Level Variation on Organic Facies Evolution. *Chem. Geol.* **206**, 199-230.

Frommherz B. (1998) Palaeoecology of Westphalian and Stephanian fluviolacustrine strata in the Saar Basin (SW Germany). PhD, Universität Würzburg.

Galimov E. M. (1985) *The biological fractionation of isotopes.* Academic Press.

Gand G., Labeyrie J., Garric J., Nel A., Schneider J., and Walter H. (1997) Dècouverte d'Arthropodes et de bivalves inédits dans le Permien continental (Lodèvois, France). *Comptes Rendus de l'Academie des Sciences de Paris, Sciences de la terre et des planètes* **325**, 891-898.

Gastaldo R. A., DiMichele W. A., and Pfefferkorn H. W. (1996) Out of the icehouse into the greenhouse; a late Paleozoic analog for modern global vegetational change. *GSA Today* **6**(10), 1-7.

Gat J. R. (1996) Oxygen and hydrogen isotopes in the hydrologic cycle. *Annu. Rev. Earth Planet. Sci.* **24**, 225-262.

Gat J. R. and Bowser C. (1991) Heavy isotope enrichment of water in coupled evaporative systems. In *Stable Isotope Geochemistry: A Tribute to Samuel Epstein*, Vol. Spec. Pub. No.3 (ed. H. P. Taylor Jr., J. R. O' Neil, and I. R. Kaplan), pp. 159-168. The Geochemical Society.

Gat J. R., Shemesh A., Tziperman E., Hecht A., Georgopoulos D., and Basturk O. (1996) The stable isotope composition of waters of the eastern Mediterranean Sea. *J. of Geophys. Res., Ser. C* **101**, 6441-6451.

Gehre M., Geilmann H., Richter J., Werner R. A., and Brand W. A. (2004) Continous flow 2H/1H and 18O/16O analysis of water samples with dual inlet precission. *Rapid Commun. Mass Spectrom.* **18**, 2650-2660.

Gelpi E., Schneider H., Mann J., and Oro J. (1970) Lipids of geochemical significance in microscopic algae 1. Hydrocarbons of geochemical significance in microscopic algae. *Phytochemistry* **9**(3), 603-612.

German-Stratigraphic-Commission. (2002) Stratigraphic table of Germany. German Stratigraphic Commission.

Giger W., Schaffner C., and Wakeham S. G. (1980) Aliphatic and olefinic hydrocarbons in recent sediments of Greifensee, Switzerland. *Geochim. Cosmochim. Acta* **44**(1), 119-129.

Golonka J. and Ford D. (2000) Pangean (Late Carboniferous-Middle Jurassic) paleoenvironment and lithofacies. *Paleogeogr. Paleoclimatol. Paleoecol.* **161**(1-2), 1-34.

Gonfiantini R. (1986) Environmental isotopes in lake studies. In *The terrestrial environment, B.* (ed. P. Fritz and J. C. Fontes), pp. 113-168. Elsevier.

Gonfiantini R., Borsi S., Ferrara G., and Panichi C. (1973) Isotopic composition of waters from the Danakil depression (Ethiopia). *Earth Planet. Sci. Lett.* **18**, 13-21.

Gonfiantini R., Roche M. A., Olivry J. C., Fontes J. C., and Zuppi G. M. (2001) The altitude effect on the isotopic composition of tropical rains. *Chem. Geol.* **181**(1-4), 147-167.

Gonfiantini R., Zuppi G. M., Eccles D. H., and Ferro W. (1979) Isotope investigations of Lake Malawi. In *Isotopes in Lake Studies*, pp. 195-207. IAEA.

Goossens H., DeLeeuw J. W., Schenck P. A., and Brassell S. C. (1984) Tocopherols as likely precursors of pristane in ancient sediments and crude oils. *Nature* **312**(5993), 440-442.

Grice K., Schaeffer P., Schwark L., and Maxwell J. R. (1997) Changes in palaeoenvironmental conditions during deposition of the Permian Kupferschiefer (Lower Rhine Basin, northwest Germany) inferred from molecular and isotopic compositions of biomarker components. *Org. Geochem.* **26**(11-12), 677-690.

Harland W. B., Armstrong R. L., Cox A. V., Craig L. E., Smith A. G., and Smith D. G. (1990) *A geologic time scale*. Cambridge University Press.

Hassan K. M. and Spalding R. F. (2001) Hydrogen isotope values in lacustrine kerogen. *Chem. Geol.* **175**(3-4), 713-721.

Hay W. W., Barron E. J., and Thompson S. L. (1990) Results of global atmospheric circulation experiments on an Earth with a meridional pole-to-pole continent. *J. Geol. Soc.* **147**, 385-392.

Hayes J. M. (2001) Fractionation of carbon and hydrogen isotopes in biosynthetic processes. *Stable Isotope Geochemistry* **43**, 225-277.

Henk A. (1993) Late orogenic basin evolution in the Variscan Internides - the Saar-Nahe Basin, Southwest Germany. *Tectonophysics* **223**(3-4), 273-290.

Hesselbo S. P., Grocke D. R., Jenkyns H. C., Bjerrum C. J., Farrimond P., Bell H. S. M., and Green O. R. (2000) Massive dissociation of gas hydrate during a Jurassic oceanic anoxic event. *Nature* **406**(6794), 392-395.

Hilkert A. W., Douthitt C. B., Schlüter H. J., and Brand W. A. (1999) Isotope ratio monitoring gas chromatography mass spectrometry of D/H by high temperature conversion isotope ratio mass spectrometry. *Rapid Commun. Mass Spectrom.* **13**(13), 1226-1230.

Huang Y., Shuman B., Wang Y., and Webb T. (2002) Hydrogen isotope ratios of palmitic acid in lacustrine sediments record late Quaternary climate variations. *Geology* **30**(12), 1103-1106.

Huang Y. S., Bol R., Harkness D. D., Ineson P., and Eglinton G. (1996) Post-glacial variations in distributions, C-13 and C-14 contents of aliphatic hydrocarbons and bulk organic matter in three types of British acid upland soils. *Org. Geochem.* **24**(3), 273-287.

Huang Y. S., Shuman B., Wang Y., and Webb T. (2004) Hydrogen isotope ratios of individual lipids in lake sediments as novel tracers of climatic and environmental change: a surface sediment test. *J. Paleolimn.* **31**(3), 363-375.

IAEA. (2001) GNIP Maps and Animations. International Atomic Energy Agency.

Ingraham N. L. and Taylor B. E. (1986) Hydrogen isotope study of large-scale meteoric water transport in northern California and Nevada. *J. Hydrol.* **85**(1-2), 183-197.

Ingraham N. L. and Taylor B. E. (1991) Light stable isotope systematics of large-scale hydrologic regimes in California and Nevada. *Water Resour. Res.* **27**(1), 77-90.

IUGS. (2002) International Stratigraphic Chart (ed. IUGS-&-Intercommission-Working-Group). International-Union-of-Geological-Sciences.

Ivlev A. A. (2001) Carbon isotope effects (13C/12C) in biological systems. *Seperation Science & Technology* **36**(8-9), 1819-1914.

Jasper J. P. (2001) Quantitative estimates of precision for molecular isotopic measurements. *Rapid Commun. Mass Spectrom.* **15**(17), 1554-1557.

Jenkyns H. C. (1985) The Early Toarcian and Cenomanian-Turonian anoxic events in Europe - Comparisons and Contrasts. *Geol. Rundsch.* **74**(3), 505-518.

Jenkyns H. C. and Clayton C. J. (1986) Black shales and carbon isotopes in pelagic sediments from the Tethyan Lower Jurassic. *Sedimentology* **33**(1), 87-106.

Jenkyns H. C. and Clayton C. J. (1997) Lower Jurassic epicontinental carbonates and mudstones from England and Wales: chemostratigraphic signals and the early Toarcian anoxic event. *Sedimentology* **44**(4), 687-706.

Kerp H. (1996) Post-Variscan late Palaeozoic Northern Hemisphere gymnosperms: The onset to the Mesozoic. *Rev. Palaeobot. Palynology* **90**(3-4), 263-285.

Koopmans M. P., Koster J., vanKaamPeters H. M. E., Kenig F., Schouten S., Hartgers W. A., deLeeuw J. W., and Sinninghe-Damsté J. S. (1996) Diagenetic and catagenetic products of isorenieratene: Molecular indicators for photic zone anoxia. *Geochim. Cosmochim. Acta* **60**(22), 4467-4496.

Koopmans M. P., Rijpstra W. I. C., Klapwijk M. M., de Leeuw J. W., Lewan M. D., and Sinninghe-Damsté J. S. (1999) A thermal and chemical degradation approach to decipher pristane and phytane precursors in sedimentary organic matter. *Org. Geochem.* **30**(9), 1089-1104.

Körner F., Schneider J. W., Hoernes S., Gand G., and Kleeberg R. (2003) Climate and continental sedimentation in the Permian of the Lodève Basin (Southern France). *Boll. Soc. Geol. It.* **2**, 185-191.

Kracht O. and Gleixner G. (2000) Isotopic analysis of pyrolysis products from spaghnum peat and dissolved organic matter from peat. *Org. Geochem.* **31**, 645-654.

Krishnamurthy R. V. and Epstein S. (1985) Tree ring D/H ratio from Kenya, East Africa and its paleoclimatic significance. *Nature* **317**(6033), 160-162.

Krishnamurthy R. V., Syrup K. A., Baskaran M., and Long A. (1995) Late Glacial Climate Record of Midwestern United States from Hydrogen Isotope Ratio of Lake Organic Matter. *Science* **269**(5230), 1565-1567.

Küspert W. (1982) Environmental changes during oil shale deposition as deduced from stable isotope ratios. In Cyclic and Event Stratification. In *Cyclic and Event Stratification* (ed. G. Einsele and A. Seilacher), pp. 482-501. Springer-Verlag.

Kutzbach J. E. and Gallimore R. G. (1989) Pangena climates: Megamonsoons of the megacontinent. *J. Geophys. Res.* **94**, 3341-3357.

Kutzbach J. E. and Ziegler A. M. (1993) Simulation of Late Permian climate and biomes with an atmospherie-ocean model: comparisons with observations. *Phil. Trans. R. Soc. London* **B**(341), 327-340.

Lange B. M. and Croteau R. (1999) Isopentenyl diphosphate biosynthesis via a mevalonate- independent pathway: Isopentenyl monophosphate kinase catalyzes the terminal enzymatic step. *Proc. Natl. Acad. Sci. U. S. A.* **96**(24), 13714-13719.

Lange O. L., Green T. G. A., and Ziegler H. (1988) Water status related photosynthesis and carbon isotope discrimination in species of the lichen genus *Pseudocyphellaria* with green or blue-green photobionts and in photosymbiodemes. *Oecologia* **75**, 494-501.

Leaney F. W., Osmond C. B., Allison G. B., and Ziegler H. (1985) Hydrogen-isotope composition of leaf water in C-3 and C-4 plants - Its relationship to the hydrogen-isotope composition of dry-matter. *Planta* **164**(2), 215-220.

Lewan M. D. (1997) Experiments on the role of water in petroleum formation. *Geochim. Cosmochim. Acta* **61**(17), 3691-3723.

Li M., Huang Y. S., Obermajer M., Jiang C., Snowdon L. R., and Fowler M. G. (2001) Hydrogen isotopic composition of individual *n*-alkanes as a new approach to petroleum correlation: case studies from the Western Canada Sedimentary Basin. *Org. Geochem.* **32**(12), 1387-1399.

Li M. W., Larter S. R., Taylor P., Jones D. M., Bowler B., and Bjøroy M. (1995) Biomarkers or not Biomarkers - a New hypothesis for the origin of pristane involving derivation from methyltrimethyltridecylchromans (Mttcs) formed during diagenesis from chlorophyll and alkylphenols. *Org. Geochem.* **23**(2), 159-167.

Lichtenthaler H. K., Rohmer M., and Schwender J. (1997) Two independent biochemical pathways for isopentenyl diphosphate and isoprenoid biosynthesis in higher plants. *Physiologia Plantarum* **101**(3), 643-652.

Lippolt H. J. and Hess J. C. (1989) Isotopic evidence for the stratigraphic position of the Saar-Nahe Rotliegend volcanism. II. Rb-Sr investigations. *Neues Jahrbuch für Geologie und Paläontologie Monatshefte* **9**, 539-552.

Littke R. (1993) *Deposition, diagenesis and weathering of organic matter-rich sediments*. Springer.

Lockheart M. J., VanBergen P. F., and Evershed R. P. (1997) Variations in the stable carbon isotope compositions of individual lipids from the leaves of modern angiosperms: Implications for the study of higher land plant-derived sedimentary organic matter. *Org. Geochem.* **26**(1-2), 137-153.

Luo Y. and Sternberg L. (1991) Deuterium heterogeneity in starch and cellulose nitrate of CAM and C_3 plants. *Phytochemistry* **30**(4), 1095-1098.
Luo Y. H. and Sternberg L. (1992) Spatial D/H heterogeneity of leaf water. *Plant Physiol.* **99**, 248-350.
Luo Y. H., Sternberg L., Suda S., Kumazawa S., and Mitsui A. (1991) Extremely low D/H ratios of photoproduced hydrogen by cyanobacteria. *Plant Cell Physiol.* **32**(6), 897-900.
Majoube M. (1971) Frationnement en oxygen-18 et en deuterium entre l'eau et sa vapeur. *J. Chim. Phys.* **58**, 1423-1436.
Mastalerz M. and Schimmelmann A. (2002) Isotopically exchangeable organic hydrogen in coal relates to thermal maturity and maceral composition. *Org. Geochem.* **33**, 921-931.
Matthews A. and Katz A. (1977) Oxygen isotope fractionation during the dolomitization of calcium carbonate. *Geochim. Cosmochim. Acta* **41**, 1431-1438.
McCrea J. M. (1950) On the isotope chemistry of carbonates and a paleotemperature scale. *Jour. Chem. Physics* **18**, 849-857.
Medina E., Lüttge U., Leal F., and Ziegler H. (1991) Carbon and hydrogen isotope ratios in Bromeliads growing under different light environments in natural conditions. *Bot. Acta* **104**(1), 47-52.
Menning M. (2001) A Permian time scale 2000 and correlation of marine and continental sequences using the Illawarra reversal (265 Ma). *Ann. Mus. Civ. Sc. Nat.* **25**, 355-362.
Menning M., Weyer D., Wendt I., Riley N. J., and Davydov V. I. (2001) Discussion on high-precision Ar-40/Ar-39 spectrum dating on sanidine from the Donets Basin, Ukraine: evidence for correlation problems in the Upper Carboniferous - Journal, Vol. 156, 1999, 527-533. *J. Geol. Soc.* **158**, 733-736.
Merlivat L. (1978) Molecular diffusivities of H_2O_{16}, HDO_{16}, and H_2O_{18} in gases. *Journeaux du Chimique et du Physique* **69**, 2864-2871.
Merlivat L. and Jouzel J. (1979) Global climatic interpretation of the deuterium-oxygen-18 relationship for precipitation. *J. of Geophys. Res., Ser. C* **84**(C8), 5029-5033.
Merritt D. A., Freeman K. H., Ricci M. P., Studley S. A., and Hayes J. M. (1995) Performance and optimization of a combustion interface for isotope ratio monitoring gas-chromatography mass-spectrometry. *Anal. Chem.* **67**(14), 2461-2473.
Meyers P. A. (1997) Organic geochemical proxies of paleoceanographic, paleolimnologic, and paleoclimatic processes. *Org. Geochem.* **27**(5-6), 213-250.
Michels R., Landais P., Philp R. P., and Torkelson B. E. (1995) Influence of pressure and the presence of water on the evolution of the residual kerogen during confined, hydrous, and high-pressure hydrous pyrolysis of Woodford Shale. *Energy Fuels* **9**(2), 204-215.
Nissenbaum A. (1972) Deuterium content of humic acids from marine and non-marine environments. *Mar. Chem.* **2**, 59-63.
O'Leary M. H. (1988) Carbon isotopes in photosynthesis. *Bioscience* **3**(5), 328-336.
Oszczepalski S. and Rydzewski A. (1987) Palaeogeography and sedimentary model of the Kupferschiefer in Poland. In *The Zechstein Facies in Europe.* (ed. Peryt, Tadeusz, and Marek), pp. 189-205. Springer-Verlag.
Otto-Bliesner B. L. (1998) Effects of tropical mountain elevations on the climate of the Late Carboniferous; climate model simulations. In *Tectonic boundary conditions for climate reconstructions*, Vol. 39 (ed. T. J. Crowley and K. C. Burke), pp. 100-115. Oxford Monographs on Geology and Geophysics.
Pagani M., Freeman K. H., and Arthur M. A. (2000) Isotope analyses of molecular and total organic carbon from Miocene sediments. *Geochim. Cosmochim. Acta* **64**(1), 37-49.
Pancost R. D., Crawford N., and Maxwell J. R. (2002) Molecular evidence for basin-scale photic zone euxinia in the Permian Zechstein Sea. *Chem. Geol.* **188**(3-4), 217-227.
Parrish J. T. (1993) Climate of the supercontinent Pangea. *J. Geol.* **101**, 215-233.
Parrish J. T. and Curtis R. L. (1982) Atmospheric circulation, upwelling, and organic-rich rocks in the Mesozoic and Cenozoic eras. *Paleogeogr. Paleoclimatol. Paleoecol.* **40**(1-3), 31-66.
Pearson A. and Eglinton T. I. (2000) The origin of *n*-alkanes in Santa Monica Basin surface sediment: a model based on compound-specific Delta C-14 and delta C-13 data. *Org. Geochem.* **31**(11), 1103-1116.
Phillips D. L. and Koch P. L. (2002) Incorporating concentration dependence in stable isotope mixing models. *Oecologia* **130**, 114-125.
Phillips T. L. and Peppers R. A. (1984) Changing patterns of Pennsylvanian coal-swamp vegetation and implications of climatic control on coal occurrence. *Int. J. Coal Geol.* **3**(3), 205-255.
Pond K. L., Huang Y. S., Wang Y., and Kulpa C. F. (2002) Hydrogen isotopic composition of individual n-alkanes as an intrinsic tracer for bioremediation and source identification of petroleum contamination. *Environ. Sci. Technol.* **36**(4), 724-728.
Quandt L., Gottschalk G., Ziegler H., and Stichler W. (1977) Isotope discrimination by photosynthetic bacteria. *FEMS Microbiol. Lett.* **1**(3), 125-128.
Radke J., Bechtel A., Gaupp R., Püttmann W., Sachse D., Schwark L., and Gleixner G. (in press) Correlation between hydrogen isotope ratios of lipid biomarkers and sediment maturity. *Geochim. Cosmochim. Acta*.
Radke M. (1988) Application of aromatic compounds as maturity indicators in source rocks and crude oils. *Mar. Pet. Geol.* **5**, 224-236.
Radke M., Welte D. H., and Willsch H. (1982) Geochemical study on a well in the Western Canada Basin - relation of the aromatic distribution pattern to maturity of organic-matter. *Geochim. Cosmochim. Acta* **46**, 1-10.
Radke M. and Willsch H. (1994) Extractable Alkyldibenzothiophenes in Posidonia Shale (Toarcian) source rocks - relationship of yields to petroleum formation and expulsion. *Geochim. Cosmochim. Acta* **58**(23), 5223-5244.
Redding C. E., Schoell M., Monin J. C., and Durand B. (1980) Hydrogen and carbon isotopic composition of coals and kerogens. In *Advances in organic geochemistry 1979.*, Vol. 12 (ed. G. Douglas and Maxwell), pp. 711-723. Pergamon.
Rees P. M., Gibbs M. T., Ziegler A. M., Kutzbach J. E., and Behling P. J. (1999) Permian climates: Evaluating model predictions using global paleobotanical data. *Geology* **27**(10), 891-894.
Reichel W. (1966) Stratigraphie, Paläogeographie des Döhlen Beckens, TU Freiberg.

Reichel W. (1984) Die Kohlelithotypen und ihre Bildungsräume in den Steinkohlenfloezen des Döhlener Beckens bei Dresden. *Hercynia* **21**(3), 319-334.

Ricci M. P., Merritt D. A., Freeman K. H., and Hayes J. M. (1994) Acquisition and processing of data for isotope-ratio-monitoring mass-spectrometry. *Org. Geochem.* **21**(6-7), 561-571.

Roden J. S. and Ehleringer J. R. (1999) Observations of hydrogen and oxygen isotopes in leaf water confirm the Craig-Gordon model under wide-ranging environmental conditions. *Plant Physiol.* **120**(4), 1165-1173.

Roden J. S., Lin G. G., and Ehleringer J. R. (2000) A mechanistic model for interpretation of hydrogen and oxygen isotope ratios in tree-ring cellulose. *Geochim. Cosmochim. Acta* **64**(1), 21-35.

Röhl H. J., Schmid-Röhl A., Oschmann W., Frimmel A., and Schwark L. (2001a) The Posidonia Shale (Lower Toarcian) of SW-Germany: an oxygen- depleted ecosystem controlled by sea level and palaeoclimate. *Paleogeogr. Paleoclimatol. Paleoecol.* **165**(1-2), 27-52.

Röhl H. J., Schmid-Röhl A., Oschmann W., Frimmel A., and Schwark L. (2001b) The Posidonia Shale (Lower Toarcian) of SW-Germany: an oxygen-depleted ecosystem controlled by sea level and palaeoclimate. *Paleogeogr. Paleoclimatol. Paleoecol.* **165**(1-2), 27-52.

Rosman K. J. R. and Taylor P. D. P. (1997) Isotopic compositions of the elements 1997. *Internat. Union of Pure and Appl. Chem.*, 1-22.

Rowley D. B., Raymond A., Parrish J. T., Lottes A. L., Scotese C. R., and Ziegler A. M. (1985) Carboniferous paleogeographic, phytogeographic, and paleoclimatic reconstructions. *Int. J. Coal Geol.* **5**(1-2), 7-42.

Rullkötter J., Leythäuser D., Horsfield B., Littke R., Mann U., Muller P. J., Radke M., Schäfer R. G., Schenk H. J., Schwochau K., Witte E. G., and Welte D. H. (1988) Organic-matter maturation under the influence of a deep intrusive heat-source - a natural experiment for quantitation of hydrocarbon generation and expulsion from a petroleum source rock (Toarcian Shale, northern Germany). *Org. Geochem.* **13**(4-6), 847-856.

Rullkötter J. and Marzi R. (1986) Oil generation in the Michigan Basin: A biological marker carbon and isotope approach. *Org. Geochem.* **10**, 817-827.

Rundel P. W., Stichler W., Zander R. H., and Ziegler H. (1979) Carbon and hydrogen isotopes of bryophytes from arid humid regions. *Oecologia* **44**, 91-94.

Sachse D., Radke J., Gaupp R., Schwark L., Lüniger G., and Gleixner G. (2004a) Reconstruction of palaeohydrological conditions in a lagoon during the 2nd Zechstein cycle through simultaneous use of δD values of individual n-alkanes and $\delta^{18}O$ and $\delta^{13}C$ values of carbonates. *Int. J. Earth Sci.* **93**, 554-564.

Sachse D., Radke J., and Gleixner G. (2004b) Hydrogen isotope ratios of recent lacustrine sedimentary *n*-alkanes record modern climate variability. *Geochim. Cosmochim. Acta* **68**(23), 4877-4889.

Sackett W. M. (1978) Carbon and hydrogen isotope effects during thermo-catalytic production of hydrocarbons in laboratory simulation experiments. *Geochim. Cosmochim. Acta* **42**(6), 571-580.

Santrock J., Studley S. A., and Hayes J. M. (1985) Isotopic Analyses Based on the Mass-Spectrum of Carbon-Dioxide. *Anal. Chem.* **57**(7), 1444-1448.

Sauer P. E., Eglinton T. I., Hayes J. M., Schimmelmann A., and Sessions A. L. (2001) Compound specific D/H ratios of lipid biomarkers from sediments as a proxy for environmental and climatic conditions. *Geochim. Cosmochim. Acta* **65**(2), 213-222.

Schäfer A. (1986) Die Sedimente des Oberkarbons und Unterrotliegenden im Saar-Nahe Becken. *Mainzer Geowissenschaftliche Mitteilungen* **15**, 239-365.

Schäfer A. (1989) Variscan molasse in the Saar-Nahe Basin (W-Germany), Upper Carboniferous and Lower Permian. *Geol. Rundsch.* **78**(2), 499-524.

Scheffler K., Hoernes S., and Schwark L. (2003) Global changes during Carboniferous-Permian glaciation of Gondwana - Linking polar and equatorial climate evolution by geochemical proxies. *Geology* **31**, 605-608.

Schiegl W. E. (1972) Deuterium content of peat as a paleoclimatic recorder. *Science* **175**, 512-513.

Schiegl W. E. and Vogel J. (1970) Deuterium content of organic matter. *Earth Planet. Sci. Lett.* **7**, 307-313.

Schimmelmann A., Boudou J. P., Lewan M. D., and Wintsch R. P. (2001) Experimental controls on D/H and C-13/C-12 ratios of kerogen, bitumen and oil during hydrous pyrolysis. *Org. Geochem.* **32**(8), 1009-1018.

Schimmelmann A., Lewan M. D., and Wintsch R. P. (1999) D/H isotope ratios of kerogen, bitumen, oil, and water in hydrous pyrolysis of source rocks containing kerogen types I, II, IIS, and III. *Geochim. Cosmochim. Acta* **63**(22), 3751-3766.

Schmid-Röhl A., Rohl H. J., Oschmann W., Frimmel A., and Schwark L. (2002) Palaeoenvironmental reconstruction of Lower Toarcian epicontinental black shales (Posidonia Shale, SW Germany): global versus regional control. *Geobios* **35**(1), 13-20.

Schmidt H. L. (2003) Fundamentals and systematics of the non-statistical distributions of isotopes in natural compounds. *Naturwissenschaften* **90**(12), 537-552.

Schmidt H. L., Werrner R. A., and Eisenreich W. (2003) Systematics of 2H-patterns of natural compounds and its importance for the elucidation of biosynthetic pathways. *Phytochem. Rev.* **2**, 61-85.

Schneider J. W. (1994) Environment, biotas and taphonomy of the Lower Perminan lacustrine Niederhäslich limestone, Döhlen basin, Germany. *Transactions of the Royal Society of Edinburgh: Earth Sciences* **34**, 453-453.

Schneider J. W. (2001) Rotliegenstratigraphie - Prinzipien und Probleme. *Beiträge zur Geologie Thüringens* **8**, 7-42.

Schneider J. W., Stanek K. P., Goebel J., Hoffmann U., Jaschke I., and Renno A. (1999) Deep fault-controlled sedimentation and volcanism; the Rotliegend Döhlen-Basin in the Elbe-Zone. In *89th annual meeting of the Geologische Vereinigung; Old crust, new problems; geodynamics and utilization; abstracts and programme; includes the final international colloquium of the DFG priority programme "Orogenic processes; quantification and modeling in the Variscan Belt".* Vol. 99-1 (ed. P. G. Dietrich, W. Franke, J. Merkel, and P. Herzig), pp. 179. Alfred-Wegener-Stiftung.

Schoell M. (1980) The hydrogen and carbon isotopic composition of methane from natural gases of various origins. *Geochim. Cosmochim. Acta* **44**(5), 649-661.

Schoell M. (1984a) Recent advances in petroleum isotope geochemistry. In *Advances in organic geochemistry 1983.*, Vol. 6 (ed. A. Schenck, W. deLeeuw, and Lijmbach), pp. 645-663. Pergamon.

Schoell M. (1984b) Stable isotopes in petroleum research. In *Advances in petroleum geochemistry*, Vol. 1 (ed. J. Brooks and D. Welte), pp. 215-245. Academic Press.

Schoell M. (1984c) *Wasserstoff- und Kohlenstoffisotope in organischen Substanzen, Erdölen und Erdgasen*. Schweitzerbart'sche Verlagsbuchhandlung.

Schoell M., Teschner M., Wehner H., Durand B., and Oudin F. L. (1983) Maturity related biomarker and stable isotope variations and their application of oil / source rock correlation in the Mahakam Delta, Kalimantan. In *Advances in organic geochemistry, 1981.*, Vol. 10 (ed. Bjoroey, M ; Albrecht, C ; Cornford, C ; de, Groot, K ; Eglinton, G ; Galimov, E ; Leythaeuser, Detlev ; Pelet, R ; Rullkoetter, and J ; Speers), pp. 156-163. Wiley & Sons.

Schwark L. and Püttmann W. (1990) Aromatic hydrocarbon composition of the Permian Kupferschiefer in the Lower Rhine Basin, NW Germany. *Org. Geochem.* **16**(4-6), 749-761.

Schwender J., Seemann M., Lichtenthaler H. K., and Rohmer M. (1996) Biosynthesis of isoprenoids (carotenoids, sterols, prenyl side- chains of chlorophylls and plastoquinone) via a novel pyruvate/glyceraldehyde 3-phosphate non-mevalonate pathway in the green alga Scenedesmus obliquus. *Biochem. J.* **316**, 73-80.

Scotese C. R. (1997) Paleogeographic Atlas. In *PALEOMAP Progress Report 90-0497*, pp. 37. Dep. Geol., U. Texas.

Seewald J. S. (2003) Organic-inorganic interactions in petroleum-producing sedimentary basins. *Nature* **426**(6954), 327-333.

Sessions A. L., Burgoyne T. W., and Hayes J. M. (2001) Determination of the H-3 factor in hydrogen isotope ratio monitoring mass spectrometry. *Anal. Chem.* **73**(2), 200-207.

Sessions A. L., Burgoyne T. W., Schimmelmann A., and Hayes J. M. (1999) Fractionation of hydrogen isotopes in lipid biosynthesis. *Org. Geochem.* **30**, 1193-1200.

Sessions A. L., Jahnke L. L., Schimmelmann A., and Hayes J. M. (2002) Hydrogen isotope fractionation in lipids of the methane-oxidizing bacterium *Methylococcus capsulatus*. *Geochim. Cosmochim. Acta* **66**(22), 3955-3969.

Sessions A. L., Sylva S. P., Summons R. E., and Hayes J. M. (2004) Isotopic exchange of carbon-bound hydrogen over geologic timescales. *Geochim. Cosmochim. Acta* **68**(7), 1545-1559.

Smith B. N. and Epstein S. (1970) Biogeochemistry of stable isotopes of hydrogen and carbon in salt marsh biota. *Plant Physiol.* **46**, 738-742.

Smith B. N. and Ziegler H. (1990) Isotopic fractionation of hydrogen in plants. *Bot. Acta* **103**(4), 335-342.

Smith J. W., Rigby D., Schmidt P. W., and Clark P. W. (1983) D/H ratios of coals and the paleolatitude of their deposition. *Nature* **302**, 322-323.

Sofer Z. and Schiefelbein C. F. (1986) Hydrogen isotope ratio determinations in hydrocarbons using the pyrolysis preparation technique. *Anal. Chem.* **58**(9), 2033-2036.

Soreghan M. J., Soreghan G. S., and Hamilton M. A. (2002) Paleowinds inferred from detrital-zircon geochronology of upper Paleozoic loessite, western equatorial Pangea. *Geology* **30**(8), 695-698.

Spero H. J., Bijma J., Lea D. W., and Bemis B. E. (1997) Effect of seawater carbonate concentration on planktonic foraminiferal carbon and oxygen isotopes. *Nature* **390**, 497-500.

Stalker L., Larter S R., and Farrimond P. (1998) Biomarker binding into kerogens: evidence from hydrous pyrolysis using heavy water (D_2O). *Org. Geochem.* **28**(3-4), 239-253.

Standen G., Boucher R. J., Rafalskabloch J., and Eglinton G. (1991) Ruthenium tetroxide oxidation of natural organic macromolecules - Messel kerogen. *Chem. Geol.* **91**(4), 297-313.

Sternberg L. (1988) D/H Ratios of Environmental Water Recorded By D/H Ratios of Plant Lipids. *Nature* **333**(6168), 59-61.

Sternberg L. and DeNiro M. J. (1983) Isotopic composition of cellulose from C3, C4, and CAM plants growing near one another. *Planta* **220**, 947-948.

Sternberg L., DeNiro M. J., and Ajie H. O. (1986) Isotopic relationships between saponifiable lipids and cellulose nitrate prepared from red, brown and green algae. *Planta* **169**(3), 320-324.

Sternberg L., DeNiro M. J., and Keeley J. E. (1984) Hydrogen, oxygen, and carbon iotope ratios of cellulose from submerged aquatic Crassulacean acid metabolism and non-Crassulacean metabolism plants. *Plant Pysiology* **76**, 68-70.

Stiller M. and Nissenbaum A. (1980) Variations of stable hydrogen isotopes in plankton from a fresh-water lake. *Geochim. Cosmochim. Acta* **44**(8), 1099-1101.

Stollhofen H. (1998) Facies architecture variations and seismogenic structures in the Carboniferous-Permian Saar-Nahe Basin (SW Germany): evidence for extension-related transfer fault activity. *Sediment. Geol.* **119**(1-2), 47-83.

Stollhofen H. (1999) Sequence stratigraphy in continental settings - examples from the Permo-Carboniferous Saar-Nahe Basin, Germany. In *West European Case Studies in Stratigraphy* (ed. H. Bock, A. Müller, R. Sweenen, and W. Zimmerle), pp. 233-260. Schweizerbart'sche Verlagsbuchhandlung.

Swart P. K. (1991) The oxygen and hydrogen isotopic composition of the Black Sea. *Deep-Sea Res. Part I* **38**, S761-S772.

Tabor N. J. and Montanez I. P. (2002) Shifts in late Paleozoic atmospheric circulation over western equatorial Pangea: Insights from pedogenic mineral d18O compositions. *Geology* **30**(12), 1127-1130.

Tabor N. J., Montanez I. P., and Southard R. J. (2002) Paleoenvironmental reconstruction from chemical and isotopic compositions of Permo-Pennsylvanian pedogenic minerals. *Geochim. Cosmochim. Acta* **66**(17), 3093-3107.

Tissot B. P. and Welte D. H. (1985) Petroleum formation and occurrence. *J. of Sed. Petrol.* **55**(6), 942-943.

Torcq F., Besse J., Vaslet D., Marcoux J., Ricou L. E., Halawani M., and Basahel M. (1997) Paleomagnetic results from Saudi Arabia and the Permo-Triassic Pangea configuration. *Earth Planet. Sci. Lett.* **148**(3-4), 553-567.

Turner P. and Magaritz M. (1981) Marine transgression, basin wide stagnation and consequent mineralization of the marl slate-Kupferschiefer. *J. Geol. Soc.* **138**(MAR), 219-219.

Vail P. R., Audemard F., Bowman S. A., Eisner P. N., and Perez-Cruz G. (1991) The stratigraphic signatures of tectonics, eustacy and sedimentation: an overview. In *Cycles and Events in Stratigraphy*, Vol. II (ed. A. Seilacher and G. Eisner). Springer.

Vaughan D. J., Sweeney M. A., Friedrich G., Diedel R., and Haranczyk C. (1989) The Kupferschiefer; an overview with an appraisal of the different types of mineralization. In *A special issue devoted to current research on mineral deposits of Europe.*, Vol. 84 (ed. Rickard and David), pp. 1003-1027. Economic Geology Publishing Company.

Veevers J. J. and Powell C. M. (1987) Late Paleozoic glacial episodes in Gondwanaland reflected in transgressive-regressive depostional sequences of Euramerica. *Geol. Soc. Am. Bull.* **98**, 475-487.

Veizer J., Godderis Y., and Francois L. M. (2000) Evidence for decoupling of atmospheric CO2 and global climate during the Phanerozoic eon. *Nature* **408**(6813), 698-701.

Visser J. N. J. (1997) Deglaciation sequences in the Permo-Carboniferous Karoo and Kalahari basins of southern Africa: A tool in the analysis of cyclic glaciomarine basin fills. *Sedimentology* **44**(3), 507-521.

Vliex M. (1994) Kohlenpetrographische und organisch-geochemische Untersuchungen an Kohlen und Sedimentgesteinen des Saar-Nahe-Beckens- Ein Beitrag über die Bedeutung geochemischer Fossilien als Anzeiger für Veränderungen der Flora zwischen dem Westfal C und dem Unterrotliegenden. PhD Thesis, Rheinisch-Westfälische Hochschule Aachen.

Vliex M., Hagemann H. W., and Püttmann W. (1994) Aromatized Arborane/Fernane Hydrocarbons as molecular indicators of floral changes in Upper Carboniferous Lower Permian strata of the Saar-Nahe Basin, Southwestern Germany. *Geochim. Cosmochim. Acta* **58**(21), 4689-4702.

Waldron S., Lansdown J. M., Scott E. M., Fallick A. E., and Hall A. J. (1999) The global influence of the hydrogen isotope composition of water on that of bacteriogenic methane from shallow freshwater environments. *Geochim. Cosmochim. Acta* **63**(15), 2237-2245.

Walker C. D., Leaney F. W., Dighton J. C., and B. A. G. (1989) The influence of transpiration on the equilibration of leaf water with atmospheric vapour. *Plant Cell Environ.* **12**, 221-234.

Wedepohl K. H. (1964) Untersuchungen am Kupferschiefer in Nordwestdeutschland - Ein Beitrag zur Deutung der Genese bituminöser Sedimente. *Geochim. Cosmochim. Acta* **28**(MAR), 305-364.

Werner R. A. and Brand W. A. (2001) Referencing strategies and techniques in stable isotope ratio analysis. *Rapid Commun. Mass Spectrom.* **15**(7), 501-519.

White J. W. C. (1988) Stable hydrogen isotope ratios in plants: A review of current theory and some potential applications. In *Stable Isotopes in Ecological Research* (ed. P. W. Rundel, J. R. Ehleringer, and K. A. Nagy), pp. 142-162. Springer.

Wieser M. E. and Brand W. A. (2000) Isotope ratio studies using mass spectrometry. In *Encyclopedia of Spectroscopy and Spectrometry*, Vol. 3 (ed. J. C. Lindon, G. E. Tranter, and J. L. Holmes), pp. 1072-1086. Academic Press.

Wilkes H., Clegg H., Disko U., Willsch H., and Horsfield B. (1998) Fluoren-9-ones and carbazoles in the Posidonia Shale, Hils Syncline, Northwest Germany. *Fuel* **77**(7), 657-668.

Xie S., Nott C. J., Avsejs L. A., Volders F., Maddy D., Chambers F. M., Gledhill A., Carter J. F., and Evershed R. P. (2000) Palaeoclimate records in compound-specific δD values of a lipid biomarker in ombrotrophic peat. *Org. Geochem.* **31**(10), 1053-1057.

Yang H. and Huang Y. S. (2003) Preservation of lipid hydrogen isotope ratios in Miocene lacustrine sediments and plant fossils at Clarkia, northern Idaho, USA. *Org. Geochem.* **34**(3), 413-423.

Yeh H. W. (1980) D/H ratios and late-stage dehydration of shales during burial. *Geochim. Cosmochim. Acta* **44**(2), 341-352.

Zegouagh Y., Derenne S., Largeau C., Bardoux G., and Mariotti A. (1998) Organic matter sources and early diagenetic alterations in Arctic surface sediments (Lena River delta and Laptev Sea, Eastern Siberia), II. Molecular and isotopic studies of hydrocarbons. *Org. Geochem.* **28**(9-10), 571-583.

Zhang B. L., Billault I., Lo X. B., Mabon F., Remaud G., and Martin M. L. (2002) Hydrogen isotopic profile in the characterization of sugars. Influence of the metabolic pathway. *J. Agric. Food Chem.* **50**(6), 1574-1580.

Ziegler A. M., Hulver M. L., and Rowley D. B. (1997) Permian world topography and climate. In *Late glacial and postglacial environmental changes; Quaternary, Carboniferous-Permian, and Proterozoic.* (ed. I. P. Martini), pp. 111-142. Oxford University Press.

Ziegler H. (1989) Hydrogen Isotope fractionation in plant tissues. In *Stable isotopes in Ecological Research* (ed. P. Rundel, J. R. Ehleringer, and K. Nagy), pp. 105-123. Springer-Verlag.

Ziegler H., Osmond C. B., Stichler W., and Trimborn P. (1976) Hydrogen isotope discrimination in higher-plants: correlations with photosynthetic pathway and environment. *Planta* **128**(1), 85-92.

Ziegler P. A. (1990) Geological atlas of western and central Europe. Shell Int. Petrol. Mij. dist. Geol. Soc. Publ., House Bath.

ACKNOWLEDGEMENTS

I gratefully thank PD Prof. Gerd Gleixner for supervising this work, for fruitful comments and ideas to keep research in isotope geochemistry going. Prof. Reinhard Gaupp for supervising this work and his comments on earlier versions of this thesis and scientific publications. My special thanks go to Prof. E. D. Schulze for being able to use laboratory equipement of the MPI for Biogeochemistry and all administrative workforces (software, workshop, administration). I would like to thank all of the workforces at MPI. The Deutsche Forschungsgemeinschaft is acknowledged for financial and scientific support during several meetings during the Schwerpunktprogramm 1054 ("*Evolution of the System Earth during the Late Palaeozoic"*).

In earth sciences, collaboration with colleagues from other institutions is mandatory and without this collaboration none of the work would have ever come to an end. Thus, I would like to thank PD Prof. L. Schwark, Prof. J. Schneider, Prof. R. Littke, Prof. W. Püttmann, Prof. A. Bechtel and coworkers, F. Körner, H. Lüschen, R. Meier, K. Scheffler. A warm thanks goes to other colleagues supporting me with their great knowledge about the samples I used in this thesis, Prof. A. Schäfer, Dr. H. Stollhofen, Dr. M. Menning, and Dr. Schubert.

I would like to express my gratitude to all isolab people at MPI in Jena. Thank you Willi, Roland, Heike and Stefan! They gave me support in all questions about isotope ratio mass spectrometry and processed isotope data for bulk samples and standards. For the elemental analysis I would like to acknowledge the central facilities lab, especially Ines Hilke. For always keeping the isotope and elemental machines in the "Gleixner Group" running I thank Steffen Rühlow. Steffen was often my last spare tyre finding a leak. Special thanks to all the people from the Gleixner Group, Oliver Kracht, Jan Rothe, Christiane Kramer and guests, Natacha Poirier, Rama Krishnamurthy, Prof. Largeau. Andrej Thiele for processing some of the 50 samples I used for analysis and Dirk Sachse for providing me with important reference data after my move to Bremen and for the nice research trip to Scandinavia.

I'm grateful to all my friends at MPI, some of them have already spread on the globe; Andrew Manning, Jo House, Ash Wood, Karen Kohfeld, Claudia Czimczik, Barbara Lühker, Brian Mantlana, Antje Weitz, Ulrike Seibt, Annett Börner and Volker Hahn. I'm pretty sure that I forgot somebody, so please scratch in your name here: _____. I appology for having missed you!!! They should be mentioned in the first line of this chapter, but as it is I would like to thank Anke Bittkau and my little son Lasse for being so pationed with me, even writing during holidays. Thank you Antje and Martin for correction and thanks to my parents.

9 Appendix

9.1 Supplementary tables – Chapter 5

Table 9.1. δD values of hydrocarbons [‰VSMOW] of the Kupferschiefer and the Posidonienschiefer. For explanation of maturation parameters see footnotes in the text and for differences in borehole depths see text in the geological settings. All δD values were determined in triplicate (σ1). Not indicated standard deviation is a single measurement. §: n=4; ¶: n=2.

	Kupferschiefer																Posidonienschiefer							
	Be42		Be38		Be41		Be30		Be27		Be35		Be22		Be33		DH44		HH20		GH 29		BH14	
compound	δD	σ1	δD	σ1	δD	σ1	δD	σ1	δD	σ1	δD	σ1	δD	σ1	δD	σ1	δD	σ1	δD	σ1	δD	σ1	δD	σ1
n-C_{12}							-104	7	-102	2			-128	8										
n-C_{13}							-109	3	-104	8			-125	4							-135	3		
n-C_{14}							-98	13	-108	5			-94	12			-162	5			-112	5		
n-C_{15}	-159	2	-153	5			-101	1	-93	4	-110	5	-128	4			-178	3			-119	9	-145	7
n-C_{16}	-133	6	-128	4	-121	4§	-103	13	-77	5	-92	2	-90	11			-163	2	-133	10¶	-102	8	-113	5
n-C_{17}	-141	1	-132	4	-120	2§	-88	2	-		-80	2	-66	8	-124	3	-176	3	-129	5¶	-76	2	-102	3
n-C_{18}	-126	6	-122	4	-132	29§	-87	7	-68	6	-74	2	-55	9	-109	1	-146	3	-204	7¶	-80	2	-96	2
n-C_{19}	-154	6	-132	5	-114	4§	-78	4	-59	8	-71	3	-57	11	-109	1	-175	2	-137	8¶	-101	3	-104	1
n-C_{20}	-118	6	-110	7	-109	3§	-81	4	-55	3	-66	1	-55	4	-102	1	-155	4	-118	13¶	-96	6	-88	2
n-C_{21}	-144	4	-123	5	-120	4§	-80	7	-59	5	-71	1	-54	12	-102	2	-170	5	-127	8¶	-92	4	-95	2
n-C_{22}	-126	4	-119	2	-125	3§	-81	1	-55	5	-74	4	-57	2	-99	1	-180	3	-118	6¶	-90	3	-92	3
n-C_{23}	-126		-122		-129	9§	-90	18	-54		-73		-63	3	-97				-114	5¶	-88	2	-94	
n-C_{24}	-116	4	-114	1	-126	4§	-84	3	-55	12	-77	1	-72	2	-98	1			-111	8¶	-104	2	-92	4
n-C_{25}	-112	2	-98	0	-133	15§	-82	1	-62	5	-77	1	-75	2	-101	1	-164		-101	10¶	-86	3	-88	2
n-C_{26}			-99	1	-129	16§	-82	2	-60	5	-89	1	-84	1	-95	1			-103	8¶	-91	4	-87	7
n-C_{27}	-110	3	-75	2	-137	14§	-76	2	-60	3	-98	1	-75	2	-111	1					-95	9		
n-C_{28}			-53	1	-139	15§	-78	1	-56	5	-88	15	-83	7	-89	3								
n-C_{29}			-102	1	-156	17§	-84	3	-74	6	-134		-83	2	-85	2								
n-C_{30}			-115	4			-90	3	-84	7	-109	10	-109	4	-97	1								
n-C_{31}			-127	4			-115	10					-85	17	-88	4								
n-C_{32}			-148	7			-				-145	3	-98	11	-101	5								
n-C_{33}			-132	5			-78	3					-88	12	-80	6								
n-C_{34}	-198	3	-191	8			-84	2					-101	9										
n-C_{35}																			-97	8				
Phytane	-281	3	-267	4	-172	3	-84	7	-81	4	-108	5	-77		-143	5	-316	1	-268	8	-130	4	-128	4
Pristane	-269	6	-249	3	-178	6					-92	2	-86	12	-150	4	-317	2	-257	4	-131	8	-117	1
mean δD $C_{11}$to C_{35} alkanes	-136		-120		-126		-88		-72		-90		-84		-99		-167		-124		-98		-100	
depth	1027		1998		2515		4719		4484		3322		4061		3784		38.1		45.1		63.1		44.20	
Rc/R_om	*0.65*		*0.81*		*0.92*		*1.08*		*1.14*		*1.16*		*1.26*		*1.3*		0.48		0.53		0.73		0.88	
MPI1	0.41		0.69		0.86		1.14		1.23		1.27		1.43		1.5		*0.4*		*0.48*		*0.83*		*1.06*	
T_{max}	419		427		432		439		441		439		433		432		*421*		*424*		*435*		*438*	
HI	432		371		285		297		295		263		366		371		*481*		*467*		*323*		*246*	
MDR	2.17		2.65		4.63		6.84		6.72		5.38		6.73		6.12		0.43		0.4		2.27		3.71	
borehole sampling depth [m]	1027		1998		2515		4719		4484		3322		4061		3784		38.1		45.1		63.1		44.2	

9.2 Supplementary tables - Chapter 6

Table 9.2. Elemental data and maturity indices of investigated samples. North East Polish Kupferschiefer (KS) samples are extracts; therefore no data from bulk sediment preparation are available. Geochemical data of the Kupferschiefer Basin samples of Poland were taken from Bechtel et al. (2001). CC: total carbonate content, Posidonienschiefer samples are from the Northern German Basin (No. DH 44) and from the Southern German Basin (No. 950874). Kupferschiefer samples are from the Lower Rhenish Basin (No. 957515) and from the North East Polish Kupferschiefer Basin (No. Be 42). [1] Döhlen Basin: Only thickness data is known (REICHEL, 1966), [2] KS: (BECHTEL et al., 2000a)

	sample number	depth [m]	CC [%]	Corg [%]	N_{tot}	S_{tot}	MPI	T_{MAX}	S1	S2	S3	HI	OI
Saar-Nahe Basin	90761	946	0	52.8	0.7	1.7	0.76	434	2.35	87.40	3.35	165	6
	90763	944	0	13.2	0.3	1.9	0.69	423	0.70	21.75	0.89	159	6
	90764	941	0	7.1	0.2	0.7	0.76	439	0.25	5.17	0.66	72	9
	90765	930	0	7.1	0.2	0.6	0.77	430	0.29	11.92	0.50	167	7
	90766	929	0	5.4	0.2	0.1	0.67	428	0.26	9.24	0.62	171	11
	90767	928	0	19.7	0.4	3.7	0.80	435	0.76	19.60	1.26	99	6
	90772	817	0	29.6	0.5	n.n.	0.60	428	0.9	60.75	2.00	205	6
	90773	816	0	2.9	0.1	0.2	0.59	431	0.09	1.96	0.54	67	18
	90774	815	0	2.1	0.1	0.0	0.60	432	0.10	7.95	0.14	92	6
	90751	1672	0	73.5	1.4	0.8	0.88	440	4.47	110.47	2.04	150	3
	90750	1670	0	32.2	0.6	0.7	0.82	436	2.04	53.69	1.56	166	4
	90782	926	0	50.1	1.0	0.6	0.82	428	2.82	101.30	3.00	202	5
	90780	925	0	77.0	1.6	0.9	0.76	437	4.60	156.43	4.00	203	5
Döhlen Basin	Z 2	n.n. [1]	0.1	12.6	0.3	0.1	0.44	431	0.20	5.92	6.14	46	48
	Zauk2/II	n.n.[1]	0.0	10.5	0.3	0.2	0.46	427	0.10	4.20	5.17	40	49
	W 669	n.n.[1]	1.5	6.1	0.3	0.1	0.48	437	0.05	1.79	3.79	29	62
	W 874	n.n.[1]	28.8	36.3	1.0	n.n.	0.78	427	1.10	64.85	22.57	180	62
Lodève Basin	SP 48	outcrop	3.2	2.9	0.2	0.1	0.76	433	0.19	9.03	0.41	301	13
	UB X	outcrop	0.7	10.4	0.1	0.2	0.54	437	0.32	29.24	0.83	281	7
Kupferschiefer Basin	Be 42	[2]1027	[2]4.3	[2]8.4	n.n.	n.n.	[2]0.41	[2]412	n.n.	n.n.	n.n.	[2]285	[2]26
	957515	612.6	3.6	0.8	n.n.	2.5	0.17	420	0.32	11.61	1.08	457	42
Posidonienschiefer Basin	DH 44	38.1	4.4	16.6	0.5	n.n.	0.48	421	2.08	79.37	1.77	481	10
	950874	outcrop	3	12.1	3.3	3.3	0.45	424	3.40	73.89	1.22	467	7

Table 9.3. $\delta^{13}C$ and δD of *n*-alkanes of the late Palaeozoic intermontane Saar-Nahe Basin and Döhlen Basin, Lodève Basin and marine Kupferschiefer Basin and Middle Mesozoic Posidonienschiefer ($\delta^{13}C$ in ‰VPDB, δD in VSMOW). All mean $\delta^{13}C$ and δD values were determined in triplicate ($\sigma 1$). Not indicated standard deviation indicates single measurements. §: n=2, ¶: n=1. Standard deviation represents δD values of hydrocarbons.

Saar-Nahe Basin

	90761		**90763**		**90764**		**90765**		**90766**		**90767**		**90772**		**90773**		**90774**		**90751**		**90750**		**90782**		**90780**	
compound	δD	σ1	δD	σ1	δD	σ1	δD	σ1	δD	σ1	δD	σ1	δD	σ1	δD	σ1	δD	σ1	δD	σ1	δD	σ1	δD	σ1	δD	σ1
n-C_{12}	-118	¶																	-104	19§						
n-C_{13}	-141	¶	-95	11			-145	¶					-167	6					-110	11						
n-C_{14}	-144	¶	-70	13			-126	9§					-168	5	-99	10			-87	8	-97	¶			-88	¶
n-C_{15}	-128	10	-145	16	-119	4	-102	7	-84	¶	-88	¶	-149	6	-114	7	-130	10	-93	10	-90	¶	-90	3	-89	6
n-C_{16}	-114	8	-83	9	-113	5	-104	7	-101	¶	-82	13	-144	6	-112	6	-118	6	-80	11	-96	13	-87	4	-99	3
n-C_{17}	-115	7	-66	7	-109	1	-98	6	-102	¶	-81	7	-135	10	-116	2	-109	7	-84	7	-100	8	-92	6	-86	0.1
n-C_{18}	-113	7	-73	7	-110	3	-96	9	-105	1	-90	9	-130	6	-109	12	-108	8	-82	6	-86	13	-70	3	-75	6
n-C_{19}	-111	6	-92	5	-93	7	-94	5	-93	12	-94	4	-140	3	-91	3	-116	5	-85	6	-85	1	-87	6	-89	4
n-C_{20}	-119	11	-64	3	-83	4	-81	4	-193	21	-92	11	-131	3	-82	5	-117	9	-52	6	-71	9	-72	4	-129	¶
n-C_{21}	-116	13	-54	2	-99	4	-97	3	-93	14	-88	12	-156	1	-90	6	-118	5	-46	4	-93	7	-80	7	-99	5
n-C_{22}	-99	7	-54	3	-98	4	-75	3	-95	10	-86	14	-136	9	-87	7	-121	9	-50	20	-80	3	-66	8	-81	¶
n-C_{23}	-103	6§	-72	¶	-100	4	-91	3	-89	6	-95	11§	-134	0.3§	-90	11	-116	6	-62	7	-92	0	-71	6	-59	14
n-C_{24}	-91	11§	-82	¶	-98	5	-101	1	-86	13	-89	14§	-137	11§	-94	8	-120	8	-73	5	-113	4	-66	7	-87	7
n-C_{25}	-123	12	-80	10	-90	7	-102	3	-158	5	-82	11§	-175	2§	-80	10	-113	6	-57	7	-145	8	-126	8	-74	5
n-C_{26}	-167	0.2	-79	2	-109	6	-140	1	-92	3	-105	35§	-156	2§	-107	5	-119	7	-42	34	-151	5	-128	12	-107	23
n-C_{27}	-121	10	-113	6	-106	3	-106	3	-92	6			-127	5§	-109	6	-153	7	-64	11	-97	11	-100	5	-92	¶
n-C_{28}	-113	18	-125	5	-116	6	-116	6	-108	8			-129	25	-119	4	-121	8	-71	36	-104	3	-87	6		
n-C_{29}	-108	3	-130	7	-114	3	-107	1	-102	10			-134	12§	-113	2	-117	4	-87	3	-111	8	-87	7		
n-C_{30}	-144	2	-151	15	-129	6	-136	6	-132	5			-131	15§	-114	9	-123	9	-117	21	-136	1	-124	7		
n-C_{31}	-135	14§	-114	9	-115	3	-99	1					-127	10§					-88	8	-109	3	-100	4		
n-C_{32}	-120	3			-121	6§								7					-88	6§		4				
pristane	-188	3	-152	7	-97	7	-147	5	-197	6	-105	13	-211	2§	-115	5	-102	10	-142	8	-142	¶	-93	8	-195	¶
phytane	-148§	14	-108	13	-113	2	-143	7	-186	5	-112	6	-190	2§	-127	1	-135	7	-122	¶	-79	2§	-122	4§	-113	7
mean *n*-C_{11} to *n*-C_{32s}	-123	20	-96	36	-107	12	-106	19	-108	29	-89	7	-142	15	-101	13	-127	29	-77	21	-103	22	-90	20	-90	16
mean $\delta D_{isoprenoids}$	-168	28	-130	31	-105	11	-145	3	-191	8	-109	5	-200	15	-121	9	-118	23	-132	14	-110	45	-108	20	-154	58

Continued Table 9.3

No.	Z2		Zauk II/2b		W669		W874		SP48		UB-X		957515		Be42		DH44		9508741	
													LRB		NE-Poland		NGB		SGB	
compound	δD	σ1	δD	σ1	δD	σ1	δD	σ1	δD	σ1	δD	σ1	δD	σ1	δD	σ1	δD	σ1	δD	σ1
n-C_{11}																				
n-C_{12}									-99	16									-202	3
n-C_{13}			-131	4					-121	4									-216	3
n-C_{14}	-108	19	-148	11	-90	12	-114	2	-128	5	-124	4§					-162	5	-186	2
n-C_{15}	-134	5	-114	3	-113	0.2	-137	4	-128	1	-119	5	-147	5	-159	2	-178	3	-166	1
n-C_{16}	-114	5	-78	6	-91	3	-123	1	-118	1	-113	8	-114	7	-133	6	-163	2	-180	26
n-C_{17}	-112	1	-86	¶	-95	29	-99	1	-128	3	-130	5	-71	10	-141	1	-176	3	-146	¶
n-C_{18}	-107	3	-67	27	-64	6	-113	2	-94	3	-104	11	-83	19	-126	6	-146	3	-148	11
n-C_{19}	-110	5			-60	4§	-116	5	-97	6	-113	5	-87	16	-154	6	-175	2	-128	7
n-C_{20}	-102	2					-121	3	-96	2	-101	10	-81	9	-118	6	-155	4	-161	2
n-C_{21}	-112	2	-45	31			-117	2	-104	3	-127	9	-99	6	-144	4	-170	5	-160	5
n-C_{22}	-107	2	-14	9			-123	2	-110	4	-114	3	-96	11	-126	4	-180	3	-163	1
n-C_{23}	-109	1	-45	22			-125	2	-103	3	-111	0.2	-105	5	-126	¶			-162	2
n-C_{24}	-107	2	-56	4			-128	4	-106	3	-100	0.2	-75	5	-116	4			-162	2
n-C_{25}	-101	2	-52	4			-134	2	-90	3	-147	37	-135	13	-112	2	-164	¶	-175	4
n-C_{26}	-100	3	-87	3	-85	4	-107	6	-109	2	-115	1§	-88						-169	3
n-C_{27}	-123	5	-91	5	-108	8	-133	3	-95	2	-98	1§	-134	15	-110	3			-142	5
n-C_{28}	-87	5	-93	1	-112	6	-101	2	-76	3	-88	¶	-87	11					-164	2
n-C_{29}	-109	13	-110	9	-118	1	-85	2	-82	4	-97	¶	-91	4					-132	39
n-C_{30}			-112	6	-118	8	-115	11	-82	15	-61	¶								
n-C_{31}									-95	8			-80	14						
n-C_{32}																				
n-C_{33}																			-142	¶
n-C_{34}															-198	3			-134	¶
Pristane	-188	2	-100	25	-186	4	-206	2	-179	24	-278	0.1	-305	11	-281	3	-316	1	-343	1
Phytane	-159	4	-73	17	-144	9	-196	0	-190	2	-208	3	-283	3	-269	6	-317	2	-265	¶
mean C_{11} to C_{34}-alkanes	-109	10	-83	35	-96	20	-117	14	-103	16	-110	19	-99	23	-136	24	-175	22	-162	23
mean $\delta D_{isoprenoids}$	-174	20	-86	19	-165	30	-201	7	-185	8	-243	50	-294	15	-275	8	-317	1	-304	55

10 Indices

10.1 Figures

10.2 Tables

Selbständigkeitserklärung

Ich erkläre hiermit, dass ich die vorliegende Arbeit selbständig und nur unter Verwendung der angegebenen Hilfsmittel, persönlichen Mitteilungen und Quellen angefertigt habe.

Jens Radke

Bremen, den 03/09/2006